Study of black holes in standard and modified gravity

Thesis submitted for the award of
Doctor of Philosophy in Science (Physics)
of
The University of Burdwan

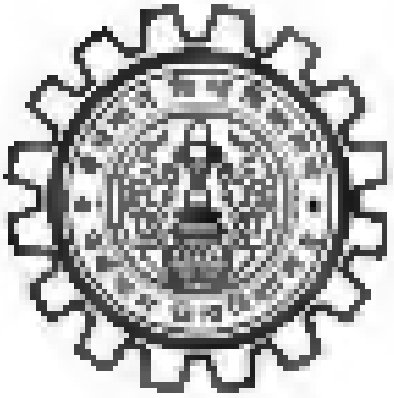

Submitted by

SOHAN KUMAR JHA

(A-Ph.D./Regn.Jer/physics/43) dated 24.06.2021

Under the Supervision of Dr. Anisur Rahaman (WBES)

Durgapur Govt. College, Durgapur, Burdwan

Work done in

Hooghly Mohsin College, Chinsurah, Hooghly

And

Durgapur Govt. College, Durgapur, Burdwan

Department of Physics
DURGAPUR GOVERNMENT COLLEGE
Accredited by NAAC with "A" Grade (2017)
[illegible] Durgapur, Paschim Bardhaman 713214

To whom it may concern

Certified that the thesis entitled **'Study of black holes in standard and modified gravity'** submitted by Sohan Kumar Jha who had got his name registered on with registration No. **B-Ph.D./Regn./sc/physics/43 dated 24/06/2022** for the award of Ph. D. (Science) degree of the University of Burdwan is based on his own work done under my supervision and that neither this thesis nor any part of it has been submitted for any degree /diploma or any other academic award before.

[illegible]
[illegible]
Durgapur Government College

Certificate from the Candidate

I do hereby declare that the subject matter embodied in the thesis "**Study of Metals based on accident and modified gravity**" is solely based on my own work done under the supervision of Dr. Ankur Purkarthi, assistant professor (W.S.) presently posted at Durgapur Government College. This thesis or any part of it has not been submitted or will not be submitted for any other academic award. I have made an effort to present it without errors. Instead, I am assuming responsibility for any mistakes if found so far.

Sahadeb Kumar Mal

Registration No : B-Phy-D-Physics/Sahadeb/43

Dated: 24.06.2023

Date:

Acknowledgement

First, I want to thank my supervisor Dr. Asutar Rakshit, for all the time and the patience invested in me throughout all my research, giving. He was able to transmit me the passion for research with supervision and long discussions where fantastic ideas emerged. I think that I could not find a better person to guide me through this experience. He taught me how to deal with new physical problems. Then, I want to thank my family for supporting me throughout this journey. It is not an easy path as those who have already walked it know. But with the guidance of my supervisor and with the support of my family, the journey was made easy.

Sukan Kumar Jha
Ph.D. scholar
Department of Physics
University of Burdwan

List of Pulications

Thesis is based on following works.

S. K. Jha, H. Barman, A. Rahaman: JCAP04 (2021) 036

S. K. Jha, A. Rahaman: Eur. Phys. J. C (2021) 81:345

S. K. Jha, S. Aziz, A. Rahaman: Eur. Phys. J. C (2022) 82:106

S. K. Jha, A. Rahaman: Eur. Phys. J. C (2023) 83:417

S. K. Jha, A. Rahaman: Eur. Phys. J. C (2023) 83:781

S. K. Jha, A. Rahaman: Eur. Phys. J. Plus 138, 84 (2023)

Additional Works done:

H. Barman, A. Rahaman and S.K.Jha: Modern Physics Letter A Vol. 36, No. 19, 2150130 (2021)

S. Aziz, S. K. Jha and A. Rahaman: Class. Quan. Grav. 38 (2021) 215004

H. Barman, A. Rahaman and S.K.Jha: Eur. Phys. J. Plus (2023) 138: 1159

List of Symbols

Notation	Description	Notation	Description
c	velocity of light	$D_{\mathcal{F}}$	fractal dimension
G	gravitational constant	$\hbar$	Planck parameter
α, β	spherical coordinates	Δx	differential parameter of Laplacian Schwarzschild metric
Γ	gamma function	$\lambda_{\mathcal{F}}$	angular parameter
ζ	Riemann zeta function	$\alpha_{\mathcal{F}}$	angle of deflection for strong gravitational lensing
λ	affine parameter	$\alpha_{\mathcal{W}}$	angle of deflection for weak gravitational lensing
λ_c	wavelength of observer	γ, β	lensing coefficients
λ_{obj}	wavelength measured at infinity	$\mathbb{R}^3$	portion of the 4th dimension
$\Phi_{\mathcal{F}}$	angular velocity of black hole	$\Delta\alpha$	magnification of the image
$T_{\mathcal{F}}$	Hawking temperature	ω	specific angular velocity of black hole
θ	charge parameter of black hole	$M_{\mathcal{F}}$	mass of black hole
$\Phi_{\mathcal{F}}$	non-rotating fractal parameter	Γ	Lorentz violating parameter
Δ	Gauss parameter	$K_{\mathcal{FF}}$	effective potential
$\Lambda_{\mathcal{F}}$	Regular parameter	$R_{\mathcal{F}}$	size of the black hole
$\Delta_{\mathcal{F}}$	deviation from circular form	κ	surface gravity
Λ	Planck constant	$r_{\mathcal{FH}}, r_{\mathcal{FC}}$	positions of event horizon
$\Gamma_{\mathcal{FC}}$	position of Cauchy horizon	$A_{\mathcal{F}}$	area of horizon
$E_{\mathcal{FC}}$	energy of photon sphere	ΔC	deviation from circularity
$\Phi_{\mathcal{F}}$	angular diameter	$\gamma_{\mathcal{F}}$	gamma ray bursts

Contents

I. INTRODUCTION

Our present description of nature is based on 2 enormously successful theories: General Relativity (GR), a classical theory describing all gravitational phenomena, and the Standard Model (SM) of particle physics, which provides a quantum description of all other interactions. General relativity has emerged as a highly successful model of gravitation and cosmology, which has so far passed many cosmological and astrophysical tests. However, there are strong indications that the theory is incomplete. The problem of quantum gravity and the question of the validity of spacetime singularities remain open. Observational data that is taken as evidence for dark energy and dark matter could indicate the need for new physics. It is widely expected that these theories are merely the low-energy limit of some more fundamental theory that would take over at the characteristic energies involved in experiments approach the Planck scale, 10^{19} GeV. Experimental information to guide the development of a Planckscale theory would, by conventional thinking, come from Planck-energy experiments, which are likely to remain unfeasible for into the future. An alternative approach is to search for small deviations from known physics (the SM and GR) in present-day experiments, with the hope that such deviations, if found, would provide information about the underlying theory. Lorentz symmetry, the idea that physical results are unchanged under rotations and boosts of the system is the pillar of both the SM and GR. Hence violations of the symmetry, if found, would provide a novel signal of new physics. Moreover, the possibility of violation of the symmetry has been demonstrated in candidates for the underlying theory, like strings. Here, we consider a special class of theory, called Standard-model, where Lorentz symmetry is spontaneously broken. The Lorentz violation arises from the dynamics of a single vector K_μ that assumes nonzero expectation value, b_μ, which is expected to zero. The nonzero value b_μ acts as a fixed background field that spontaneously breaks Lorentz symmetry.

II. THEORY OF GENERAL RELATIVITY: EINSTEIN'S EQUATION

In 1907 Einstein published his special theory of relativity. While this theory has been able to predict many observed phenomena, it was not complete in two ways. To explain matter and energy changing the geometry of spacetime, Einstein proposed a new theory (hereby known as general theory relativity. This theory is characterized by a set of dynamical equations expressed as: Einstein Field Equations showing how gravitational interaction as a result of spacetime curvature is associated energy. Albert Einstein published this new theory Gravity as a tensor equation in 1915. Movement of the body under gravitational field is almost completely described by geodetic equation. Einstein used three principles in his development of general theory of relativity namely Mach Principle, Equality Principle and Covariance principle. Einstein's field equations are given by

$$R_{ij} - \frac{1}{2}g_{ij}R = -\kappa T_{ij} \qquad (1)$$
$$\Rightarrow G_{ij} = -\kappa T_{ij}$$

Their inverted form of the above equation is

$$R_{ij} = -\kappa T_{ij} - \frac{1}{2}g_{ij}T) \qquad (2)$$

Here $G_{ij} = R_{ij} - \frac{1}{2}g_{ij}R$ are the components of Einstein tensor and T is defined by $T = g^{ij}T_{ij}$, g_{ij} being components of metric tensor. If the spacetime has signature $(-,+,+,+)$ then equation (1) becomes

$$R_{ij} - \frac{1}{2}g_{ij}R = \kappa T_{ij} \qquad (3)$$
$$\Rightarrow G_{ij} = \kappa T_{ij}$$

which is inverted form is

$$R_{ij} = \kappa T_{ij} - \frac{1}{2}g_{ij}T) \qquad (4)$$

By solving Einstein's equations, one obtains the Schwarzschild metric:

$$ds^2 = -\left(1 - \frac{2M}{r}\right)dt^2 + \left(1 - \frac{2M}{r}\right)^{-1} - r^2(d\theta^2 + \sin^2\theta d\phi^2). \qquad (5)$$

where M is the mass of the Kerr black hole in units of length and $G = c = 1$ for the entire thesis. Since the coefficient of the particle do not depend on t, and the metric does not have any cross terms involving time-like and time-like components, it is a static metric. The metric has two singularities, one at $r = 0$ and another at $r = 2M$. The first one cannot be removed using a change of coordinates, but the second one can be removed using a different choice of coordinates. It is called event horizon. Since the metric is metric and spherically symmetric, E, the conserved energy per unit mass of the particle and L, the angular momentum per unit mass, both with respect to an observer stationary at infinity, are constants of motion. Here, we study circular motion of a particle around the black hole and the proper period of the particle in the circular orbit is found out to be

$$\tau = \frac{r^{3/2}}{M} - 2\pi \frac{r^{3/2}}{\sqrt{2M}} \sqrt{1 - \frac{3M}{r}}. \tag{6}$$

Periastron shift also studied for Schwarzschild black hole. For small eccentricity, the precessing orbits showed. Light Gravitational redshift and Pound-Rebka Gravity for Schwarzschild black hole are also studied.

The Kerr solution, which describes a rotating black hole in the spacetime, is actually the solution of Einstein's equations in vacuum. In other words, the metric in exterior of an usually rotating body. The Kerr metric, in Boyer-Lindquist coordinate reads [1]

$$ds^2 = -\left(1 - \frac{2Mr}{\rho^2}\right) dt^2 - \frac{4Mr a \sin^2\theta}{\rho^2} dt\,d\phi + \frac{\rho^2}{\Delta} dr^2 + \rho^2 d\theta^2 + \frac{A \sin^2\theta}{\rho^2} d\phi^2, \tag{7}$$

where $a = \frac{J}{M}$, J being the angular momentum of the black hole and

$$\begin{aligned} \rho^2 &= r^2 + a^2 \cos^2\theta, \\ \Delta &= r^2 - 2Mr + a^2, \\ A &= (r^2 + a^2)^2 - \Delta a^2 \sin^2\theta. \end{aligned} \tag{8}$$

The equation $\Delta = 0$ has two real solutions when $a \leq M$. The larger of the two solutions gives the Event horizon (r_+) and the smaller one gives the Cauchy horizon (r_-). The region given by $g_{tt} > 0$ is called ergo-sphere. It is possible, even particle can remain static within the ergo-sphere. The region between Event horizon and the static limit surface is called ergosphere. We also study motion, gravity and Hawking temperature for the Kerr black hole. Penrose-gogging which is unique to rotating black holes are also studied here. Black hole shadows for Kerr black hole are studied here.

In [26] Bai obtained a charged rotating BH solution which came to be known as the Kerr-Sen (KS) solution. The resulting charged metric in Boyer-Lindquist coordinates (t, r, θ, ϕ) is [1]

$$ds^2 = -\left(1 - \frac{2Mr}{\rho^2}\right) dt^2 - \frac{4Mr a \sin^2\theta}{\rho^2} dt\,d\phi + \frac{\rho^2}{\Delta} dr^2 + \rho^2 d\theta^2 + \frac{A \sin^2\theta}{\rho^2} d\phi^2, \tag{9}$$

where

$$\rho^2 = r^2 + a^2 \cos^2\theta, \quad \Delta = r^2 - 2Mr + a^2, \text{ and } A = (r^2 + a^2)^2 - \Delta a^2 \sin^2\theta. \tag{10}$$

where $r = Q/M$, Q being the charge of the black hole. Here we also study Hawking temperature and other effects for the Kerr-Sen black hole.

III. EXTENSION OF LORENTZ SYMMETRY BREAKING AND THE STANDARD MODEL

General relativity and the standard model of particle physics are two very successful field theoretic models that exist so far describe our Universe. The formulation of both these theories is based on the well established Lorentz symmetry. However, the regime of applicability and the nature of energy scales describing the Universe by these two theories are profoundly different. The general relativity describes the gravitational interactions and it is a classical field theory in the curved spacetime and there is no direct way to include the quantum effect. On the contrary, the standard model describes the other fundamental interactions and it is the quantum field theory in the flat spacetime that neglects all gravitational effects, but to study the physical system in the vicinity of the Planck scale $(10^{-35}\,\mathrm{m})$, the effect due to gravity cannot be ignored, since the gravitational interaction is strong enough in this energy scale. Therefore, the study of physics in the vicinity of the Planck scale necessarily needs the unification of general relativity

[illegible]

[illegible]

$$[illegible] \tag{11}$$

[illegible]

$$[illegible] \tag{12}$$

[illegible]

$$[illegible] \tag{13}$$

[illegible]

$$[illegible] \tag{14}$$

[illegible]

$$[illegible] \tag{15}$$

[illegible]

$$[illegible] \tag{16}$$

[illegible]

$$[illegible] \tag{17}$$

[illegible]

$$[illegible] \tag{18}$$

[illegible]

$$[illegible] \tag{19}$$

[illegible]

$$[illegible] \tag{20}$$

[illegible]

V. [illegible] NONCOMMUTATIVE [illegible] BLACK HOLE

[illegible]

$$[illegible] \quad (23)$$

where

$$[illegible]$$

[illegible]

$$[illegible] \quad (24)$$

[illegible]

$$[illegible] \quad (25)$$

[illegible]

$$[illegible]$$

[illegible]

$$[illegible]$$

and

$$[illegible]$$

[illegible]

[illegible]

[illegible]

[illegible]

[illegible]

[illegible]

[illegible]

[illegible]

[illegible]

[illegible]

[illegible]

[illegible]

[illegible]

[illegible] (10)

where

$$\rho = \frac{\sigma_{xy} - \mu_x \mu_y}{\sqrt{(\sigma_{x^2} - \mu_x^2)(\sigma_{y^2} - \mu_y^2)}} \tag{11}$$

$$= \frac{\sum_{i=1}^{n} x_i y_i - n \bar{x} \bar{y}}{\sqrt{\left(\sum_{i=1}^{n} x_i^2 - n \bar{x}^2\right)\left(\sum_{i=1}^{n} y_i^2 - n \bar{y}^2\right)}}$$

$$= \frac{n \sum_{i=1}^{n} x_i y_i - \sum_{i=1}^{n} x_i \sum_{i=1}^{n} y_i}{\sqrt{\left[n \sum_{i=1}^{n} x_i^2 - \left(\sum_{i=1}^{n} x_i\right)^2\right]\left[n \sum_{i=1}^{n} y_i^2 - \left(\sum_{i=1}^{n} y_i\right)^2\right]}}$$

and

$$\rho = \frac{\sigma_{xy} - \mu_x \mu_y}{\sqrt{(\sigma_{x^2} - \mu_x^2)(\sigma_{y^2} - \mu_y^2)}} \tag{12}$$

$$= \frac{\sum_{i=1}^{n} x_i y_i - n \bar{x} \bar{y}}{\sqrt{\left(\sum_{i=1}^{n} x_i^2 - n \bar{x}^2\right)\left(\sum_{i=1}^{n} y_i^2 - n \bar{y}^2\right)}}$$

$$= \frac{n \sum_{i=1}^{n} x_i y_i - \sum_{i=1}^{n} x_i \sum_{i=1}^{n} y_i}{\sqrt{\left[n \sum_{i=1}^{n} x_i^2 - \left(\sum_{i=1}^{n} x_i\right)^2\right]\left[n \sum_{i=1}^{n} y_i^2 - \left(\sum_{i=1}^{n} y_i\right)^2\right]}}$$

[illegible] regression [illegible] [illegible] [illegible]

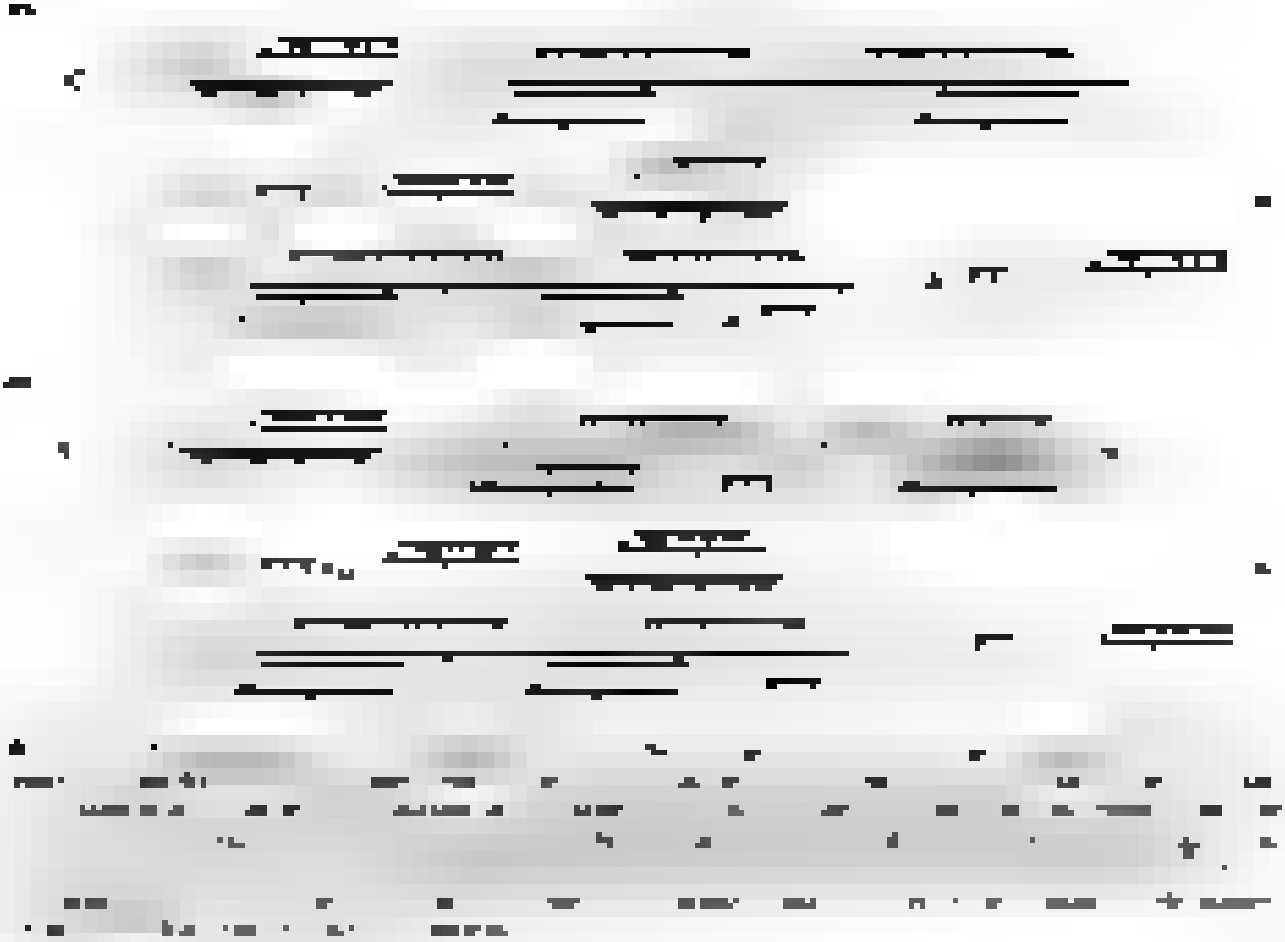

Introduction

Chapter 1

Now, equation (11.3) becomes

$$\delta S = \int \sqrt{-g}\, R_{\mu\nu}\, \delta g^{\mu\nu}\, d^4x \tag{11.4}$$

Now, we can write the variation of the Ricci tensor as

$$\delta R_{\mu\nu} = \nabla_\lambda \left(\delta \Gamma^\lambda_{\mu\nu} \right) - \nabla_\nu \left(\delta \Gamma^\lambda_{\mu\lambda} \right) \tag{11.5}$$

Substituting above two equations we get

$$\delta S = \int \sqrt{-g}\, R_{\mu\nu}\, \delta g^{\mu\nu}\, d^4x + \int \sqrt{-g}\, g^{\mu\nu} \left[\nabla_\lambda \left(\delta \Gamma^\lambda_{\mu\nu} \right) - \nabla_\nu \left(\delta \Gamma^\lambda_{\mu\lambda} \right) \right] d^4x \tag{11.6}$$

Now, we can write

$$\int \sqrt{-g}\, g^{\mu\nu} \nabla_\lambda \left(\delta \Gamma^\lambda_{\mu\nu} \right) d^4x = \int \nabla_\lambda \left(\sqrt{-g}\, g^{\mu\nu} \delta \Gamma^\lambda_{\mu\nu} \right) d^4x - \int \nabla_\lambda \left(\sqrt{-g}\, g^{\mu\nu} \right) \delta \Gamma^\lambda_{\mu\nu}\, d^4x \tag{11.7}$$

According to the Gauss theorem we get

$$\int \nabla_\lambda \left(\sqrt{-g}\, g^{\mu\nu} \delta \Gamma^\lambda_{\mu\nu} \right) d^4x = \int \sqrt{-g}\, g^{\mu\nu} \delta \Gamma^\lambda_{\mu\nu}\, dS_\lambda \tag{11.8}$$

Then we get

$$\int \sqrt{-g}\, g^{\mu\nu} \nabla_\lambda \left(\delta \Gamma^\lambda_{\mu\nu} \right) d^4x = \int \sqrt{-g}\, g^{\mu\nu} \delta \Gamma^\lambda_{\mu\nu}\, dS_\lambda - \int \nabla_\lambda \left(\sqrt{-g}\, g^{\mu\nu} \right) \delta \Gamma^\lambda_{\mu\nu}\, d^4x \tag{11.9}$$

Now, we can write the second term of the variation of the Einstein-Hilbert action as

$$\int \sqrt{-g}\, g^{\mu\nu} \nabla_\nu \left(\delta \Gamma^\lambda_{\mu\lambda} \right) d^4x = \int \nabla_\nu \left(\sqrt{-g}\, g^{\mu\nu} \delta \Gamma^\lambda_{\mu\lambda} \right) d^4x - \int \nabla_\nu \left(\sqrt{-g}\, g^{\mu\nu} \right) \delta \Gamma^\lambda_{\mu\lambda}\, d^4x \tag{11.10}$$

Note that $\delta \Gamma^\lambda_{\mu\nu}$ is the variation of the Levi-Civita connection and is defined by $g^{\mu\nu}$. If the spacetime has a boundary, we require $\delta \Gamma^\lambda_{\mu\nu}$ to vanish on the boundary. Then we get

$$\int \nabla_\nu \left(\sqrt{-g}\, g^{\mu\nu} \delta \Gamma^\lambda_{\mu\lambda} \right) d^4x = \int \sqrt{-g}\, g^{\mu\nu} \delta \Gamma^\lambda_{\mu\lambda}\, dS_\nu = 0 \tag{11.11}$$

where we have used the following equation

$$\nabla_\lambda \left(\sqrt{-g}\, g^{\mu\nu} \right) = 0 \tag{11.12}$$

Equations (11.4) and (11.11) can be written as Einstein's field equations

1. Solutions of Einstein's field equation

Einstein's field equations are non-linear and hence difficult to solve. However, certain symmetries in the problem can be used to find solutions of Einstein's field equations for different physical situations. Let us find some solutions which are relevant for astrophysics and cosmology.

1 Schwarzschild solution

The first exact solution of Einstein's equations was found by Karl Schwarzschild in 1916. He obtained the solution for a vacuum spherically symmetric gravitational field produced by a non-rotating spherical mass. For such a field, the line element, in spherical polar coordinates (t, r, θ, ϕ), is given by

$$ds^2 = \left(1 - \frac{2GM}{rc^2}\right) c^2 dt^2 - \left(1 - \frac{2GM}{rc^2}\right)^{-1} dr^2 - r^2 d\theta^2 - r^2 \sin^2\theta\, d\phi^2 \tag{1.1}$$

Lemma Let $g_{\mu\nu}$ be a solution of the vacuum Einstein field equations, then the metric $\tilde{g}_{\mu\nu}$ defined by

$$\tilde{g}_{\mu\nu} = \frac{\partial x^\alpha}{\partial \tilde{x}^\mu}\frac{\partial x^\beta}{\partial \tilde{x}^\nu} g_{\alpha\beta}, \quad \det\left(\frac{\partial x^\alpha}{\partial \tilde{x}^\mu}\right) = 1 \tag{1}$$

Lemma Let $\mathcal{M}$ be the manifold of the black hole in local coordinates and $\mathcal{M} = \mathbb{R}^4$ for the entire cluster. Suppose the coefficients of the metric g are expanded in r and the metric does not have any cross terms involving dr or $d\theta$ and the determinant of g is -1.

Proof Hamiltonian

The contact manifold $\mathcal{M}$ is $\mathbb{R}^4$ and the contact form α is $dz - p\,dq$. The Reeb vector field can be expressed using a change of coordinates, but the associated flow can be determined using diffeomorphisms and isotopies. Within the horizon $r = 2M$, all future directions point towards the singularity. Once we cross the horizon, r becomes a time coordinate and t becomes a space coordinate, so the singularity is no longer in the future. All trajectories end at the singularity. If we could move faster than light, we could escape the singularity, but we cannot. Thus, the singularity is inevitable once a black hole forms.

Definition (Particle)

Here, we consider the gravitational interaction between a point mass m and a rigid body $\mathcal{B}$ with mass distribution $\rho(\mathbf{x})$. The potential energy of the system is given by

$$U = -G\int_{\mathcal{B}} \frac{m\,\rho(\mathbf{x})}{|\mathbf{x} - \mathbf{x}_0|}\,dV$$

Here, $\mathbf{x}_0 = \frac{\mathbf{p}}{m}$ is the center of mass of the rigid body, and $\mathbf{p}$ is the total momentum of the particle with respect to the stationary observer. The Hamiltonian $H(\mathbf{p}, \mathbf{L})$ of the system is

$$H(\mathbf{p}, \mathbf{L}) = \frac{|\mathbf{p}|^2}{2m} + U(\mathbf{p}, \mathbf{L}) \tag{2}$$

where $\mathbf{L}$ is the angular momentum about the center of mass. Hamilton's equations give

$$\frac{d\mathbf{x}_0}{dt} = \frac{\mathbf{p}}{m} \tag{3}$$

Hence, we see that the angular momentum is conserved with respect to an observer who is stationary relative to the center of mass.

3 Motion of a particle in a gravitational field

Now, we study the gravitational interaction between a point mass m and a rigid body $\mathcal{B}$. For this, we consider the equations

$$\left|\frac{d^2\mathbf{x}_0}{dt^2}\right| = \left|\frac{GM}{|\mathbf{x}_0|^2}\right| = \left|\frac{GM}{|\mathbf{x}_0|^2}\right| + \left|\frac{GM}{|\mathbf{x}_0|^2}\right| \tag{4}$$

Using the equations (3) and (4), we obtain

$$\frac{d}{dt}\left|\frac{d\mathbf{x}_0}{dt}\right| = \left|\frac{d\mathbf{x}_0}{dt}\right| \cdot \left|\frac{d^2\mathbf{x}_0}{dt^2}\right| \tag{5}$$

Now, consider the following two equations:

$$\frac{d\mathbf{x}_0}{dt} = \frac{\mathbf{p}}{m}, \qquad \frac{d\mathbf{p}}{dt} = 0 \tag{6}$$

The first equation gives

$$\mathbf{x}_0 = \frac{\mathbf{p}}{m}t + \frac{\mathbf{p}_0}{m} \tag{7}$$

[illegible]

$$[illegible]$$

[illegible]

$$[illegible]$$

[illegible]

$$[illegible]$$

[illegible]

$$[illegible]$$

[illegible]

$$[illegible]$$

[illegible]

$$[illegible]$$

Experimental test of general theory of relativity

[illegible]

The precession shift of Mercury

[illegible]

$$[illegible]$$

[illegible]

$$[illegible]$$

[illegible]

A.2.3 Bending of light

One of the observational results given by general theory of relativity is the bending of light by gravity. In the absence of gravity, light travels in a straight line. But in the presence of gravity, light travels in curved paths. Light rays passing near massive bodies are bent towards them. Hence the direction of the light coming from a star is slightly changed when it passes near the sun. This change in the direction of light coming from the star is known as the deflection of light. Consequently, the star appears to be displaced from its actual position in the sky. Such displacements have been observed during total solar eclipses. Observations of the positions of stars near the sun have been made during solar eclipses and compared with their positions when the sun is in other parts of the sky. The observations confirm the predictions based on general theory of relativity.

A.2.4 Gravitational time delay

Gravitational time delay is one of the important tests of general relativity. The signals sent to and fro between the planets A and B must pass close to the sun. When the planet A is on the far side of the sun relative to the planet B, the signal sent from planet A to planet B has to travel a longer distance than when the planet A is on the near side of the sun relative to the planet B. As a result, the signal sent from planet A takes longer time to reach the planet B when the planet A is on the far side of the sun relative to the planet B than when the planet A is on the near side of the sun relative to the planet B. This delay in reaching the signal due to gravitational field of the massive object is known as gravitational time delay.

A.2.5 Gravitational Redshift

Now, we consider the case of a photon. The proper mass of the photon is zero. Hence the gravitational potential energy is given by

$$\qquad \frac{GM}{r}m \qquad (A.2.5)$$

Assume the wavelength of radiation emitted by the source of light is λ_0. Then we have

$$\qquad \qquad \frac{hc}{\lambda_0}(1+z) \qquad (A.2.6)$$

Here the relation between the wavelength λ_0 of radiation received on earth and the wavelength λ_e received at the source. The redshift z is defined by

$$z = \frac{\lambda_0 - \lambda_e}{\lambda_e} \qquad (A.2.7)$$

and we get

$$1 + z = \frac{GM}{rc^2} \qquad (A.2.8)$$

A.2.6 Energy conservation and equivalence principle

From the standard definition, the gravitational force is given by

$$F = \frac{GMm}{r^2} \qquad (A.2.9)$$

where the gravitational potential ϕ is defined by

$$\phi = -\frac{GM}{r} \quad \text{or} \quad F = -m\nabla\phi \qquad (A.2.10)$$

The conservation of the 4-momentum of a moving object is given by

$$p^\mu = (E/c, \mathbf{p}) \quad \text{or} \quad p^\mu = (mc, 0, 0, 0) \qquad (A.2.11)$$

The momentum component of the 4-momentum is given by

$$p = \frac{E}{c^2}v = \frac{mv}{\sqrt{1 - v^2/c^2}} \qquad (A.2.12)$$

[illegible]

where [illegible]

$$[illegible]$$

[illegible]

$$[illegible]$$

[illegible]

[illegible]

[illegible]

$$[illegible]$$

where [illegible]

$$[illegible]$$

[illegible]

[illegible]

$$[illegible]$$

[illegible]

$$[illegible]$$

[illegible]

Figure 1 The numerical domain for the solution of the Laplace equation in the physical space.

We can now make the plot that the equation is the solution of the Laplace equation in the domain.

3.3.2 Spatial fluid surface and impedance

We describe how the temperature at the surface is described by $\rho_{ijk} = 0$. For a stationary particle, we have $\rho_{ijk} = 0$ at the boundary. Thus

$$\rho_{ijk} = \frac{\partial}{\partial x_i} \tag{3.61}$$

For $\rho_{ijk} = 0$, the above equation is satisfied and hence, without the surface ρ_{ijk} the stationary particle is the stationary. We therefore define the surface ρ_{ijk} as the fluid surface.

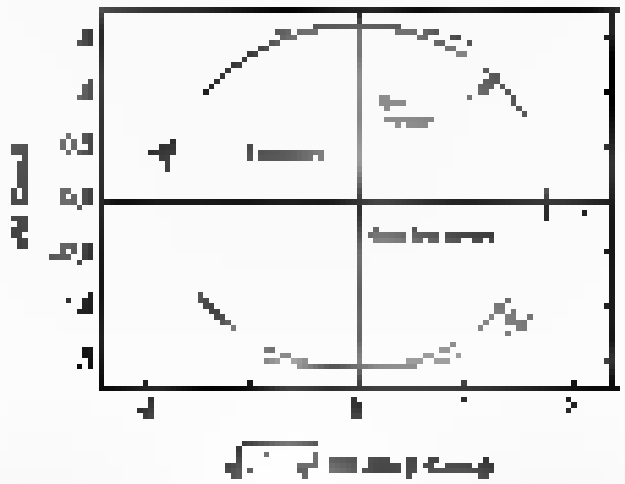

Figure 2 Fluid surface impedance and static fluid surface. See text for details.

The motion of the fluid surface is given by

$$\rho_{ijk} = \ln + \tag{3.62}$$

The fluid surface is the surface on which the pressure is constant and the surface is the surface. The impedance is the ratio of the pressure to the velocity. The impedance is the ratio of the pressure to the velocity. The impedance is the ratio of the pressure to the velocity.

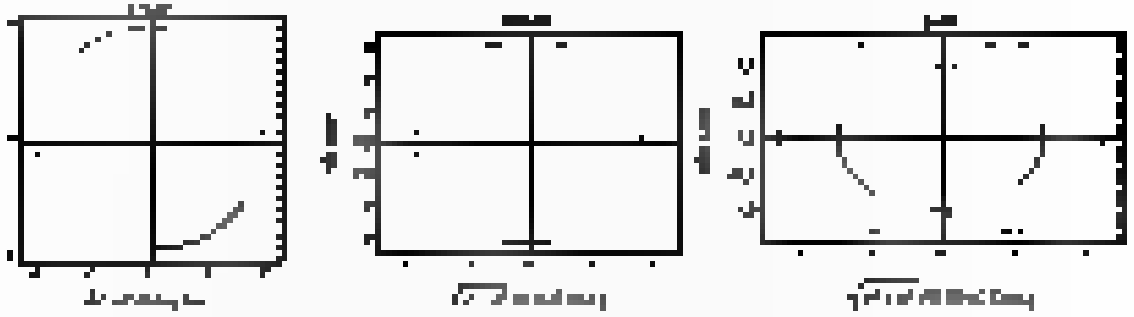

Figure 3 Variation of temperature with

3.13 Surface gravity and Hawking temperature

The surface gravity is given by [24]

$$= \frac{}{} \frac{}{} \tag{3.43}$$

where $\equiv$ and $\frac{}{}$ is the velocity measured by a stationary observer at infinity, we get

$$\frac{}{} = \frac{}{} \tag{3.44}$$

The Hawking temperature can be obtained from surface gravity using the relation

$$T_H = \frac{}{} \tag{3.45}$$

Thus, the Hawking temperature is

$$\frac{}{} \tag{3.46}$$

3.14 Covariant and contravariant differential equations of motion

Covariant components of velocity u_μ and u_ν are covariant, but in the contravariant components they are reduced to the velocity of light c. We now apply the principle covariance to obtain the equations of motion. For the energy equation, we have

$$\frac{}{} = \qquad \qquad \tag{3.47}$$

Substituting the values of coefficients, we get

$$\frac{}{} = \qquad \qquad \tag{3.48}$$

where L gives the components of the angular momentum of the particle normal to the equatorial plane per unit mass. For a particle of rest mass m_0, the quantity E is the energy of the particle per unit mass and is positive for the approaching case, and E is the energy of the particle per unit mass.

For the angular momentum equation, we have

$$\frac{}{} \qquad \qquad \tag{3.49}$$

Now we obtain the relation

$$\frac{}{} = \frac{}{} \qquad \qquad \tag{3.50}$$

[illegible]

[illegible]

$$[illegible] \tag{[illegible]}$$

where [illegible]

$$[illegible] \tag{[illegible]}$$

[illegible]

$$[illegible] \tag{[illegible]}$$

where [illegible]

$$[illegible]$$

$$[illegible] \tag{[illegible]}$$

The above equation yields

$$[illegible] \tag{[illegible]}$$

and

$$[illegible] \tag{[illegible]}$$

where [illegible]

$$[illegible] \quad \text{and} \quad [illegible] \tag{[illegible]}$$

Equations [illegible]

$$[illegible]$$

$$[illegible]$$

$$[illegible] \tag{[illegible]}$$

where [illegible] is the affine parameter and

$$[illegible] \tag{[illegible]}$$

6.13 Rutherford scattering

Rutherford investigated the scattering of alpha particles by a target consisting of a very thin foil of gold. He found that the number of alpha particles scattered through an angle θ is proportional to $\csc^4(\theta/2)$. This result is now known as the Rutherford scattering formula. It can be derived by considering the repulsive Coulomb force between the alpha particle and the gold nucleus. The force is given by

$$F = \frac{1}{4\pi\varepsilon_0}\frac{(2e)(Ze)}{r^2} \qquad [1]$$

where Ze is the charge on the gold nucleus and $2e$ is the charge on the alpha particle. The force is directed along the line joining the two particles, so the angular momentum of the alpha particle about the nucleus is conserved. Let b be the impact parameter of the alpha particle, and let v_0 be its initial speed. Then the initial angular momentum of the alpha particle about the nucleus is $mv_0 b$, where m is the mass of the alpha particle. Let v be the speed of the alpha particle when it is a very large distance from the nucleus. Then conservation of angular momentum gives

$$mvr\sin\phi = mv_0 b \qquad [2]$$

where r is the distance between the alpha particle and the nucleus, and ϕ is the angle between the velocity vector of the alpha particle and the radius vector from the nucleus to the alpha particle. When the alpha particle is very far from the nucleus, $\phi \approx \theta$, and $r \approx \infty$. Therefore, in this limit, $vb = v_0 b$, or $v = v_0$. Conservation of energy gives

$$\frac{1}{2}mv_0^2 = \frac{1}{2}mv^2 + \frac{1}{4\pi\varepsilon_0}\frac{2Ze^2}{r} \qquad [3]$$

Solving equation [2] for r and substituting into equation [3], we obtain

$$\frac{1}{2}mv_0^2 = \frac{1}{2}mv^2 + \frac{1}{4\pi\varepsilon_0}\frac{2Ze^2}{mvb}\sin\phi \qquad [4]$$

Solving equation [4] for $\sin\phi$, we obtain

$$\sin\phi = \frac{\pi\varepsilon_0 mvb}{Ze^2}\left(v - v_0\right) \qquad [5]$$

Now, $v \approx v_0$, so we can write $v = v_0 + \Delta v$, where $\Delta v \ll v_0$. Substituting into equation [5], we obtain

$$\sin\phi = \frac{\pi\varepsilon_0 mv_0 b}{Ze^2}\Delta v \qquad [6]$$

Since $\Delta v \ll v_0$, ϕ is small, and $\sin\phi \approx \phi$. Therefore, equation [6] becomes

$$\phi = \frac{\pi\varepsilon_0 mv_0 b}{Ze^2}\Delta v \qquad [7]$$

Squaring equation [7], we obtain

$$\phi^2 = \left(\frac{\pi\varepsilon_0 mv_0 b}{Ze^2}\right)^2(\Delta v)^2 \qquad [8]$$

Now, $(\Delta v)^2 \ll v_0^2$, so we can write $(\Delta v)^2 = \alpha v_0^2$, where $\alpha \ll 1$. Substituting into equation [8], we obtain

$$\phi^2 = \left(\frac{\pi\varepsilon_0 mv_0 b}{Ze^2}\right)^2\alpha v_0^2 \qquad [9]$$

Solving equation [9] for b, we obtain

$$b = \frac{Ze^2}{\pi\varepsilon_0 mv_0^2}\frac{\phi}{\sqrt{\alpha}} \qquad [10]$$

Now, α is the fraction of the incident kinetic energy that is transferred to the alpha particle when it is scattered through an angle θ. Therefore, α is a function of θ. The exact form of this function depends on the details of the scattering process, but we can write $\alpha = f(\theta)$, where $f(\theta)$ is some unknown function. Then equation [10] becomes

$$b = \frac{Ze^2}{\pi\varepsilon_0 mv_0^2}\frac{\phi}{\sqrt{f(\theta)}} \qquad [11]$$

where ϕ is the angle between the velocity vector of the alpha particle and the radius vector from the nucleus to the alpha particle. When the alpha particle is very far from the nucleus, $\phi \approx \theta$. Therefore, equation [11] becomes

$$b = \frac{Ze^2}{\pi\varepsilon_0 mv_0^2}\frac{\theta}{\sqrt{f(\theta)}} \qquad [12]$$

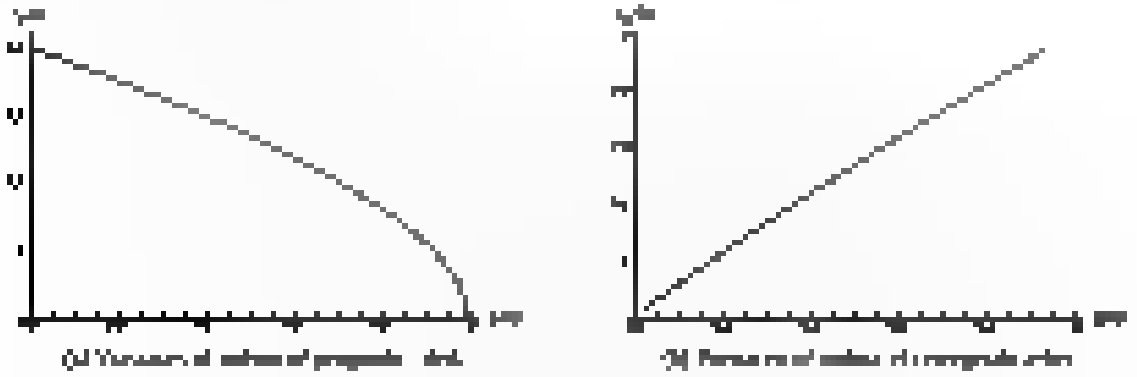

(a) Impact parameter versus scattering angle (b) Impact parameter versus scattering angle

As we can see from the above figure, the motion of photons around a black hole is affected by the presence of the black hole. The photons are deflected by the gravitational field of the black hole, and some of them are captured by the black hole. The photons that are captured by the black hole are lost forever, and they do not contribute to the brightness of the black hole. The photons that are deflected by the black hole can be used to study the properties of the black hole, such as its mass and spin.

The motion of photons around a black hole is described by the Schwarzschild metric, which is a solution to the Einstein field equations of general relativity. The Schwarzschild metric is given by

$$ds^2 = -\left(1 - \frac{2GM}{rc^2}\right)c^2dt^2 + \left(1 - \frac{2GM}{rc^2}\right)^{-1}dr^2 + r^2(d\theta^2 + \sin^2\theta\, d\phi^2)$$

where G is the gravitational constant, M is the mass of the black hole, c is the speed of light, r is the radial coordinate, θ is the polar angle, and ϕ is the azimuthal angle. The Schwarzschild metric is a spherically symmetric solution to the Einstein field equations, which means that it is the same in all directions.

3.3 Black hole shadow

The black hole shadow is the region of the sky that appears dark because the light from the stars behind the black hole is bent around the black hole and does not reach the observer. The size and shape of the black hole shadow depend on the mass and spin of the black hole, as well as the observer's distance from the black hole.

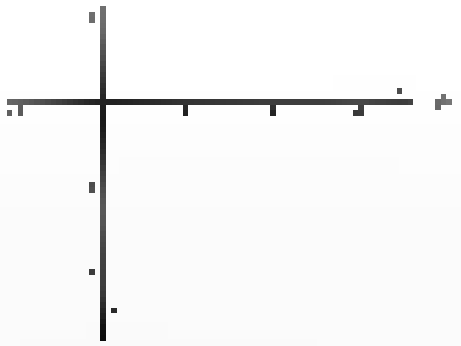

Figure 1 Black hole shadow in the equatorial plane

The radius of the apparent shape of a black hole is the boundary of the shadow. The shape of the shadow that is seen by an observer in the sky is described by the following celestial coordinates:

$$\alpha(p,o) = \lim_{r_o \to \infty} \frac{r^2 p^t}{p^r} = -\xi_{(\phi)}$$

$$\beta(p,o) = \lim_{r_o \to \infty} \frac{r^2 p^\theta}{p^r} = \pm\sqrt{\eta_{\theta\theta}\left(p^\theta + \xi_{(\phi)}\right)^2 + \left(\xi_{(\phi)}\right)^2}$$

Here, α and β are the celestial coordinates of the photon in the sky, r_o is the radial coordinate of the observer, p^t, p^r, p^θ, and p^ϕ are the components of the photon's four-momentum, and $\xi_{(\phi)}$ and $\eta_{\theta\theta}$ are the components of the black hole's metric tensor. The shape and size of the black hole shadow depend on the mass and spin of the black hole, as we will see in the next section.

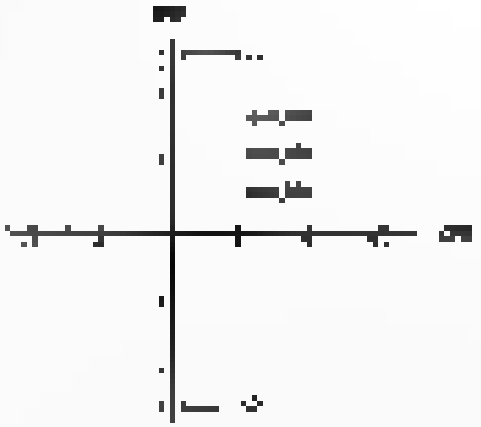

Figure 1: Penrose diagram for the Schwarzschild-anti-de Sitter spacetime.

As we can see from the plot, the Schwarzschild-anti-de Sitter black hole is static.

1.4 Reissner-Nordström black holes

In [3], a four-dimensional charged black hole solution was found by solving the Einstein-Maxwell equations in the presence of a negative cosmological constant. The Einstein-Hilbert action with a cosmological constant is

$$S = \frac{1}{16\pi G}\int d^4x\sqrt{-g}\left(R - 2\Lambda - \frac{1}{4}F_{\mu\nu}F^{\mu\nu}\right) \tag{1.41}$$

where R is the Ricci scalar, and $F_{\mu\nu}$ is the electromagnetic field strength tensor defined as

$$F_{\mu\nu} = \partial_\mu A_\nu - \partial_\nu A_\mu \tag{1.42}$$

where A_μ is the electromagnetic potential given by

$$A_\mu = (A_t, A_r, 0, 0) \tag{1.43}$$

Here A_t is the electric potential, which is the time component of the electromagnetic potential, and A_r is the magnetic potential. The line element is given by

$$ds^2 = -\frac{\Delta(r)}{r^2}dt^2 + \frac{r^2}{\Delta(r)}dr^2 + r^2(d\theta^2 + \sin^2\theta\, d\phi^2) \tag{1.44}$$

where

$$\Delta(r) = r^2 - 2Mr + Q^2 + \frac{r^4}{L^2} \tag{1.45}$$

Here M is the mass of the black hole, Q is the charge of the black hole, and L is the radius of curvature of the anti-de Sitter spacetime. The Ricci scalar is given by

$$R = -\frac{12}{L^2} \tag{1.46}$$

The metric (1.44) represents a charged black hole solution with spherical symmetry. The event horizon of the black hole is located at $\Delta(r) = 0$.

[illegible] Known boundaries and edge problems

The [illegible] and the [illegible] are given by the solution of [illegible]

$$[illegible] \quad (1)$$

and the boundary of the [illegible] is

$$[illegible] \quad (2)$$

The [illegible] and edge problems of the Kernel Block Bootstrap are shown below.

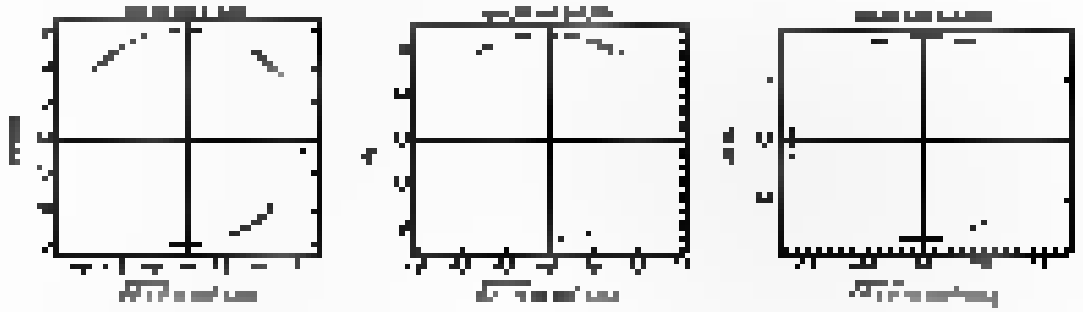

Figure [illegible]

The [illegible] are [illegible] from above. [illegible]
There is also [illegible] of [illegible]

$$[illegible] \quad (3)$$

The [illegible] are [illegible]

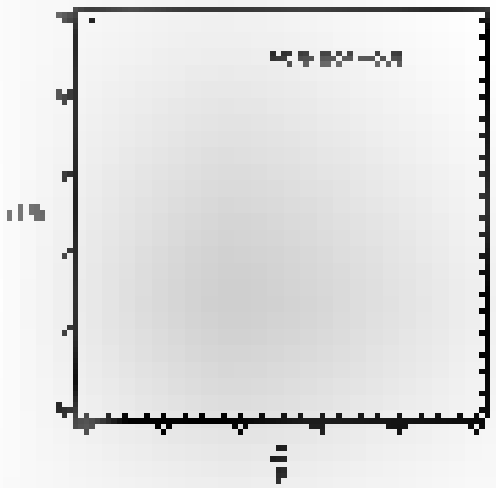

Figure [illegible]

The [illegible] and the [illegible] are [illegible] [illegible] [illegible]

B.1.3 Surface gravity and Hawking temperature

The surface gravity of the Kerr-Newman black hole, corresponding to Eq. (A5), is given by

$$\kappa = \frac{\sqrt{r_+^2 - a^2} \quad}{2Mr_+ \quad \sqrt{r_+^2 - a^2}} \tag{C 1}$$

Then the Hawking temperature, using the relation

$$T_H = \frac{\kappa}{2\pi} \tag{C 2}$$

is given by

$$T_H = \frac{\sqrt{r_+^2 - a^2} \quad}{4\pi M \left[2Mr_+ \quad \sqrt{r_+^2 - a^2} \right]} \tag{C 3}$$

B.1.4 Wave equations

Following the same procedure as before we will need the wave equations for null geodesics in the background of the black hole, which are given by

$$\frac{\partial \Psi}{\partial t} = \pm \sqrt{\Delta} \left(\frac{\partial \Psi}{\partial r} \right) \mp \frac{a}{\Sigma} \left(\frac{\partial \Psi}{\partial \phi} \right)$$

$$= \pm \sqrt{\frac{\Delta}{\Sigma}} \left(\sqrt{\Sigma} \frac{\partial \Psi}{\partial r} \right) \mp \frac{a}{\sqrt{\Sigma}} \left(\frac{1}{\sqrt{\Sigma}} \frac{\partial \Psi}{\partial \phi} \right)$$

$$\Rightarrow \frac{\partial \Psi}{\partial t} = \pm \sqrt{\frac{\Delta}{\Sigma}} \frac{\partial}{\partial r^*} \left(\sqrt{\Sigma} \Psi \right) \mp \frac{a}{\sqrt{\Sigma}} \left(\frac{1}{\sqrt{\Sigma}} \frac{\partial \Psi}{\partial \phi} \right) \tag{B1}$$

where Ψ is a scalar wave function and

$$\Delta(r) = r^2 + a^2 + 2M^2 \quad 2M \left[r^2 + a^2 \right]^{1/2} \quad \Sigma = r^2 + a^2 + 1 \quad a^2 \sin^2 \theta \tag{C 4}$$

B.1.5 Spherical orbit and Black hole shadow

On the equatorial plane, the null spherical orbits are given by the equation $r = 2M$. For non-zero spin, where we have $a \neq 0$ and $a \neq 0$. For such orbits, the solution of Eq. (1.4) gives the constant value of the conserved quantities of these spherical orbits, for the Kerr-Newman black hole, as given by

$$= \frac{\left[2Mr \quad r^2 + a^2 \right] \left[r^2 + a^2 + 1 \right] \left[2Mr \quad a^2 \right]}{a \left[2Mr \quad r^2 + a^2 \right]}$$

$$= \frac{a^2 \left[2Mr \quad r^2 + a^2 \right] \left[r^2 + a^2 \right] \left[2Mr \quad a^2 \right]}{a \left[2Mr \quad r^2 + a^2 \right]^2}.$$

The non-zero spherical radius is given by

$$r_{sph} = \quad \left[\quad \right]$$

$$R_{sph} = \quad \left[\quad \right] \tag{C 5}$$

We plot the behaviour of r_{sph} with a in the following graph.

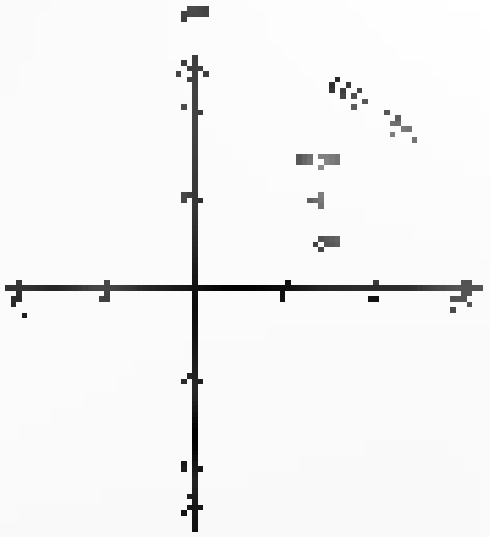

Figure [illegible] The diagram of the relative transverse velocity of the particle. It is used for [illegible]

Assume an inertial frame of reference in which the particle moves with velocity v. The relative velocity of the particle with respect to the black hole is

3.3 The deviation from the circular orbit (β_{11}) and the shape (R_{11}) of the attractor

Hadad and Mureika et al. [20] introduced the parameter β to describe the deviation from the circular orbit of the particle (β_{11} was the same β_{11} of the attractor, except in the black hole attractor, for simplicity, we have dropped the subscript). For the two particles, $r_1(\phi) = r_0(1 + \beta\cos\phi)$ and $r_2(\phi) = r_0(1 - \beta\cos\phi)$, respectively, where r_0 is the radius of the circular orbit, β is the deviation parameter, and ϕ is the angular position of the particle on the circle.

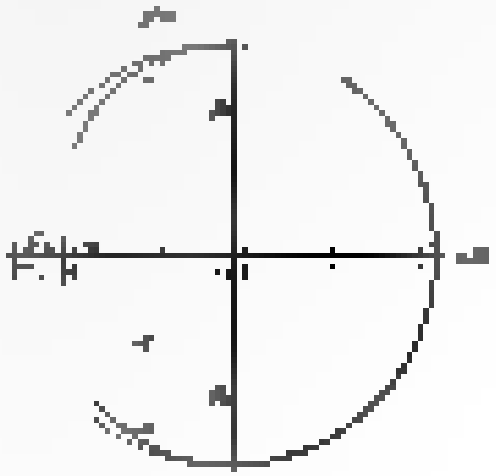

Figure [illegible] A schematic of the black hole and the attractor. The black hole is at the origin, and the attractor is at the point $(r_0, 0)$. The particle is at the point (r, θ). The angle ϕ is the angle between the line connecting the black hole and the attractor and the line connecting the black hole and the particle.

The equation for the relative velocity is

$$v = \frac{\dots}{\dots} \qquad (3.8)$$

Substituting these expressions for r_1 and r_2 into the equation for the relative velocity, we get

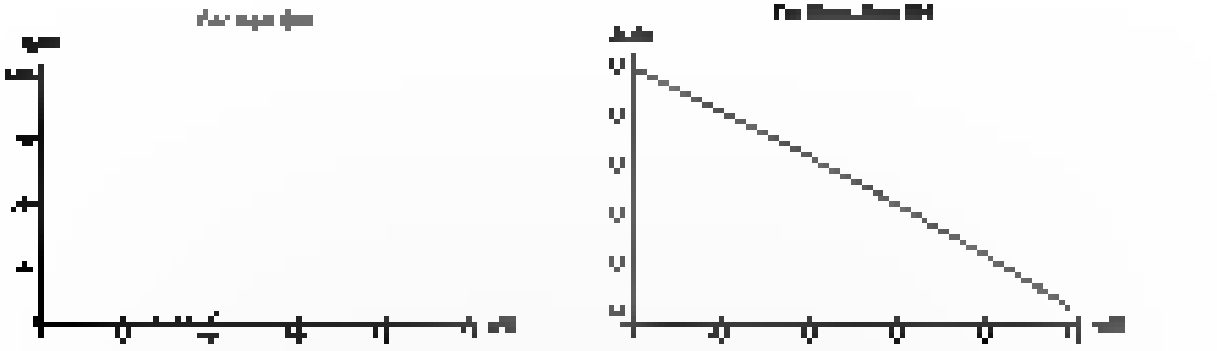

Figure 11: The figure on the left side represents the evolution of the mass of a Schwarzschild black hole with time. The figure on the right side represents the evolution of the radius of the black hole with time. Both are plotted in units of M_0 and r_{s0} respectively.

Integrating Eq. (3.41) and Eq. (3.42), we obtain

$$M(t) = M_0 \left(1 - \frac{t}{t_0}\right)^{1/3} \tag{3.43}$$

Below we show the evolution of the Schwarzschild and Kerr-Sen black holes:

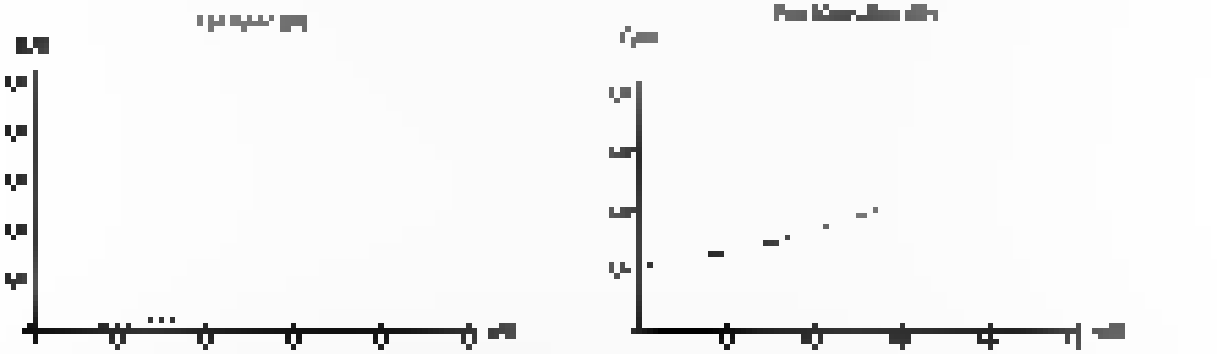

Figure 12: The figure on the left side represents the evolution of the mass of a Kerr-Sen black hole with time. The figure on the right side represents the evolution of the horizon radius of a Kerr-Sen black hole with time. Both are plotted in units of M_0 and r_{s0} respectively.

As we can see from the above plots, the evolution curves for the mass and the horizon radius of the black hole are continuous.

3.3.3 Black Hole Energy Emission

We know that a black hole emits radiation and this mass of the black hole decreases with time. We have also seen that the previous calculations related to the evolution of the mass of the black hole are valid only in the low energy limit. In this limit, the black hole emits radiation in the form of photons. In this section, we will calculate the energy emission rate of the black hole. We also want to include the effects of the high energy limit. In this limit, the black hole emits radiation in the form of photons and gravit

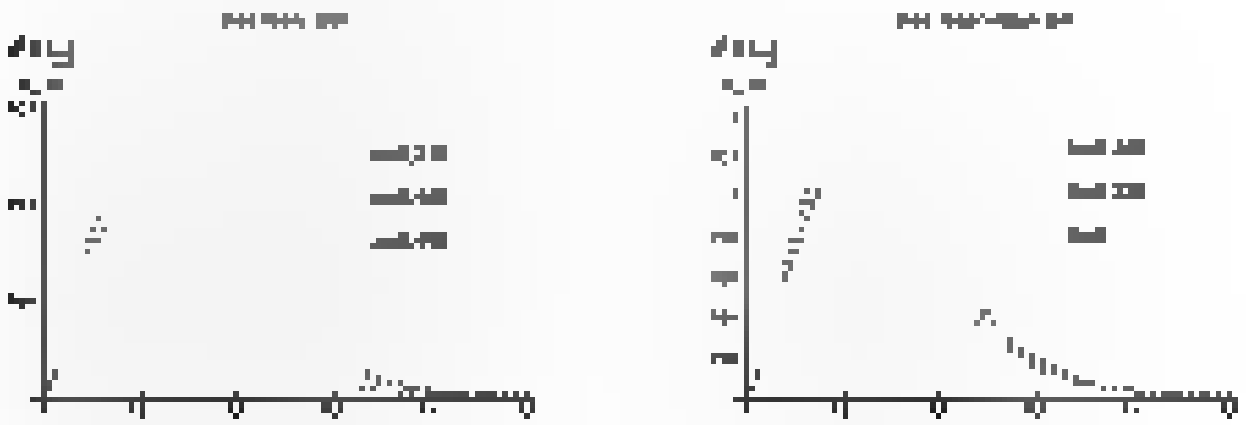

Figure 13: The figure on the left shows how the number of stable circular orbits for Kerr black holes with low and high spin parameters. The figure on the right shows the region of instability for circular orbits around Kerr black holes.

In the following table we list the number of stable circular orbits for Kerr black holes with low and high spin parameters.

Chapter 2

[illegible]

$$[illegible]$$

[illegible]

$$[illegible]$$

[illegible]

$$[illegible]$$

[illegible]

$$[illegible]$$

[illegible]

$$[illegible]$$

[illegible]

$$[illegible]$$

Here [illegible]

$$[illegible]$$

[illegible]

$$[illegible]$$

[illegible]

$$[illegible]$$

[illegible]

$$[illegible]$$

[illegible]

$$[illegible] \quad \text{and} \quad [illegible]$$

In the absence of matter, Einstein's equations reduce to

$$R_{\mu\nu} = 0 \quad \Rightarrow \quad g^{\alpha\beta} R_{\alpha\mu\beta\nu} = 0 \tag{2.1}$$

with

$$R_{\mu\nu} = \partial_\alpha \Gamma^\alpha_{\mu\nu} - \partial_\nu \Gamma^\alpha_{\mu\alpha} + \Gamma^\alpha_{\mu\nu}\Gamma^\beta_{\alpha\beta} - \Gamma^\alpha_{\mu\beta}\Gamma^\beta_{\nu\alpha}$$

$$\Gamma^\alpha_{\mu\nu} = \frac{1}{2} g^{\alpha\beta}\left(\partial_\mu g_{\nu\beta} + \partial_\nu g_{\mu\beta} - \partial_\beta g_{\mu\nu}\right) \tag{2.2}$$

2.1 Schwarzschild-like solutions in static spherically symmetric black hole solutions

In this chapter we discuss some of the salient features of the Schwarzschild-like black hole solutions in static, spherically symmetric circumstances of the modified Einstein equations (2.1). The solutions have been obtained by Mannheim et al. [4] by assuming that the spherical source gathered by the mass M is of the form

$$\rho_m = \rho_0 \left(\frac{r_0}{r}\right)^3 + \rho_0 \left(\frac{r_0}{r}\right)^2 \tag{2.3}$$

where ρ_0 and r_0 are constants of dimensions $[M][L]^{-3}$ and $[L]$ respectively. With these assumptions, the Einstein field equations for the gravitational field $g_{\mu\nu}$ which describes the spacetime around a static, spherically symmetric source of mass M and density ρ_m are found to be [4]

$$\frac{dM}{dr} = 4\pi r^2 \rho_m \left(1 - \frac{2M}{r}\right)^{-1} \quad \Rightarrow \quad M = 4\pi \rho_0 r_0^3 \ln\left(\frac{r}{r_0}\right) + 2\pi \rho_0 r_0^2 r \tag{2.4}$$

where the parameter r_0 is determined by $r_0 = 2M$ which is known as Schwarzschild radius. Although the density has a structural similarity with the Schwarzschild metric, it is known to be very different from the usual one that is used to describe the following Schwarzschild metric

$$ds^2 = \left(1 - \frac{2M}{r}\right) dt^2 - \left(1 - \frac{2M}{r}\right)^{-1} dr^2 - r^2 d\Omega^2 \tag{2.5}$$

3 Hawking temperature

The Hawking temperature is given by

$$T_H = \frac{\hbar c^3}{8\pi G M k_B} \tag{3.1}$$

Where $\hbar$ is the reduced Planck constant, c is the speed of light, G is the gravitational constant, M is the mass of the black hole, and k_B is the Boltzmann constant. Using Dirac's relation in the above equation we obtain the Hawking temperature for the mass M as

$$T_H = \frac{\hbar c^3}{8\pi G M k_B} = \frac{\hbar c}{4\pi r_0 k_B} \tag{3.2}$$

In other words, the above expression shows that the r_0 parameter represents the Hawking temperature of the black hole. In the limit $r \to r_0$, we obtain $T_H = \frac{\hbar c}{4\pi r_0 k_B}$, which is the Hawking temperature for the Schwarzschild black hole.

4.2.3 Blackbody line broadening and absorption/filling processes

In our first consideration of the radiative processes in the broadening process. To this end, we employ the methods that are to establish the gravitational redshift and the redshifting of emitted photons. The interaction of matter is only understandable with the radiation which is manifested by the blackbody spectrum and under the influence of the gravitational field. In order to derive the line broadening we first consider the background as

$$\sigma = \frac{2\pi^5}{15 h^3 c^2} (kT)^4 \qquad (4.28)$$

And the wavelength of radiation is proportional to the peak of the spectrum at a distance, the corresponding gravitational

$$\lambda = \frac{2\pi r^3}{GM} \qquad (4.29)$$

For the relation between the wavelength λ of radiation emitted at r and the wavelength λ_0 received at infinity, we the redshift z defined by

$$z = \frac{\lambda_0 - \lambda}{\lambda} \qquad (4.30)$$

we get

$$z = \frac{GM}{rc^2} \qquad (4.31)$$

where in the range we that for between we will be approximated. These approximations are not applied to the [illegible] in the case of the blackbody spectrum and we will not do so here.

Consider the case of a photon emitted from the surface of a star with a gravitational field. The line and the relationship between the energy and the wavelength are now helpful to us here to compute the wavelength of the photon at the point of the observation. In the gravitational field of the star the photon loses energy. A simple physical explanation is to consider the photon as a particle having mass in such a way that the photon is accelerated by the gravitational field of the star. The energy of the photon is then given by

$$E = h\nu = \frac{hc}{\lambda}$$

where ν is the frequency of the signal in the rest frame of the [illegible]. Now we calculate the energy of the photon in the Schwarzschild-like frame of the gravitational field. This is the [illegible] of the [illegible] of the photon in this coordinate system. The energy of the photon is then given by

$$E' = \frac{hc}{\lambda'} = \frac{hc}{\lambda\left(1 - \frac{2GM}{rc^2}\right)}$$

with λ' [illegible]. This is the wavelength of the photon as it is observed at infinity. The [illegible] of the photon is then [illegible] the [illegible] of the gravitational field. The [illegible] of the photon is then [illegible] by the [illegible] of the gravitational field. The [illegible] of the photon is then [illegible] by the [illegible] of the gravitational field.

$$\lambda' = \lambda\left(1 - \frac{2GM}{rc^2}\right)^{-1}$$

$$\lambda' \approx \lambda\left(1 + \frac{2GM}{rc^2}\right)$$

$$\lambda' = \lambda + \frac{2GM\lambda}{rc^2}$$

where the final expression follows from the normalization of the scalar product. The relative Lorentz factor between two observers moving with four-velocities u_1^μ and u_2^μ is given by $\gamma_{12} = -u_1 \cdot u_2$. Note that γ_{12} is also independent of the choice of coordinates. For the Schwarzschild-anti-de Sitter black hole, the redshift experienced by a photon emitted at r_1 and observed at r_2 is therefore given by

$$1 + z = \frac{\omega_1}{\omega_2} = \frac{\sqrt{-g_{tt}(r_2)}}{\sqrt{-g_{tt}(r_1)}} \tag{2.34}$$

where ω_1 and ω_2 are the frequencies of the photon as measured by observers at r_1 and r_2, respectively. For a photon emitted at r_1 and observed at infinity, we have

$$1 + z = \frac{1}{\sqrt{-g_{tt}(r_1)}} \tag{2.35}$$

Using the explicit form of the Schwarzschild-anti-de Sitter metric, we find

$$z = \frac{1}{\sqrt{1 - \frac{2M}{r} + \frac{r^2}{L^2}}} - 1 \tag{2.36}$$

where L is related to the cosmological constant Λ by $\Lambda = -3/L^2$. Since L is positive, the redshift z is always positive for $r > 0$. The redshift z diverges at the horizon $r = r_+$, where g_{tt} vanishes, and approaches zero as $r \to \infty$.

2.5 Surface Gravity

We have already seen that the surface gravity of a black hole is defined as the acceleration due to gravity at the horizon as measured by an observer at infinity. For a general static spherically symmetric metric of the form

$$ds^2 = -f(r)dt^2 + \frac{dr^2}{f(r)} + r^2 d\Omega^2 \tag{2.37}$$

where $f(r)$ is a function of r only, the surface gravity is given by

$$\kappa = \frac{1}{2}\left|\frac{df}{dr}\right|_{r=r_+} \tag{2.38}$$

where r_+ is the largest root of $f(r) = 0$. For the Schwarzschild-anti-de Sitter black hole, we have

$$f(r) = 1 - \frac{2M}{r} + \frac{r^2}{L^2} \tag{2.39}$$

The surface gravity is then given by

$$\kappa = \frac{1}{2}\left|\frac{df}{dr}\right|_{r=r_+} = \frac{1}{2}\left|\frac{2M}{r^2} + \frac{2r}{L^2}\right|_{r=r_+} \tag{2.40}$$

where r_+ is the largest root of $f(r_+) = 0$. Since r_+ is a root, we have

$$\frac{2M}{r_+} = 1 + \frac{r_+^2}{L^2} \tag{2.41}$$

Substituting this into the expression for κ, we obtain

$$\kappa = \frac{1}{2}\left|\frac{1}{r_+} + \frac{3r_+}{L^2}\right| \tag{2.42}$$

The Hawking temperature T_H is related to the surface gravity by $T_H = \kappa/2\pi$. Thus, we have

$$T_H = \frac{1}{4\pi}\left|\frac{1}{r_+} + \frac{3r_+}{L^2}\right| \tag{2.43}$$

It is clear that the surface gravity for the Schwarzschild-anti-de Sitter black hole depends on the cosmological constant in an explicit manner. While the redshift experienced by a photon emitted at the horizon and observed at infinity is given by $1 + z = 1/\sqrt{-g_{tt}(r_+)}$. This is the expression of surface gravity that we have

$$\kappa = \frac{M}{r_+^2} - \frac{r_+}{L^2} = \frac{1}{2r_+}\left(1 - \frac{3r_+^2}{L^2}\right) \tag{2.44}$$

It shows that the surface gravity for the Schwarzschild-anti-de Sitter black hole depends on the cosmological constant in an explicit manner. While the redshift experienced by a photon emitted at the horizon and observed at infinity is given by $1 + z = 1/\sqrt{-g_{tt}(r_+)}$. This is the expression of surface gravity that we have

3 Quantum radiation from black holes in anti-de Sitter background

In order to study the quantum effects of a scalar field on the background of a black hole in anti-de Sitter spacetime, we need to solve the wave equation for a massless scalar field in the curved background. For a massless scalar field, we have

$$\Box\Phi = \frac{1}{\sqrt{-g}}\partial_\mu\left(\sqrt{-g}\,g^{\mu\nu}\partial_\nu\Phi\right) = 0 \tag{3.1}$$

where g is the determinant of the metric tensor $g_{\mu\nu}$. For the Schwarzschild-anti-de Sitter black hole, we have

$$\sqrt{-g} = r^2 \tag{3.2}$$

Case A: In the case where energy per unit mass of the particle relative to a stationary observer at infinity. We have one more information regarding the motion, namely

$$r^2\frac{d\phi}{d\tau} = \text{constant} \tag{C 10}$$

where ϕ is the angular coordinate in the orbital plane. Let us now introduce an affinity. Using the above two equations we obtain

$$\left(\frac{dr}{d\phi}\right)^2 = \frac{r^4}{L^2}\left[\frac{E^2}{m^2} - \left(1+\frac{L^2}{r^2}\right)\left(1-\frac{2M}{r}\right)\right] \tag{C 11}$$

For circular orbits, the following two conditions

$$\frac{dr}{d\phi} = 0 \quad \text{and} \quad \frac{d^2r}{d\phi^2} = 0 \tag{C 12}$$

must be satisfied. The first condition gives us the same result as that obtained in Eq. (C) and the second condition, after some simplifications, turns out to be

$$r^2 - \frac{L^2}{m^2}r + 3M\frac{L^2}{m^2} = 0 \tag{C 13}$$

The quadratic equation (C 13) yields the following solution for

$$\frac{L}{m} = \pm\sqrt{\frac{r^2}{3M}\left(r \mp \sqrt{r^2 - 12M^2}\right)} \tag{C 14}$$

Case B: The expression for $\frac{L}{m}$ is the same as that given in Eq. (C 14). We get the following expression for $\frac{E}{m}$ using equations (C 11) and (C 12)

$$\frac{E}{m} = \left(1-\frac{2M}{r}\right)\sqrt{\frac{r}{r-3M}} \tag{C 15}$$

Now, the first order stability of the equation (C 15) for $r > 3M$ implies that the energy of a particle in circular orbit must decrease with decreasing radius of the orbit. The above information leads us to compute the time period of revolution of the orbiting particle as follows

$$\frac{dt}{d\phi} = \frac{r^2}{L} = \frac{r^2}{\pm\sqrt{\frac{r^2}{3M}\left(r \mp \sqrt{r^2-12M^2}\right)}} \tag{C 16}$$

Thus, the proper period of the particle in the circular orbit is found out to be

$$T = \int_0^{2\pi} \frac{r^2}{\sqrt{\frac{r^2}{3M}\left(r \mp \sqrt{r^2-12M^2}\right)}}\,d\phi \tag{C 17}$$

My thesis work is the proper generalization of the above result in the backdrop of background spacetime which is the anti-de Sitter-Schwarzschild background and it does not depend on Λ. If we look at the expression of a general non-circular orbit, we find that the time period of the particle in the background spacetime is explicitly dependent on the Λ term. Also, the Λ term has a significant role in the expression for the circular orbit. We would like to mention that the results we have derived are the generalization of the results in [48]. A careful look into the expression for the energy in Eq. (C 15) reveals that it coincides with the equation (17) of the article [48] when the only massless particle is considered. Such a result for the circular orbit for the particle obtained here is in agreement with the article [48]. In the future work, we intend to study the motion of particles in the background spacetime of the black hole solution in the presence of a cosmological constant Λ under the perturbation of the Hamiltonian. The problem in the Schwarzschild background was studied in [49]. The modification of perturbation will be worthwhile for getting an idea of the motion of the particle in the background spacetime. Besides, both the circular orbit and the effective potential are supposed to appear as the essential tools for the study of the gravitational lensing in the background spacetime. Before going to study the motion of particles in the background spacetime, we may also intend to give a brief discussion of Poynting-Robertson effect.

4.3 An illustration of Snyder algebra

Here we discuss the general Snyder algebra. The covariant generalization of the canonical Poisson bracket algebra is given by

$$\{x_\mu, x_\nu\} = \theta_{\mu\nu} + \theta_{\mu\rho}\, p^\rho + \theta_{\nu\rho}\, p^\rho + \theta_{\mu\rho}\, p^\rho p^\sigma \qquad \{x_\mu, p_\nu\} = \eta_{\mu\nu} \qquad \{p_\mu, p_\nu\} = 0 \tag{3.11}$$

where $\theta_{\mu\nu} = \theta\, \epsilon_{\mu\nu\rho\sigma} L^{\rho\sigma}$ is the Lorentz covariant angular momentum. If we set $\theta_{\mu\nu} = 0$ then the above Poisson algebra reduces to the ordinary Snyder noncommutative model with which we are concerned in our present article. So presently the algebra reads

$$\{x_\mu, p_\nu\} = \eta_{\mu\nu} \qquad \{x_\mu, x_\nu\} = \theta_{\mu\nu} \qquad \{p_\mu, p_\nu\} = 0 \tag{3.12}$$

In order to study the corresponding quantum algebra, we first express the above algebra in terms of the polar coordinates in momentum space and subsequently quantize the algebra in the usual framework of Snyder. We now obtain the algebra in the polar coordinates. The radial momentum p and the polar coordinates are connected to usual Cartesian coordinates as follows

$$p = |\vec{p}| = \sqrt{p_1^2 + p_2^2 + p_3^2} \qquad \theta = \tan^{-1}\frac{p_2}{p_1} \tag{3.13}$$

Therefore the momenta corresponding to the polar coordinates can be written as

$$p_1 = p\cos\theta\sqrt{1 - \frac{p_3^2}{p^2}} \qquad p_2 = p\sin\theta\sqrt{1 - \frac{p_3^2}{p^2}} \qquad p_3 = p\cos\phi \tag{3.14}$$

where ϕ is simply the momentum in the z direction. Using the Snyder algebra (3.12) it is straightforward to see that the phase space in the polar coordinates or the Snyder space has the symplectic structure and acquires the following modified form

$$\{r, p\} = 1 + \theta p^2 \qquad \{r, \phi\} = \frac{\phi}{p} \qquad \{r, \theta\} = \frac{\theta}{p}$$

$$\{p, \phi\} = \frac{\phi}{r} + \theta p \qquad \{p, \theta\} = \frac{\theta}{r} + \theta p \qquad \{\phi, \theta\} = \frac{\phi\theta}{p^2}$$

$$\{r, r\} = \theta \qquad \{r, p\} = 1 + \theta p^2 \qquad \{r, \phi\} = \{r, \theta\} = 0$$

$$\{p, p\} = 0 \qquad \{p, \phi\} = -\frac{p\phi}{r} \qquad \{p, \theta\} = -\frac{p\theta}{r}$$

$$\{\phi, \phi\} = 0 \qquad \{\phi, \theta\} = \frac{\phi\theta}{p^2} \qquad \{\theta, \theta\} = 0 \tag{3.15}$$

The above algebra will be useful to study the motion of particle in a central potential background

2.1 Motion of Particle in Bumblebee background in the Snyder orbit

[illegible]

$$[illegible]$$

[illegible]

$$[illegible]$$

[illegible]

[illegible]

[illegible]

[illegible]

[illegible]	[illegible]	[illegible]	[illegible]	[illegible]	[illegible]
[illegible]	[illegible]	[illegible]	[illegible]		
[illegible]	[illegible]	[illegible]	[illegible]		
[illegible]	[illegible]	[illegible]	[illegible]		[illegible]
[illegible]	[illegible]	[illegible]	[illegible]		
[illegible]	[illegible]	[illegible]	[illegible]	[illegible]	
[illegible]	[illegible]	[illegible]	[illegible]		[illegible]

[illegible]

2 [illegible]

[illegible]

Chapter 3

Non-commutative Kerr-like black hole

In this chapter we discuss non-commutative Kerr-like black hole which we have studied in [32]. Kerr-like black hole is the rotating counterpart of non-rotating solution [33] investigated in the context of non-commutative geometry inspired by Moyal product [34]. According to the prescription of Smailagic and Spallucci [34], the non-commutative Kerr-Schild metric in Boyer-Lindquist coordinates can be written down as [35, 36]

$$g_{\mu\nu} = \eta_{\mu\nu} + \frac{2Mr}{\rho^2}\left(\frac{\Gamma(3/2, r^2/4\theta)}{\Gamma(3/2)}\right)^2 l_\mu l_\nu \tag{3.1}$$

where $\eta_{\mu\nu}$ is the metric of flat spacetime and θ is the non-commutative parameter. The mass M and spin a of the black hole are related to the ADM mass M_{ADM} and the total angular momentum J of the spacetime as $M_{ADM} = M$ and $J = Ma$. The null vector l_μ is given by

$$l_\mu = \left(1, \frac{rx + ay}{r^2 + a^2}, \frac{ry - ax}{r^2 + a^2}, \frac{z}{r}\right) \tag{3.2}$$

In the limit $r \gg \sqrt{\theta}$, Eq. (3.1) reduces to

$$ds^2 = -\left(1 - \frac{2Mr}{\rho^2}\right)dt^2 + \frac{\rho^2}{\Delta + a^2}dr^2 + \rho^2 d\theta^2 + \left(r^2 + a^2 + \frac{2Mra^2}{\rho^2}\sin^2\theta\right)d\phi^2 - \frac{4Mra}{\rho^2}\sin^2\theta\, d\phi\, dt \tag{3.3}$$

The non-commutative black hole metric (3.3) is obtained by the gravitational field equations sourced by a non-linear electrodynamics field

$$\mathcal{L} = \frac{\mathcal{P}}{4\pi\theta}\exp\left(-\frac{\mathcal{P}}{4\theta}\right) \tag{3.4}$$

The spacetime metric (3.3) of the non-commutative black hole reduces to the Kerr metric in the limit $\theta \to 0$. The event horizon of the non-commutative black hole is determined by the equation

$$g^{rr} = 0, \tag{3.5}$$

which has a unique, largest real root r_h in the form

$$r_h = 2M\left[1 + \cos\left(\frac{1}{3}\cos^{-1}\left(-\frac{a}{M}\right)\right)\right] \tag{3.6}$$

in a very elaborate manner. With the help of this metric, we have studied the thermodynamics and stability of non-commutative black hole [32]. In Ref. [32], we have calculated the Hawking temperature, entropy, specific heat capacity, and free energy of non-commutative black hole. The Hawking temperature is given by

$$T_H = \frac{\kappa}{2\pi} = \frac{\sqrt{M^4 - a^2\left(\frac{2\theta}{\pi}\right)^{3/2}\Gamma\left(\frac{3}{2}, \frac{M^2}{2\theta}\right)^2}}{2\pi\left(2M^2 - a^2\left(\frac{2\theta}{\pi}\right)^{3/2}\Gamma\left(\frac{3}{2}, \frac{M^2}{2\theta}\right)^2\right)}, \tag{3.7}$$

where

$$\kappa = \frac{\sqrt{-g}}{g^{rr}}\frac{\partial g^{rr}}{\partial r}\Big|_{r=r_h}, \quad \sqrt{-g} = \rho^2\sin\theta, \quad g^{rr} = \frac{\Delta + a^2}{\rho^2}, \quad \Delta = r^2 - 2Mr + a^2, \quad \rho^2 = r^2 + a^2\cos^2\theta.$$

The main point is that the entanglement is not significant when the [illegible] are [illegible] and tends to be large when [illegible] the parameter [illegible] plays [illegible] Although there has been proposed [illegible] in the [illegible] [illegible] have the ability to [illegible] and [illegible] the [illegible] [illegible] [illegible] The parameter [illegible] [illegible] [illegible]

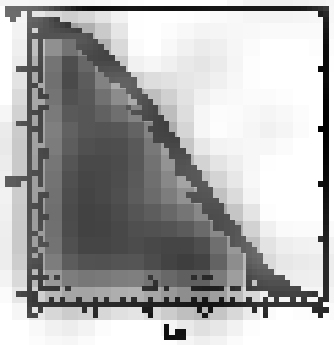

Figure 2: [illegible] [illegible]

[illegible] [illegible] [illegible] [

5.6 Photon orbit and black hole shadow

Here, we are going to discuss the black hole shadow related to the standard theory. Such a black hole shadow is caused by massless [131]. There are several studies related to the black hole shadow. Here, we will get the equation of motion [132]. In order to study the shadow, we introduce two conserved quantities and which are defined by

$$\frac{}{} \quad \text{and} \quad = \frac{}{} \tag{5.41}$$

where is and is the energy the total component of the angular momentum and the Carter constant respectively. In the background geometry, by the symmetry, we have a conserved quantity in terms of the four-momentum

$$= \frac{}{} \qquad = \frac{}{}$$

$$= \frac{}{} = \qquad \text{and} \qquad \frac{}{} \tag{5.42}$$

where is the affine parameter and

$$= \int \frac{}{\sqrt{}} \qquad = \qquad \text{and} \qquad = \int \frac{}{\sqrt{}} \tag{5.43}$$

The radial equation of motion can be written down in the following form

$$\frac{}{} + V_{\text{eff}} = \tag{5.44}$$

The effective potential is given as

$$V_{\text{eff}} = \frac{}{} \qquad \text{and} \qquad = \tag{5.45}$$

Considering the case of , we describe the unstable spherical orbit as the equatorial circular orbit of . We plot the potential as a function of with various values of . In the equatorial spherical symmetric orbit

Figure 5.5: The left and the right panels show the effective potential for the photon orbit and the corresponding orbits respectively in various values of with and .

Figure 5.6: The left and the right panels show the effective potential for the photon orbit and the corresponding orbits respectively for various values of with and .

Figure . The left panel illustrated the effective potential for prograde orbits and right panel illustrated the prograde orbits for various values of with

The plots depicted above show that the turning points for prograde orbits shift towards left as a [illegible] Also plot of with of prograde and retrograde orbits for different values of spin parameter are given below

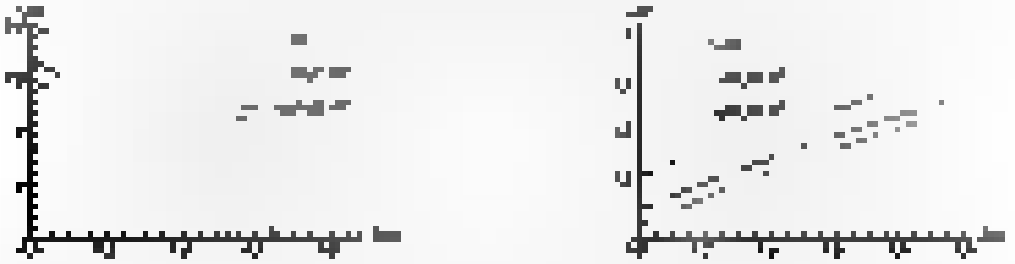

Figure . The left panel shows the variation of critical impact parameter with and right panel shows the numerical and analytical fit for prograde orbits for various values of and

It can be concluded from plots above that critical radius for prograde as well as retrograde orbits, decreases with an increase in the spin parameter of the black hole. For a static galactic black hole, we have [illegible] and for the maximally rotating galactic black hole, [illegible] Therefore, the angular size of the shadow as seen by a distant observer can be obtained as [illegible] is given by

$$\theta \approx \frac{[\text{illegible}]}{[\text{illegible}]} \approx \frac{[\text{illegible}]}{[\text{illegible}]} \tag{3.39}$$

In the above calculation we have assumed that the source and observer are located at [illegible] Here we have considered a [illegible] which is [illegible] from the black hole. If we consider a [illegible] then the shape of the shadow will be distorted. The distortion parameter is given by

$$\delta = \lim_{r_0 \to \infty} \frac{r_0}{\sqrt{r_0^2 - r_c^2}} = [\text{illegible}] \tag{3.40}$$

$$\delta = \lim_{r_0 \to \infty} \frac{r_0 \sin\theta_0}{\sqrt{r_0^2 - r_c^2}} = [\text{illegible}] \tag{3.41}$$

where [illegible] are the celestial coordinates of the photon as seen by an observer [illegible] [illegible] [illegible].

We have shown in the plot below the variation of [illegible] with respect to [illegible] for different values of [illegible]

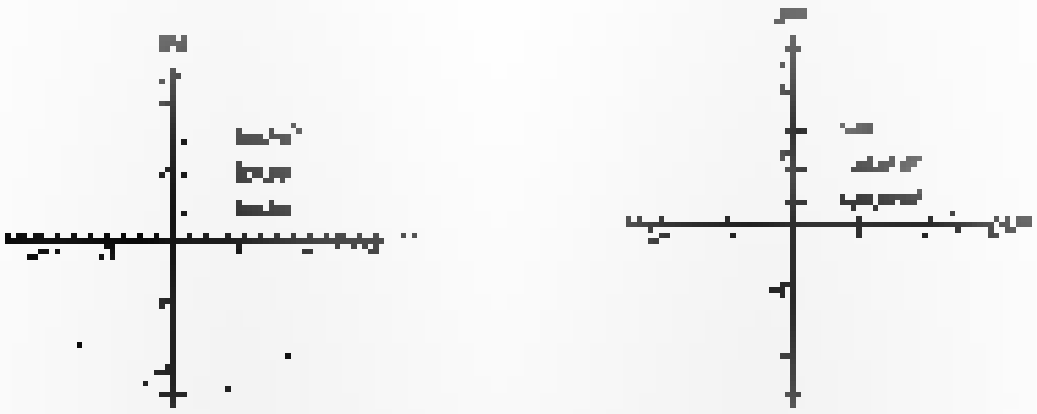

Figure 5: The left panel gives the edge of the shadow for various values of ϵ_C with $\theta_0 = 17/20\pi$ and $\theta_0 = \pi/2$. The right panel gives the edge of the shadow for various θ_0 with $\epsilon_C = 0.2$ and $\epsilon_C = 0$.

From the above plots, we observe that the size of the shadow increases with an increase in ϵ_C whereas it decreases with increase in θ_0.

5.5 Deviation from the circularity ϵ_C and the size R_S of the black hole shadow

Using the parameters which are introduced for Hioki and Maeda [23], we measure the deviation from the circularity ϵ_C and the size R_S of the shadow cast by the black hole.

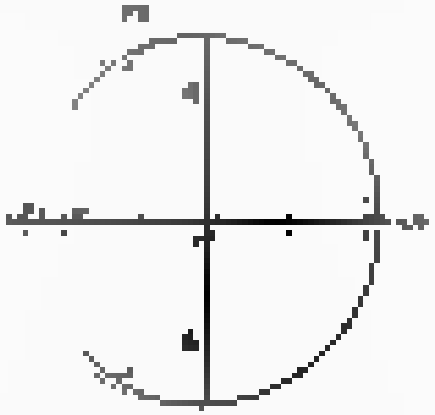

Figure 6: The black hole shadow and the reference circle used to define the deviation from circularity ϵ_C and the radius R_S.

For the following given parameters, we consider three points (x_1, y_1), (x_2, y_2) and (x_3, y_3) which are on the edge of the shadow. In terms of the shadow and the size of the reference circle, respectively, we have

$$R_S = \frac{\sqrt{(x_1 - x_2)^2 + (y_1 - y_2)^2}}{2\sin\left(\frac{1}{2}\arccos\left(\frac{(x_1 - x_2)(x_1 - x_3) + (y_1 - y_2)(y_1 - y_3)}{\sqrt{(x_1 - x_2)^2 + (y_1 - y_2)^2}\sqrt{(x_1 - x_3)^2 + (y_1 - y_3)^2}}\right)\right)}$$

and

$$\epsilon_C = \frac{|R_S - r_d|}{R_S}$$

In the following, the parameters θ_0 and ϵ_C are numerically determined for the black hole. The θ_0 and ϵ_C are the observables which are used to find the parameters of the black hole.

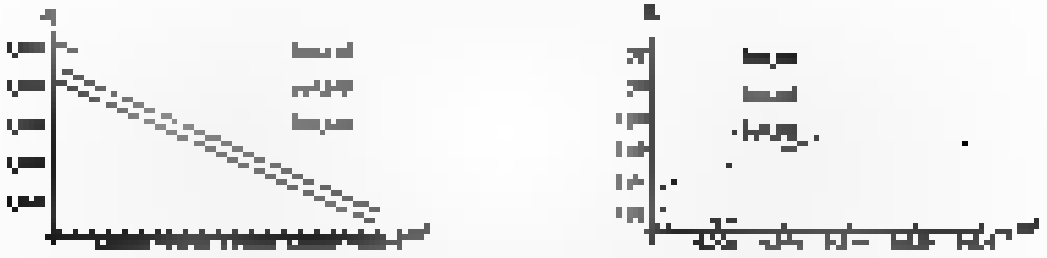

Figure 11: The left-hand figure shows the entropy of the [illegible] as a function of [illegible]. The right-hand figure shows the [illegible] with [illegible].

From the above plots we observe that the [illegible] with the increase of [illegible]. For fixed values of [illegible] and [illegible] the [illegible] with [illegible] and [illegible] with [illegible]. For fixed values of [illegible] and [illegible] with [illegible].

5.4 Computation of entropy generation rate

In this part we calculate the possible variability of the entropy generation in Kerr-Newman-de Sitter-anti-de Sitter (KN-dS) black hole [13]. In the vicinity of the black hole event horizon, the Kerr-de Sitter black hole does not exhibit any stationary region. We therefore find the entropy generation rate for the KN-dS black hole. The entropy generation rate is given by

$$r_{+} = r_{+} \tag{3.23}$$

Using the above equation, the entropy generation rate is obtained [16] as

$$\frac{dS}{dt} = \frac{1+R_2}{|\dot{r}|} \tag{3.24}$$

where $\dot{r}$ = [illegible] is the [illegible] entropy generation rate. In the figure

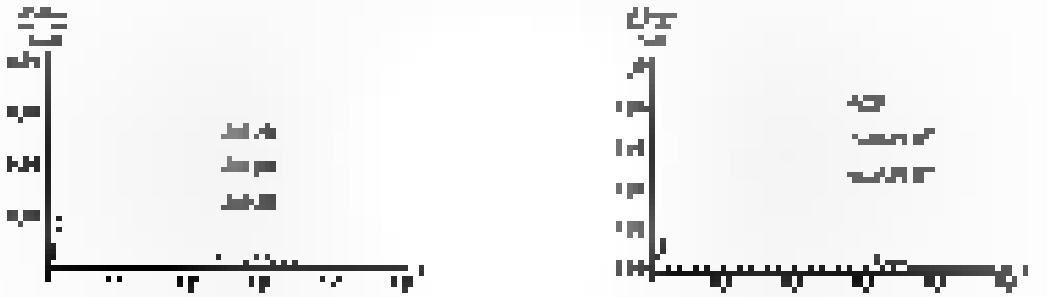

Figure 12: The graphical [illegible] of the [illegible] as a function of [illegible] for the fixed values of [illegible] and [illegible]. The right-hand panel represents the [illegible] with [illegible] and [illegible].

Figure 13: The [illegible] as a function of [illegible] for the fixed values of [illegible].

6. COMPUTATION OF ENTRY MASSING RATIO

Chapter 4

Kerr-Sen-like black hole

In this chapter we consider the process for Kerr-Sen-like black hole and study the energy extraction of it. The Kerr-Sen-like spacetime is derived by [74] where we have shown that the Kerr-Sen-like solution is also a solution of the low-energy heterotic string theory. In addition, we study the energy extraction of the Kerr-Sen-like black hole using the Penrose process [75, 76]. According to the development of Kerr, the geometrical form of the rotating stationary axisymmetric black hole spacetime can be written down in Boyer-Lindquist coordinates and given in the following manner

$$ds^2 = \ldots \qquad (4.1)$$

In between Eq. (4.1) and Eq. (4.2) We can see the metric coefficient [4.2] is complete the given spherical-like equations. If we consider that the black hole is spherical, [4.2] can be written down as

$$= \ldots \qquad (4.2)$$

In the case where the metric components like g_{tt} and g_{rr} of the rotating black hole are written down as a function of r and θ only, the components $g_{t\phi}$ and $g_{r\theta}$ vanish. Now we have

$$\begin{aligned} & g_{tt} = g_{tt} \\ & + \ldots \\ & \ldots \\ & = \ldots \end{aligned} \qquad (4.3)$$

where g_{tt} and g_{rr} are functions of r and θ. Also, the spherical metric $g_{\theta\theta}$ is written as

$$g_{\theta\theta} = \ldots \qquad (4.4)$$

in a straightforward manner. Therefore, the corresponding components of the Kerr-Sen-like black hole are

$$\begin{aligned} & \ldots \\ & = \ldots \\ & \ldots \\ & \ldots \end{aligned} \qquad (4.5)$$

where the primed symbol is used to denote the corresponding components in spherical-like coordinates. We now consider the following transformation equations

$$\ldots$$

$$\frac{\partial \ln L}{\partial \theta_j} \tag{4.4}$$

and the quantity $I(\theta)_{jk}$ is the corresponding covariance

$$I(\theta)_{jk} = E\left[\frac{\partial \ln L}{\partial \theta_j}\frac{\partial \ln L}{\partial \theta_k}\right] = -E\left[\frac{\partial^2 \ln L}{\partial \theta_j \partial \theta_k}\right] \tag{4.5}$$

Applying equation (4.4) we obtain the system of equations $R_{11}\,\alpha_1 + R_{12}\,\alpha_2 = R_{1y}$, $R_{21}\,\alpha_1 + R_{22}\,\alpha_2 = R_{2y}$ for unique estimates of the β_j. The generalized least squares estimates, which are needed for our purposes, are

$$\begin{aligned} R_{1y} &= R_{11}\beta_1^{(0)} + R_{12}\beta_2^{(0)} + \beta_1^{(0)} R_{1y} \\ R_{2y} &= R_{21}\beta_1^{(0)} + R_{22}\beta_2^{(0)} + \beta_2^{(0)} R_{2y} \\ \beta_1^{(1)} &= \beta_1^{(0)} + \alpha_1 \\ \beta_2^{(1)} &= \beta_2^{(0)} + \alpha_2 \end{aligned} \tag{4.6}$$

where β_0 the variance R_{1y} & β_{00} are given by

$$\begin{aligned} R_{1y} &= \frac{\beta_{00}}{\beta_0^2} + \frac{\beta_1 \left| \beta_0 \quad \beta_{01} \right| + 2\beta_0 \beta_{1y}}{\beta_0 \quad \beta_0^2} \\ \beta_0 &= \frac{\beta_1}{2\beta_0 \quad \beta_1} \quad \beta_{00} \quad \beta_0^2 \beta_1 \quad \left| \beta_0 \beta_1^{(1)} \right| \\ \beta_{00} &= \frac{\beta_0 \beta_1}{2\beta_0 \quad \beta_1} \quad \frac{\beta_0^2 \quad \beta_1}{\beta_0 \beta_1} \quad \frac{\beta_0}{\beta_0 \beta_1^{(1)}} \end{aligned} \tag{4.7}$$

where β_1 β_0 · The distinction would respond to variables · and it was denoted by multiplication and a response β_0 in the Eq. (4.7). Note the R_{1y} is implied from β_{1y} variables. Then the plan to test β_1 is a matrix of two variables

$$\begin{aligned} \text{var} \quad \beta_1 \quad \beta_{00} \quad \beta_{01} \quad \beta_0 \\ \beta_0 \quad \beta_1 = \frac{\beta_1 \beta_{00}}{\beta_0 \quad \beta_1} \end{aligned} \tag{4.8}$$

A key purpose is to obtain the expression of β_0

$$\frac{\beta_0 \beta_1}{\beta_0 \beta_1 \quad \beta_0 \beta_1} \tag{4.9}$$

We have an β_0 variance and parameter variables · applying the condition β_0 · and finally which is

$$\beta_0 \beta_1 \tag{4.10}$$

where β_0 · β_0 Since we use the estimates with respect to β_0 we have

$$\begin{aligned} \beta_0 &= \frac{\beta_0}{\beta_0} \quad \frac{\beta_0}{\beta_0} \quad \beta_0 \frac{\beta_0}{\beta_0} \\ \beta_1 \quad \beta_0 &= \frac{\beta_0}{\beta_0} \quad \frac{\beta_0}{\beta_0} \quad \beta_0 \frac{\beta_0}{\beta_0} \end{aligned} \tag{4.11}$$

$$= \sqrt{3}\frac{\partial}{\partial x}\frac{\partial}{\partial z} + \frac{\partial}{\partial y}\frac{\partial}{\partial z}\sqrt{3}$$

$$\frac{\partial}{\partial t} = \frac{\partial}{\partial x} \quad \frac{\partial}{\partial y}\frac{\partial}{\partial z}$$

A combination of Eqs. (3.18) and (3.19) reveals that the following equation holds

$$= \quad \tag{3.20}$$

After inserting the expressions for $\ldots$ and $\ldots$ in Eq. (3.20), we find

$$= \frac{\partial}{\partial x}\frac{\partial}{\partial z} + \frac{\partial}{\partial y}\frac{\partial}{\partial z} + \frac{\partial}{\partial z}\frac{\partial}{\partial z} + \frac{\partial}{\partial z}\frac{\partial}{\partial z}$$

$$= \frac{\partial}{\partial x}\frac{\partial}{\partial z} + \frac{\partial}{\partial y}\frac{\partial}{\partial z} + \frac{\partial}{\partial z}\frac{\partial}{\partial z} + \frac{\partial}{\partial z}\frac{\partial}{\partial z}$$

$$= \frac{\partial}{\partial x}\frac{\partial}{\partial z} + \frac{\partial}{\partial y}\frac{\partial}{\partial z} + \frac{\partial}{\partial z}\frac{\partial}{\partial z} + \frac{\partial}{\partial z}\frac{\partial}{\partial z} \tag{3.21}$$

Within the derivation above, we have made use of the fact that $\ldots$ and $\ldots$ are independent of $\ldots$ and $\ldots$, respectively. We thus have

$$\frac{\partial}{\partial} \quad \quad \text{and} \quad \tag{3.22}$$

Inserting Eq. (3.22) into Eq. (3.21) and rearranging terms, we find

$$= \frac{\partial}{\partial x}\frac{\partial}{\partial z} + \frac{\partial}{\partial y}\frac{\partial}{\partial z} + \frac{\partial}{\partial z}\frac{\partial}{\partial z} + \frac{\partial}{\partial z}\frac{\partial}{\partial z} \tag{3.23}$$

This can be written as

$$= \quad \tag{3.24}$$

which gives the following

$$= \quad \tag{3.25}$$

By inserting the expressions $= \ldots$ and $= \ldots$ into Eq. (3.25), we obtain

$$= \tag{3.26}$$

From comparing Eq. (3.26) with Eq. (3.23), we find that

$$= \frac{\partial}{\partial x}\frac{\partial}{\partial z} + \frac{\partial}{\partial y}\frac{\partial}{\partial z} + \frac{\partial}{\partial z}\frac{\partial}{\partial z} + \frac{\partial}{\partial z}\frac{\partial}{\partial z} \tag{3.27}$$

Eq. (3.27) is a differential equation for $\ldots$ which can be solved by separation of variables. Integrating both sides of Eq. (3.27) and taking the exponential function of the result, we obtain for the solution of the Hamilton–Jacobi equation the following:

$$= \quad \frac{\partial}{\partial x}\frac{\partial}{\partial z} + \frac{\partial}{\partial y}\frac{\partial}{\partial z} + \frac{\partial}{\partial z}\frac{\partial}{\partial z} + \frac{\partial}{\partial z}\frac{\partial}{\partial z} \tag{3.28}$$

where $\ldots$ is an integration constant. Finally, we insert the expressions for the Hamiltonian and the momentum $\ldots$ and $\ldots$ from Eq. (3.17) and Eq. (3.22), respectively, into Eq. (3.28) and obtain for the Hamilton–Jacobi equation in the Hamiltonian gauge the result

$$= \quad \frac{\partial}{\partial x}\frac{\partial}{\partial z} + \frac{\partial}{\partial y}\frac{\partial}{\partial z} + \frac{\partial}{\partial z}\frac{\partial}{\partial z} + \frac{\partial}{\partial z}\frac{\partial}{\partial z} \tag{3.29}$$

where

$$\Delta = \frac{R - 2M}{r^2 + a^2} \qquad \text{and} \qquad \Sigma = r^2 + a^2 \cos^2\theta \tag{3.1}$$

If $a = 0$ the metric reduces to the usual Reissner-Nordström metric and for $a = 0$ and $Q = 0$ it becomes

$$ds^2 = -\left(1 - \frac{2M}{r}\right) dt^2 + \left(1 - \frac{2M}{r}\right)^{-1} dr^2 + r^2 d\Omega^2. \tag{3.2}$$

where $d\Omega^2$ is the metric on the unit 2-sphere [10]. The quantity $R(r,\theta)$ represents the gravitational redshift of a photon emitted from the equatorial plane at radius r and received by an observer at infinity. For a photon emitted in the direction perpendicular to the radius vector in the equatorial plane, $R(r,\theta)$ is given by

$$R(r,\theta) = \sqrt{\frac{r^2 + a^2 + 2Ma^2/r}{r^2 - 2Mr + a^2}} \tag{3.3}$$

where r is the radius of the point in the equatorial plane at which the photon is emitted and M is the mass of the black hole. For a photon emitted in the direction perpendicular to the radius vector in the equatorial plane, $R(r,\theta)$ is given by

$$R(r,\theta) = \sqrt{\frac{r^2 + a^2 + 2Ma^2/r}{r^2 - 2Mr + a^2}} \tag{3.4}$$

The parameter a is the angular momentum per unit mass of the black hole.

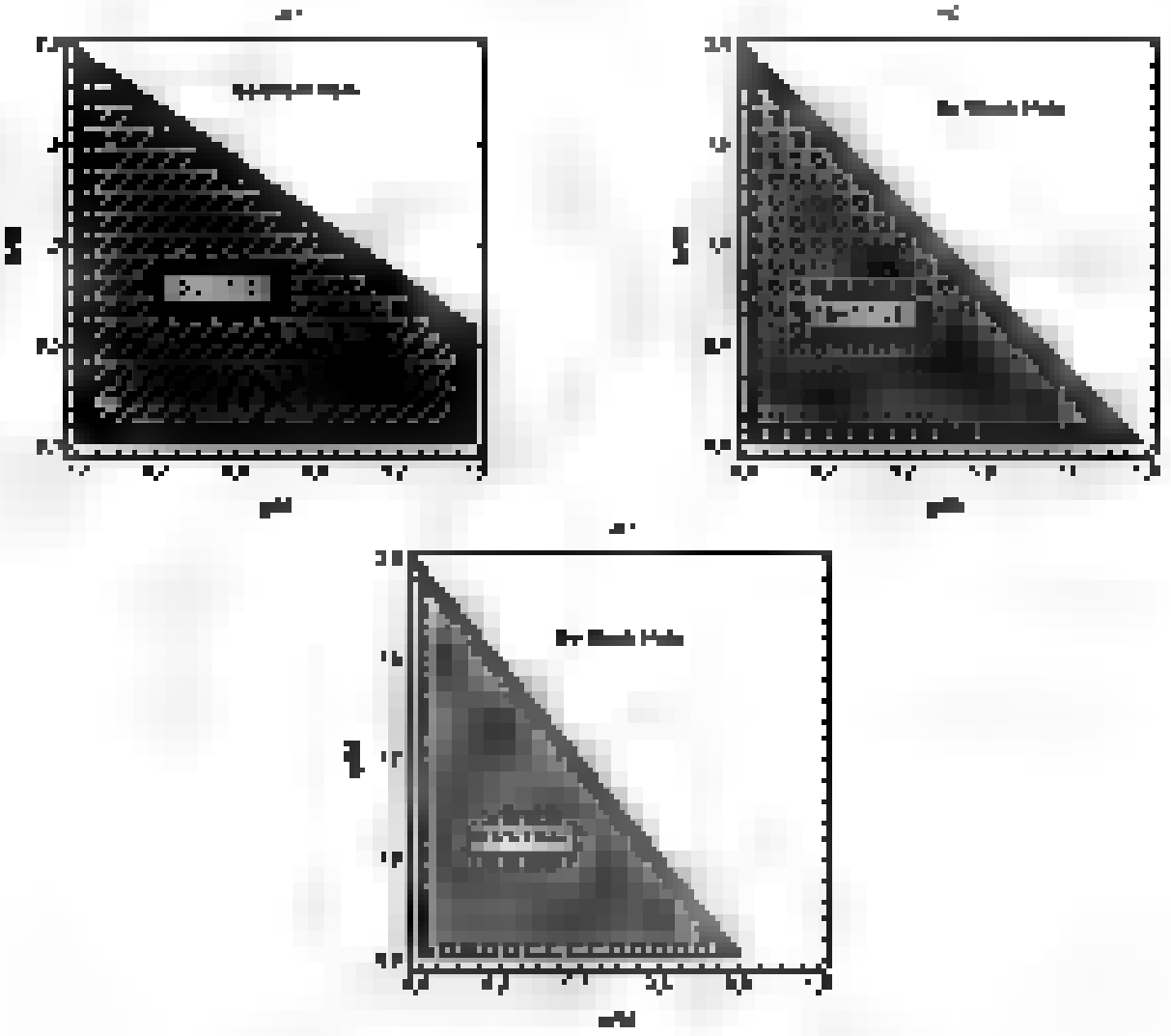

Figure 3. The shadow of a black hole for different values of a.

From the above we see that the parameter values for which we have black hole ... [illegible] ... are tabulated below.

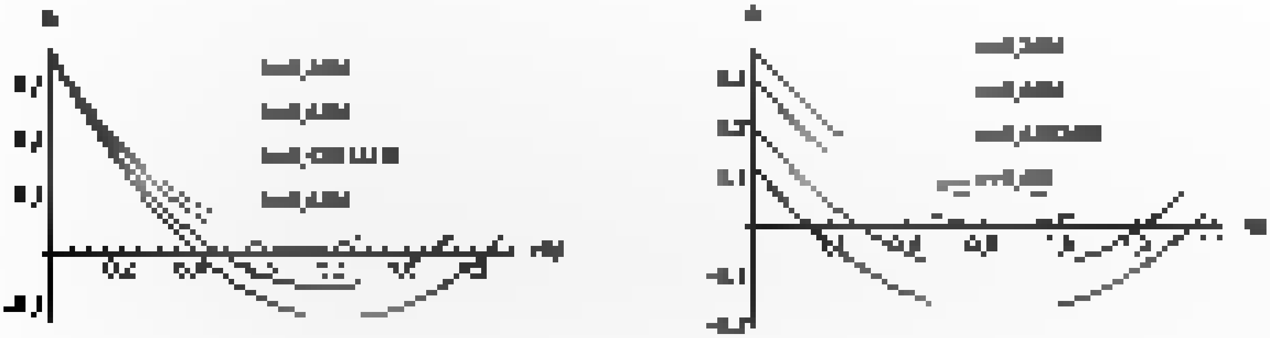

Figure 3: The left ... [illegible] ... the right ... [illegible]

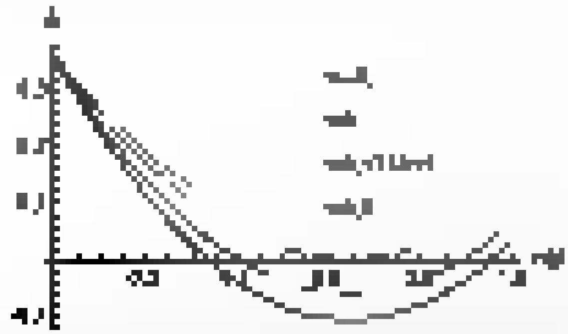

Figure 4: ... [illegible] ...

From the above plots we see that there exist critical values ... [illegible] ... we have black holes and for ... [illegible] ... we have naked singularity. Similarly, ... [illegible] ... we have black holes; for ... [illegible] ... we have naked singularity. For example, ... [illegible] ...

[illegible]

$$[illegible] \qquad (4.29)$$

The real positive solutions of above equation give radial coordinates of ergosphere given by

$$[illegible] \qquad (4.30)$$

Hence the ... [illegible] ... are bound to ... around the black hole. Ergosphere is the region that lies between the ... [illegible] ... From the plots below we observe that the shape of the ergosphere strongly depends on parameters ... [illegible]

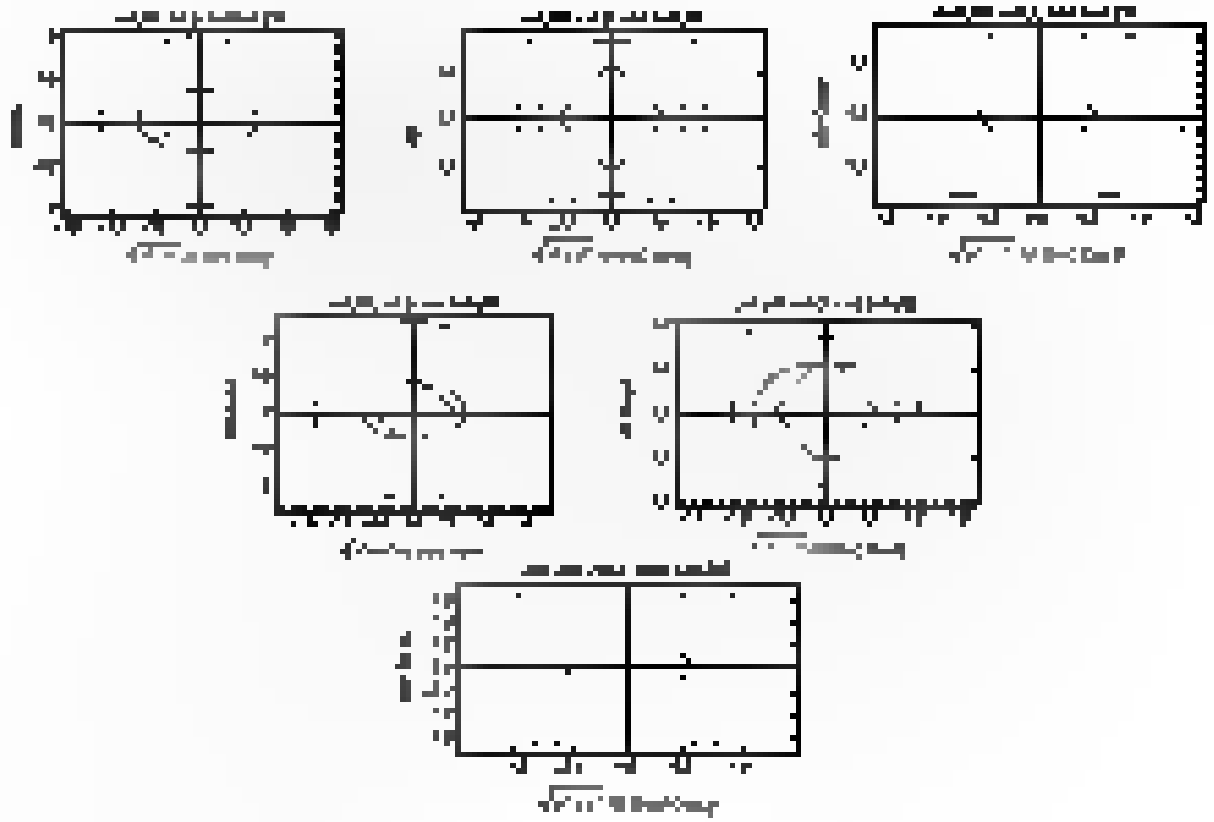

Figure 4. The event horizon of a black hole as a function of its mass M and angular momentum J. Left: the Kerr black hole.

Angular velocity of the black hole at the event horizon

$$\Omega_H = \frac{a}{2Mr_+} \tag{4.30}$$

4. Hawking temperature

The Hawking temperature of a black hole is given by [18]

$$T_H = \frac{\hbar}{2\pi k_B} \kappa = \frac{\hbar}{2\pi k_B} \sqrt{-\frac{1}{2} \nabla_\mu \chi_\nu \nabla^\mu \chi^\nu} \tag{4.31}$$

where $\chi^\mu = \partial_t + \Omega_H \partial_\phi$ is the Killing vector field that is null on the horizon. Substituting the expressions for Ω_H and r_+ from Eqs. (4.30) and (4.29), we obtain

$$T_H = \frac{\hbar}{4\pi k_B} \frac{\sqrt{M^2 - a^2}}{M + \sqrt{M^2 - a^2}} \tag{4.32}$$

4.1. Photon orbit and black hole shadow

In order to study black hole shadows, we introduce the two celestial parameters ξ and η, which are defined by

$$\xi = \frac{L_z}{E} \quad \text{and} \quad \eta = \frac{Q}{E^2}. \tag{4.33}$$

[illegible] [illegible] [illegible] [

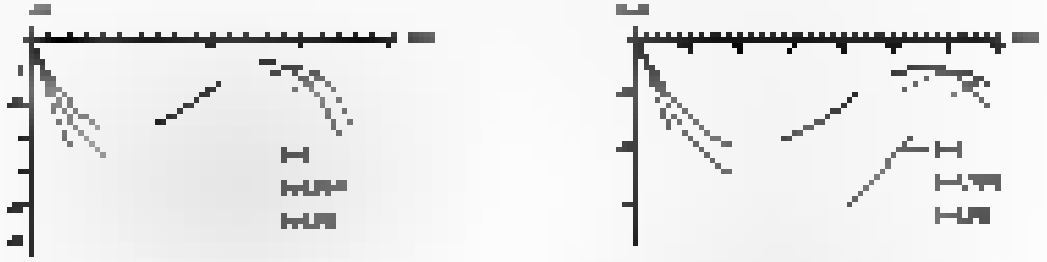

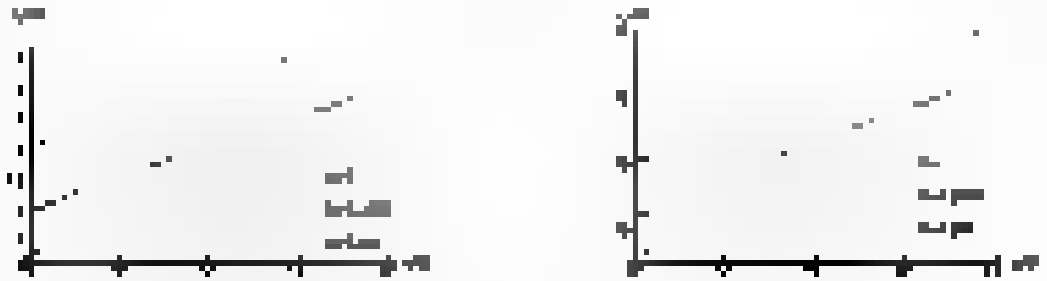

The radial equation of motion can be written down in the form

$$\left(\frac{dr}{d\tau}\right)^2 + V_{\rm eff}^2 = E^2, \tag{4.6}$$

The effective potential $V_{\rm eff}(r)$ reads

$$V_{\rm eff}^2 = \left(1 - \frac{2M}{r} + \frac{Q^2}{r^2}\right)\left(\frac{L^2}{r^2} + 1\right) \qquad (r > r_+ = M + \sqrt{M^2 - Q^2}) \tag{4.7}$$

Here we put $V_{\rm eff}(r_+) = 0$ and $V_{\rm eff}(\infty) = 1$.

The unstable spherical orbit on the equatorial plane is given by the equation $dV_{\rm eff}/dr = 0$. The plot $V_{\rm eff}$ against r for various values of Q with a fixed L is given in the left panel of Fig. 2. The plot $1/b^2 = V_{\rm eff}^2/L^2$ for various values of Q is given in the right panel of Fig. 2. These plots show that the photon orbiting the black hole, which is the turning point of the effective potential, is determined by b. When $b = b_c$, the turning point is an unstable spherical orbit and the photon tends asymptotically to it. When $b < b_c$, the turning point is the minimum of the effective potential and the photon is scattered by the black hole. When $b > b_c$, the photon is captured by the black hole. The critical value b_c corresponds to the radius of the photon sphere or the black hole shadow [6], which is also called the capture cross section [8] in the scattering problem of massless particles. The photon sphere is the surface of the sphere of light rays that are trapped by the black hole. The black hole shadow is the dark area in the sky as seen by a distant observer, which is caused by the photon sphere. We can also see the photon sphere and the black hole shadow in the left panel of Fig. 3.

4. PHOTON ORBIT AND IMAGE PROJECTION

[illegible] [illegible] [illegible] [

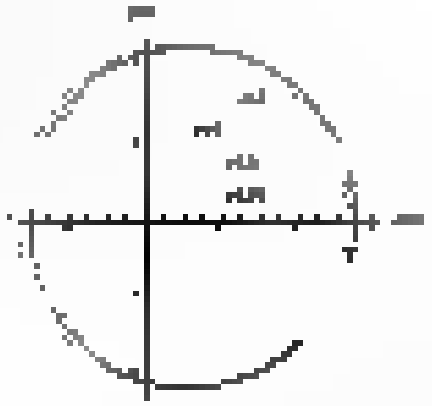

Figure 4.12: The diagram shows the relative positions of the observer, the photon sphere, and the source.

The Fig. 4.12 shows the relative positions of the observer, the photon sphere, and the source. The angle ψ is the deviation of the photon's path from the straight line connecting the source and the observer. The angle α is the angular separation between the source and the observer. The angle β is the angular separation between the observer and the point where the photon's path intersects the photon sphere. The angle γ is the angular separation between the point where the photon's path intersects the photon sphere and the source. The angle δ is the angular separation between the point where the photon's path intersects the photon sphere and the point where the photon's path intersects the photon sphere again. The angle ϵ is the angular separation between the point where the photon's path intersects the photon sphere again and the source. The angle ζ is the angular separation between the point where the photon's path intersects the photon sphere again and the observer. The angle η is the angular separation between the point where the photon's path intersects the photon sphere again and the point where the photon's path intersects the photon sphere again. The angle θ is the angular separation between the point where the photon's path intersects the photon sphere again and the point where the photon's path intersects the photon sphere again. The angle ι is the angular separation between the point where the photon's path intersects the photon sphere again and the point where the photon's path intersects the photon sphere again. The angle κ is the angular separation between the point where the photon's path intersects the photon sphere again and the point where the photon's path intersects the photon sphere again. The angle λ is the angular separation between the point where the photon's path intersects the photon sphere again and the point where the photon's path intersects the photon sphere again. The angle μ is the angular separation between the point where the photon's path intersects the photon sphere again and the point where the photon's path intersects the photon sphere again. The angle ν is the angular separation between the point where the photon's path intersects the photon sphere again and the point where the photon's path intersects the photon sphere again. The angle ξ is the angular separation between the point where the photon's path intersects the photon sphere again and the point where the photon's path intersects the photon sphere again. The angle $\omicron$ is the angular separation between the point where the photon's path intersects the photon sphere again and the point where the photon's path intersects the photon sphere again. The angle π is the angular separation between the point where the photon's path intersects the photon sphere again and the point where the photon's path intersects the photon sphere again. The angle ρ is the angular separation between the point where the photon's path intersects the photon sphere again and the point where the photon's path intersects the photon sphere again. The angle σ is the angular separation between the point where the photon's path intersects the photon sphere again and the point where the photon's path intersects the photon sphere again. The angle τ is the angular separation between the point where the photon's path intersects the photon sphere again and the point where the photon's path intersects the photon sphere again. The angle υ is the angular separation between the point where the photon's path intersects the photon sphere again and the point where the photon's path intersects the photon sphere again. The angle ϕ is the angular separation between the point where the photon's path intersects the photon sphere again and the point where the photon's path intersects the photon sphere again. The angle χ is the angular separation between the point where the photon's path intersects the photon sphere again and the point where the photon's path intersects the photon sphere again. The angle ψ is the angular separation between the point where the photon's path intersects the photon sphere again and the point where the photon's path intersects the photon sphere again. The angle ω is the angular separation between the point where the photon's path intersects the photon sphere again and the point where the photon's path intersects the photon sphere again.

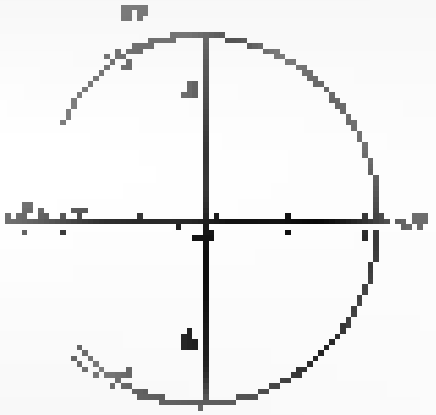

Figure 4.13: A schematic diagram of the photon sphere and the photon's path. The diagram shows the relative positions of the observer, the photon sphere, the source, and the photon's path.

For the following three parameters, we have considered the parameter α_1 as α, α_2 as $\alpha + \Delta\alpha$, $r_1(\theta)$ as $r(\theta)$, and $r_2(\theta)$ as $r(\theta + \Delta\theta)$. Here, $\Delta\alpha$ and $\Delta\theta$ are the angular displacement between the observer and the source, and the photon's path respectively. So we have

$$\Delta\alpha = \int_{r_1}^{r_2} \frac{dr}{r^2 \sqrt{\frac{1}{b^2} - \frac{1}{r^2}\left(1 - \frac{2M}{r}\right)}}$$

and

$$\Delta\theta = \int_{r_1}^{r_2} \frac{dr}{r^2 \sqrt{\frac{1}{b^2} - \frac{1}{r^2}\left(1 - \frac{2M}{r}\right)}}$$

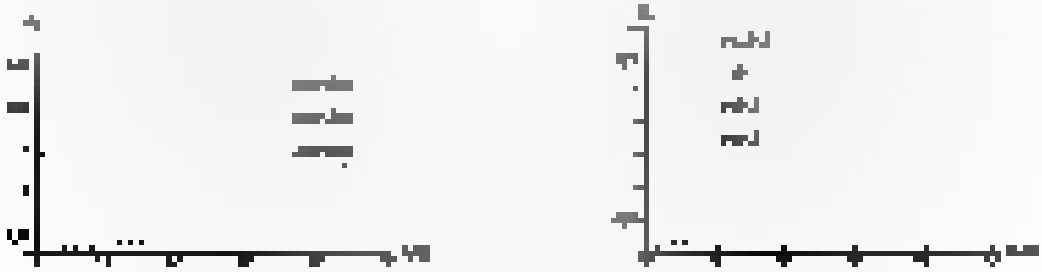

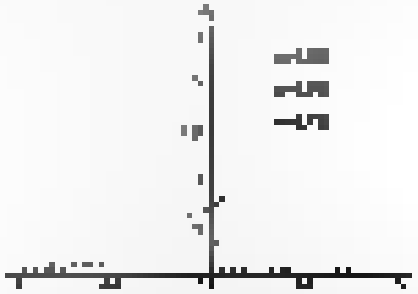

4.3 Energy emission rate

$$\frac{dE}{dt} = \frac{\cdots}{\cdots} \tag{4.10}$$

[illegible] the following asymptotic analysis [illegible] the electromagnetic radiation. [illegible] and [illegible] from the main text. Using [illegible] the above equations gives

$$\frac{dE}{dt} = \frac{[illegible]}{[illegible]} \tag{4.11}$$

where $\omega = \frac{[illegible]}{[illegible]}$ is the angular velocity of the black hole. Using [illegible] gives [illegible] plots [illegible] the black hole frequency [illegible] Fig. 4.10 and Fig. 4.11. [illegible] Fig. 4.10 [illegible] gives the [illegible] the black hole frequency. Black [illegible] the [illegible] [illegible] The figure [illegible] the [illegible] of the electromagnetic frequency [illegible] [illegible] and [illegible].

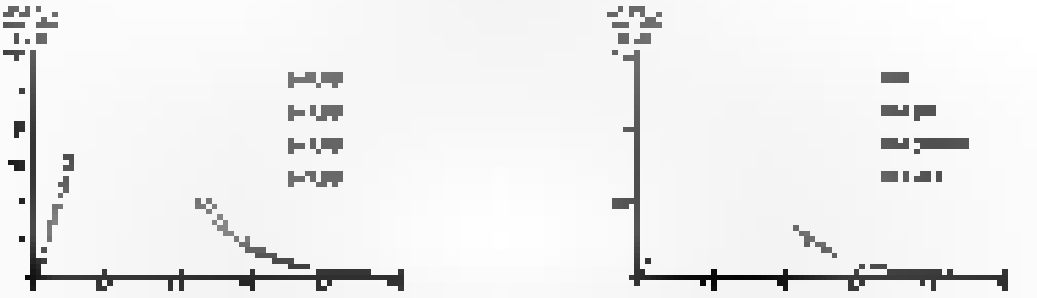

Figure 4.10: The [illegible] [illegible] [illegible]

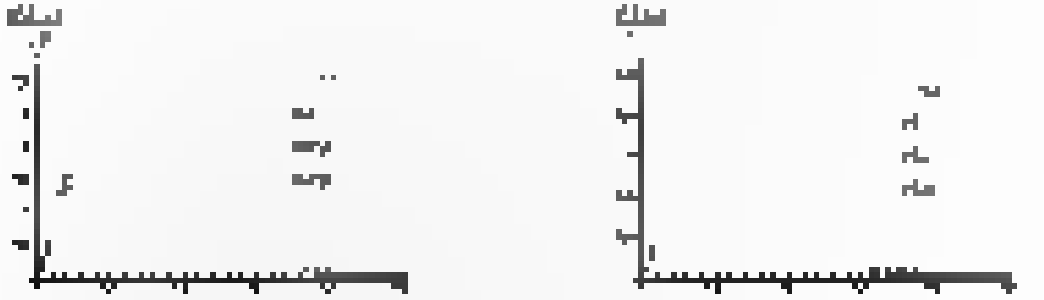

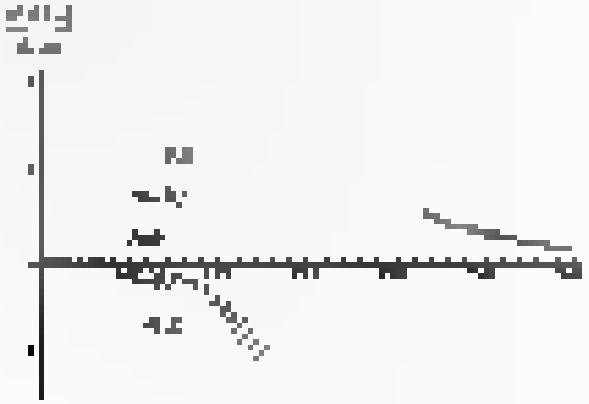

4.4 Comparison between Schwarzschild-like, Kerr-like and Kerr-Sen-like Black holes

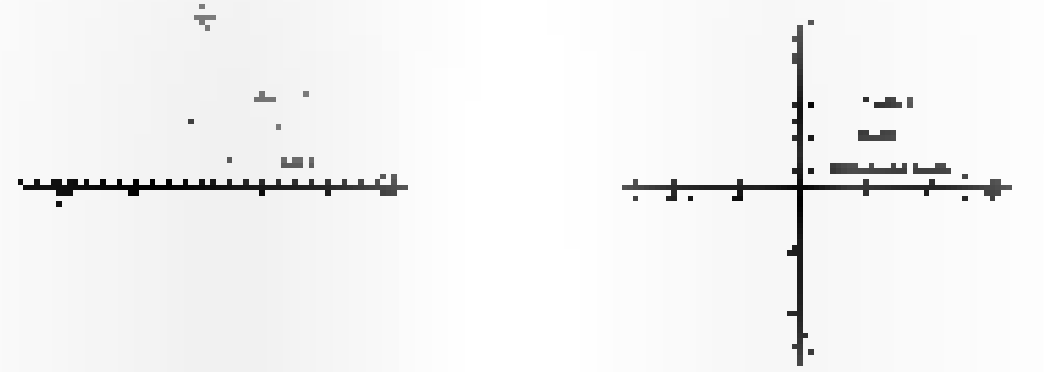

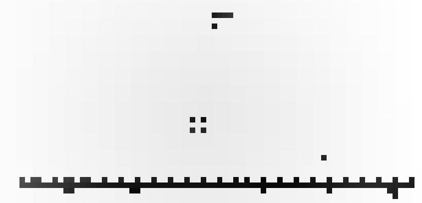

[illegible]

Bending of light

[illegible]

with [illegible] The corresponding [illegible] [illegible] and the [illegible]

$$[illegible]$$

with [illegible] and [illegible]

Chapter 5

$$\cdots \tag{6.3}$$

where $\cdots$ is the effective parameter and

$$\cdots \tag{6.4}$$

In equation (6.4) we introduced two dimensionless parameters $\cdots$ and $\cdots$, which are defined by

$$\cdots \tag{6.5}$$

where $\cdots$ and $\cdots$ are the energy, the radial component of the angular momentum, and the mass of the particle, respectively.

In terms of $\cdots$ the region of the nuclear potential is defined by [26]

$$\cdots \tag{6.6}$$

where $\cdots$ and $\cdots$ are respectively the frequency of photons and the interaction photon frequency. In the general theory of relativity, the radial motion of the photon depends on the distance from the photon to the gravitational field. Besides, the electric neutral frequency has the expression [26]

$$\cdots \tag{6.7}$$

where $\cdots$ is the concentration of electrons in the electromagnetic plasma. The mass and the charge of the electron are respectively determined by $\cdots$ and $\cdots$. We now consider a radial power-law density $\cdots$

$$\cdots \tag{6.8}$$

where $\cdots$ is the density number at the radial position of the most edge of plasma and $\cdots$ is the index. Therefore, we have

$$\cdots \tag{6.9}$$

where $\cdots$ is the Riemann zeta function $\cdots$ is the Gamma function [26] and we have

$$\cdots \tag{6.10}$$

6 Effective potential and Critical radius

Now for specific form of the metric coefficients (6.12), we have studied various aspects of photon geodesics in [13] and the explicit form of the effective potential given in Eq. (6.3). The radial equation of motion and the effective potential $\cdots$ is the same form

$$\cdots \tag{6.11}$$

The effective potential $\cdots$ is the same as the form

$$\cdots \tag{6.12}$$

Now that we have both the $\cdots$ and $\cdots$

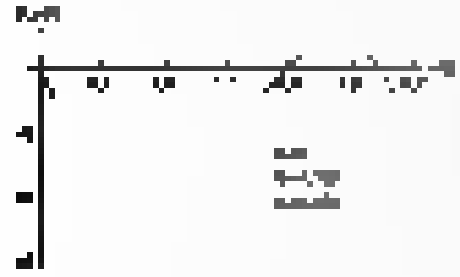

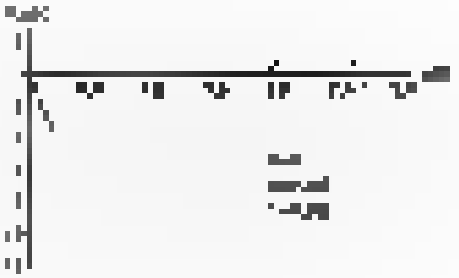

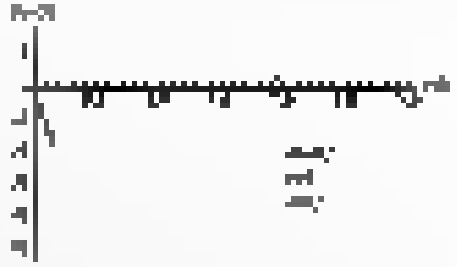

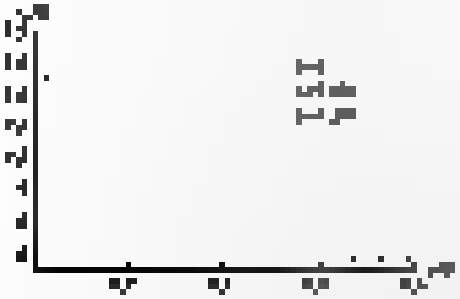

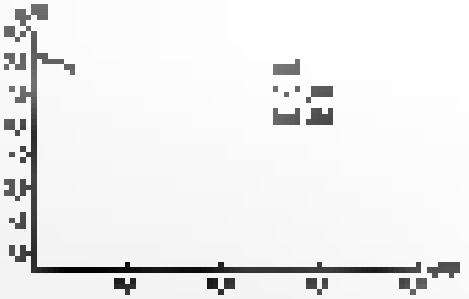

...dial 2nd Eq. (5.1) we find that the turning point is the root of the equation $r^2 - 2Mr + a^2 = 0$. For $M > a$ there are two horizons at $r_\pm = M \pm \sqrt{M^2 - a^2}$. The ergosphere is the region between the outer horizon and the outer boundary of the ergosphere, which touches the horizon at the poles and reaches its maximum radius in the equatorial plane. The right hand side of Eq. (5.1) is a complicated function of r and θ. In Fig. 5.1 we show the plot of the event horizon and the ergosphere. We find that the boundary of the shadow is affected by the rotation of the black hole. As the black hole rotates faster, the shadow becomes more distorted.

5.1 Photon orbit and black hole shadow

For a given spherical photon orbit, where the radius is a constant, the equations of motion for photons in the equatorial plane ($\theta = \pi/2$) are given by the geodesic equations of the Hamiltonian

$$H = 0 \quad \text{and} \quad \frac{dR}{dr} < 0 \tag{5.14}$$

where

$$R(r) = \left[\frac{r^2 + b^2 - a^2}{r^2 + a^2} \right]^2 - \left[\frac{a^2 + b^2 + r^2}{r^2 + a^2} \right] \left[\frac{b^2 + a^2 + r^2}{r^2 + a^2} \right]$$

and

$$\frac{dR}{dr} = \frac{2r}{(r^2 + a^2)^2} \left[\frac{r^2 + b^2 - a^2}{r^2 + a^2} \right] - \left[\frac{2r}{r^2 + a^2} - \frac{2r(a^2 + b^2 + r^2)}{(r^2 + a^2)^2} \right] \left[\frac{b^2 + a^2 + r^2}{r^2 + a^2} \right]$$

$$- \frac{2r}{(r^2 + a^2)^2} \left[\frac{b^2 + a^2 + r^2}{r^2 + a^2} \right] \tag{5.15}$$

For a spherical photon orbit, r is a constant, so we obtain from the equations

$$R(r) = 0 \quad \text{and} \quad \frac{dR}{dr} = 0 \tag{5.16}$$

which give

$$b = \frac{r^2(r^2 + a^2) - a^2(r^2 - a^2)}{a(r^2 - a^2)} \left[\frac{r^2 + a^2}{r^2 - a^2} \right]^{1/2}$$

$$\eta = \frac{r^2(r^2 + a^2)^2 - a^2(r^2 - a^2)^2}{a^2(r^2 - a^2)^2} \left[\frac{r^2 + a^2}{r^2 - a^2} \right]$$

$$- \frac{r^2(r^2 + a^2) - a^2(r^2 - a^2)}{a^2(r^2 - a^2)} \left[\frac{r^2 + a^2}{r^2 - a^2} \right]$$

$$+ \frac{4r^2}{(r^2 - a^2)^2} \left[r^2(r^2 + a^2) - a^2(r^2 - a^2) \right] \left[\frac{r^2 + a^2}{r^2 - a^2} \right]$$

$$- \frac{4r^2}{(r^2 - a^2)^2} \left[r^2(r^2 + a^2) - a^2(r^2 - a^2) \right] \left[\frac{r^2 + a^2}{r^2 - a^2} \right]$$

$$+ \frac{4r^2}{(r^2 - a^2)^2} \left[r^2(r^2 + a^2) - a^2(r^2 - a^2) \right] \left[\frac{r^2 + a^2}{r^2 - a^2} \right]$$

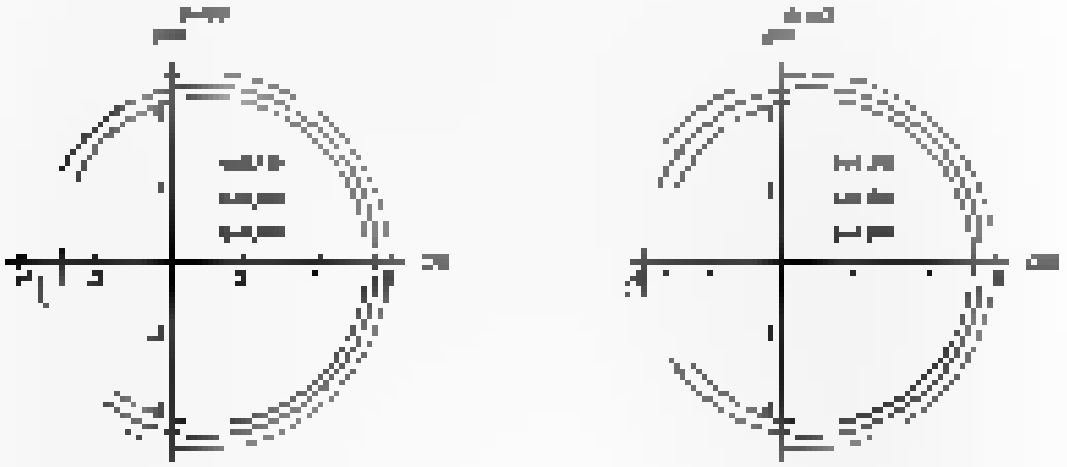

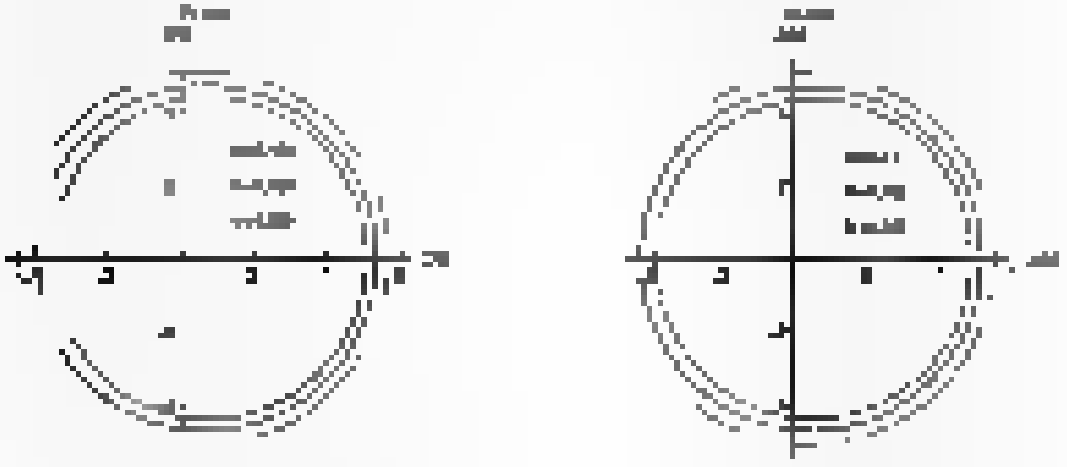

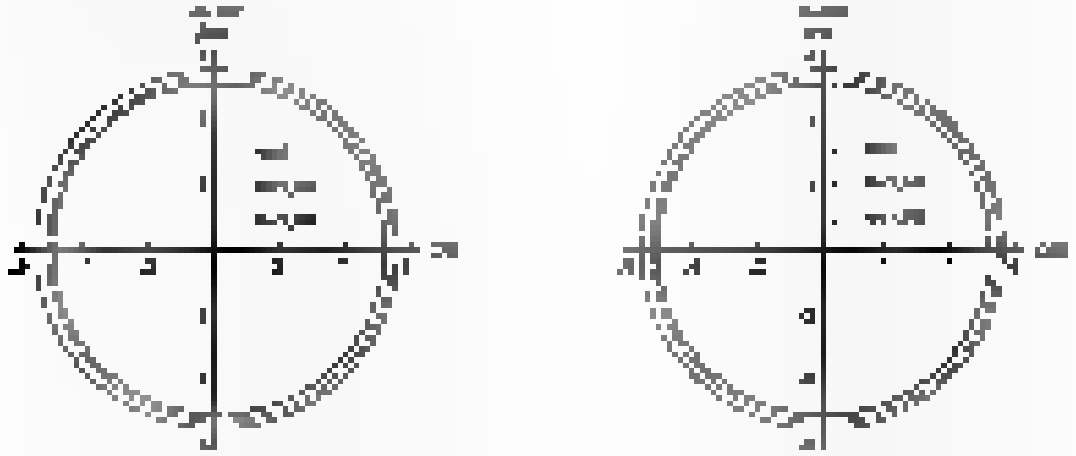

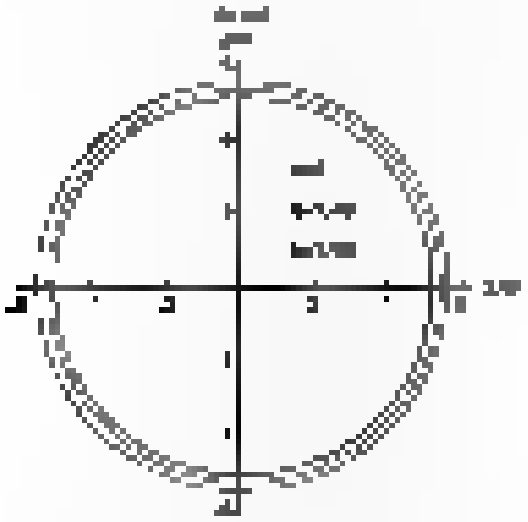

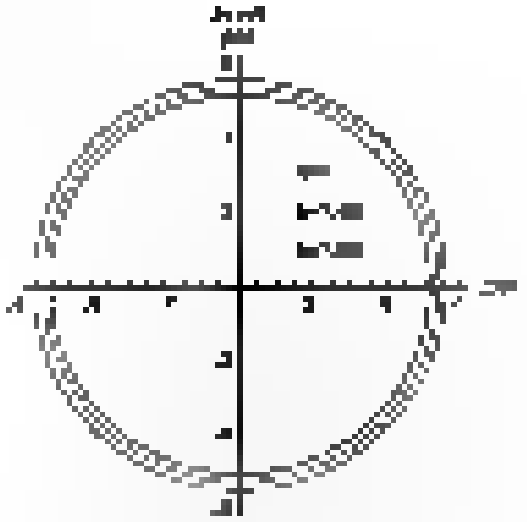

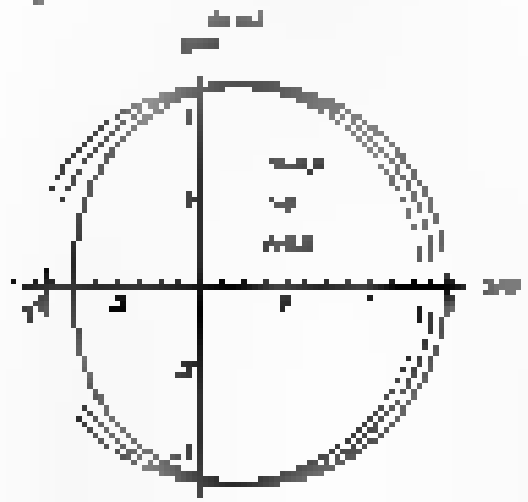

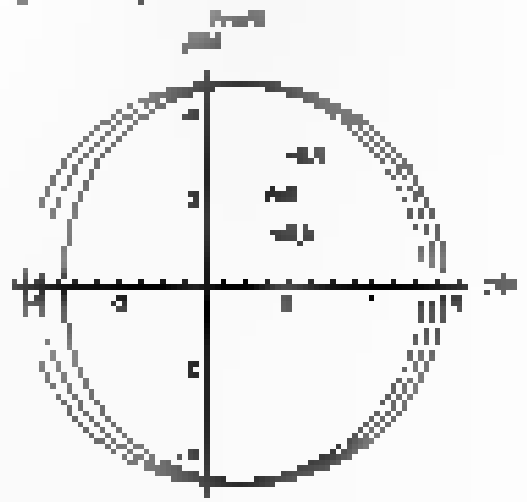

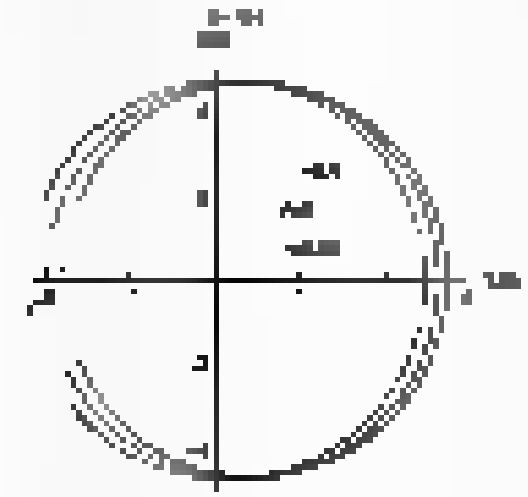

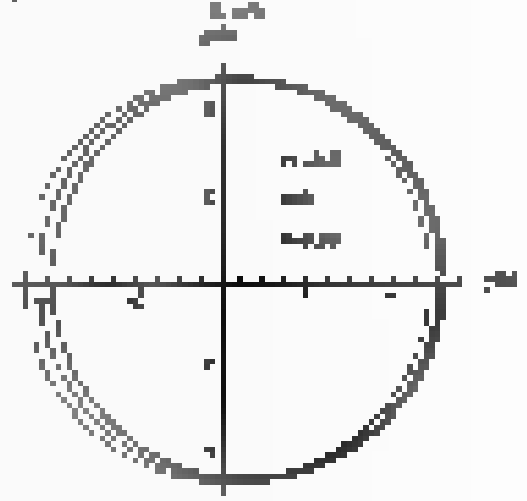

[illegible]

5.5 The deviation from the circular form of the shadow [illegible] and the size [illegible] of the shadow

[illegible]

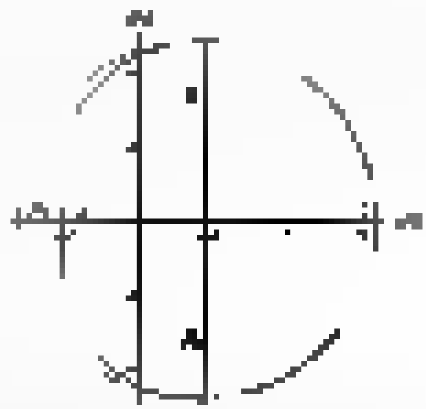

[illegible]

[illegible]

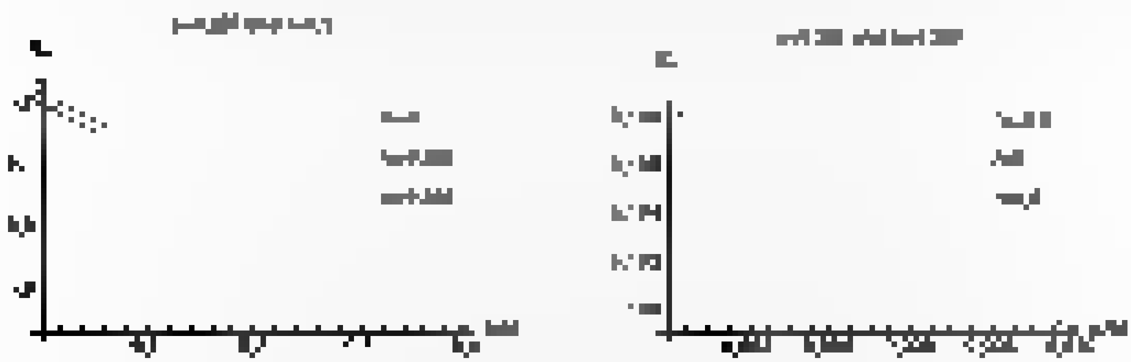

[illegible]

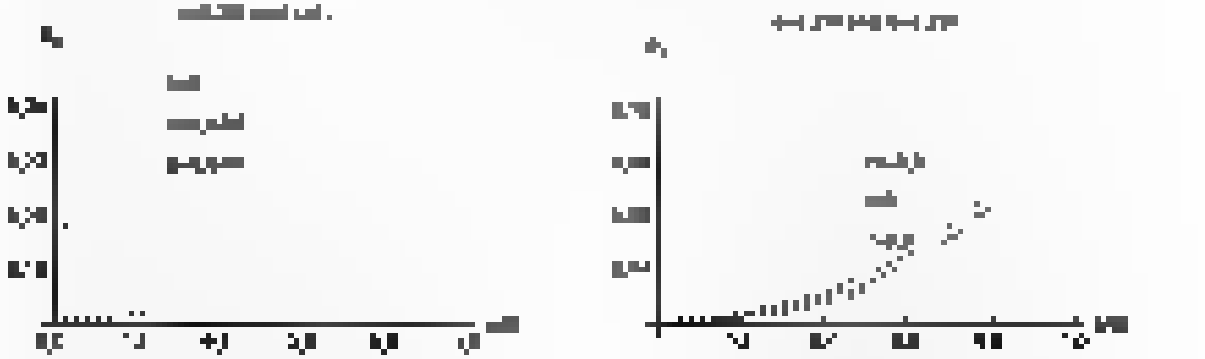

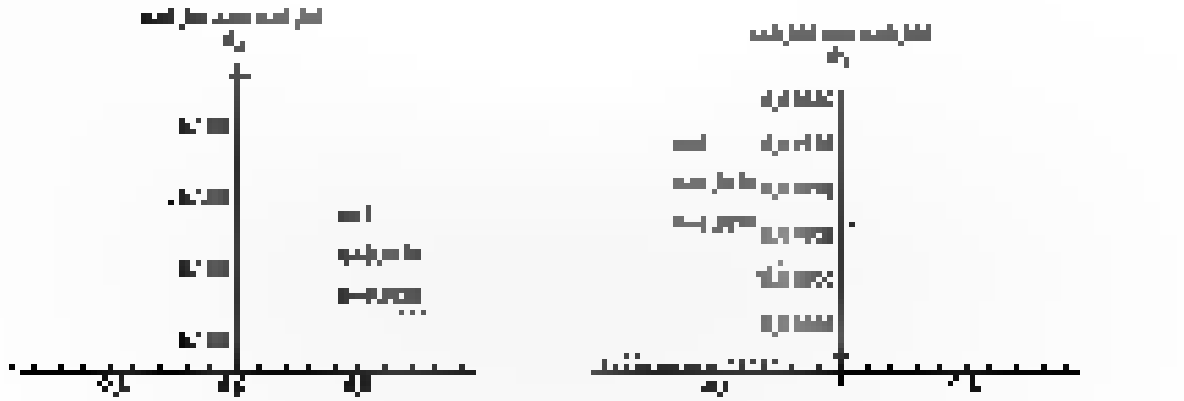

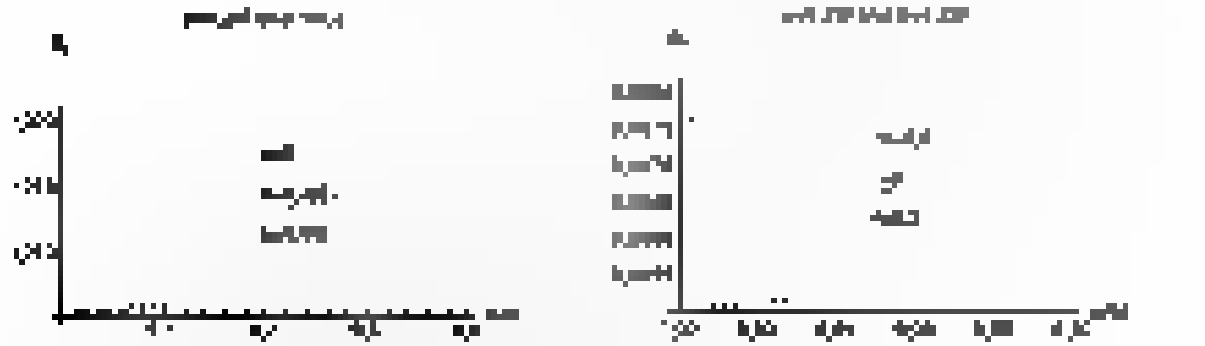

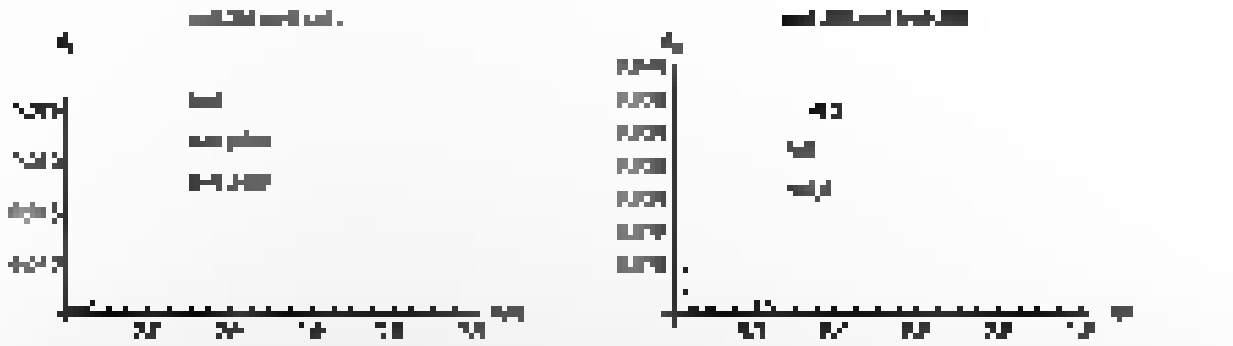

Figure 5.4: The figure on the left side represents the variation of the velocity of the block with time when the damping coefficient is zero. The figure on the right side represents the variation of the velocity of the block with time when the damping coefficient is non-zero.

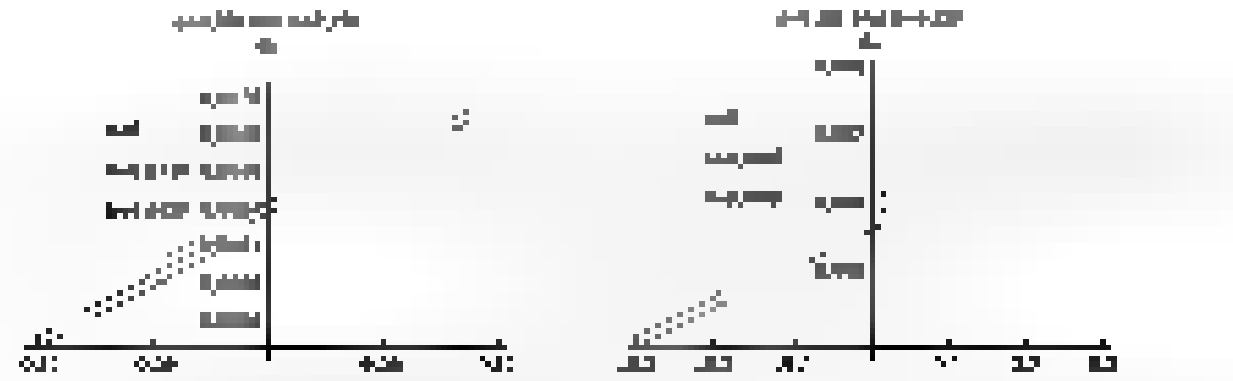

Figure 5.5: The figure on the left side represents the variation of the velocity of the block with time when the damping coefficient is zero. The figure on the right side represents the variation of the velocity of the block with time when the damping coefficient is non-zero.

Here, we have plotted the velocity of the block with time for two different values of the damping coefficient. We have taken the mass of the block to be 1 kg and the spring constant to be 1 N/m. The initial velocity of the block is 1 m/s. The figure on the left side represents the variation of the velocity of the block when the damping coefficient is zero. The figure on the right side represents the variation of the velocity of the block when the damping coefficient is non-zero.

Table 5.1: Comparison of the theoretical and experimental values of the time period of the block.

In this table, we have compared the theoretical and experimental values of the time period of the block. We have also calculated the percentage error in the time period of the block.

5.5 The effect of energy dissipation

In the real world, we do not have a perfect spring. As a result, some of the energy of the block is dissipated in the form of heat and other forms of energy. This is called damping. In this section, we will study the effect of damping on the motion of the block. We will also study the effect of damping on the energy of the block. We will also study the effect of damping on the energy of the block. We will also study the effect of damping on the energy of the block.

The following [illegible]

$$[illegible] \tag{5.1}$$

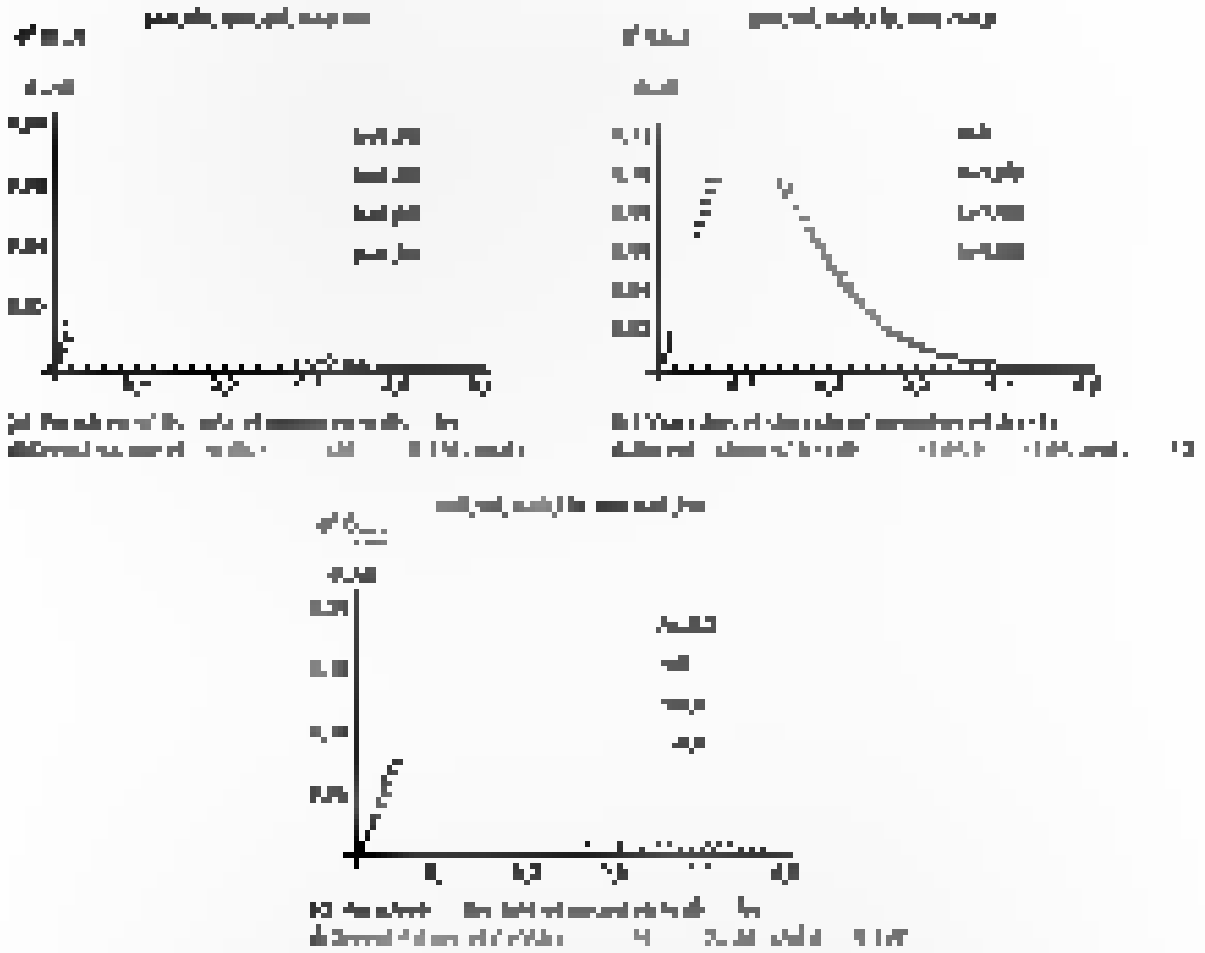

Figure 5.4: [illegible]

The Fig. 5.4(a) we have studied how the energy emitted per unit area will behave with the variation of the temperature. It will be observed that the rate of emission is higher for smaller values of the temperature. The reason is the more values of temperature for smaller wavelength. The energy emitted by the body is proportional to the fourth power of the temperature. Hence the energy emitted by the body increases very rapidly with the temperature. The [illegible]

Chapter 6

3 Multiple-Source Scattering of Time-Harmonic Waves by Convex Obstacles

In this section we apply the results of the previous section to the problem of scattering of time-harmonic waves by convex obstacles. We first consider the case of a single obstacle and then extend the results to the case of multiple obstacles. The problem of scattering of time-harmonic waves by convex obstacles is governed by the Helmholtz equation with appropriate boundary conditions. The Helmholtz equation is given by

$$\nabla^2 u + k^2 u = 0 \qquad (3.1)$$

where u is the scattered wave, k is the wavenumber, and ∇^2 is the Laplacian operator. The boundary conditions are given by

$$u = -u_{inc} \quad \text{on } \partial\Omega \qquad (3.2)$$

where u_{inc} is the incident wave and $\partial\Omega$ is the boundary of the obstacle. The solution to the Helmholtz equation can be represented as a single-layer potential

$$u(x) = \int_{\partial\Omega} \sigma(y)\, \Phi(x,y)\, ds(y) \qquad (3.3)$$

where σ is the density function and $\Phi(x,y)$ is the fundamental solution to the Helmholtz equation. The density function σ is determined by the boundary condition (3.2). The single-layer potential (3.3) is a solution to the Helmholtz equation for any density function σ. The boundary condition (3.2) is satisfied if the density function σ is chosen appropriately. The density function σ is determined by the integral equation

$$-u_{inc}(x) = \int_{\partial\Omega} \sigma(y)\, \Phi(x,y)\, ds(y), \quad x \in \partial\Omega \qquad (3.4)$$

This integral equation is a Fredholm integral equation of the first kind. The kernel $\Phi(x,y)$ is singular when $x = y$. The singularity is integrable. The integral equation (3.4) is ill-posed. The ill-posedness is due to the fact that the kernel $\Phi(x,y)$ is smooth. The smoothness of the kernel implies that the integral operator is compact. The compactness of the integral operator implies that the integral equation (3.4) is ill-posed.

To solve the integral equation (3.4) we use the method of moments. The method of moments is a numerical method for solving integral equations. The method of moments is based on the idea of approximating the unknown function σ by a linear combination of basis functions. The basis functions are chosen to be piecewise constant functions. The piecewise constant basis functions are defined as

$$\phi_j(x) = \begin{cases} 1, & x \in \Delta_j \\ 0, & \text{otherwise} \end{cases} \qquad (3.5)$$

where Δ_j is the jth element of the boundary $\partial\Omega$. The boundary $\partial\Omega$ is divided into N elements $\Delta_1, \Delta_2, \ldots, \Delta_N$. The unknown function σ is approximated by

$$\sigma(x) \approx \sum_{j=1}^{N} \sigma_j \phi_j(x) \qquad (3.6)$$

where σ_j are the unknown coefficients. The coefficients σ_j are determined by the boundary condition (3.2). The boundary condition (3.2) is satisfied at the midpoints of the elements Δ_j. The midpoints of the elements Δ_j are denoted by x_i. The boundary condition (3.2) is satisfied at the midpoints x_i by the equation

$$-u_{inc}(x_i) = \sum_{j=1}^{N} \sigma_j \int_{\Delta_j} \Phi(x_i,y)\, ds(y), \quad i = 1, 2, \ldots, N \qquad (3.7)$$

The integral equation (3.7) is a system of N linear equations in N unknowns. The system of linear equations can be written in matrix form as

$$A\sigma = b \qquad (3.8)$$

where A is the $N \times N$ matrix with entries $A_{ij} = \int_{\Delta_j} \Phi(x_i,y)\, ds(y)$, σ is the vector of unknown coefficients σ_j, and b is the vector with entries $b_i = -u_{inc}(x_i)$. The matrix A is dense. The matrix A is ill-conditioned. The ill-conditioning of the matrix A is due to the fact that the kernel $\Phi(x,y)$ is smooth. The smoothness of the kernel implies that the integral operator is compact. The compactness of the integral operator implies that the matrix A is ill-conditioned. The ill-conditioning of the matrix A can be overcome by using a regularization method. The regularization method is based on the idea of adding a small perturbation to the matrix A. The perturbed matrix is denoted by A_ε. The perturbed matrix A_ε is given by

$$A_\varepsilon = A + \varepsilon I \qquad (3.9)$$

where ε is a small positive number and I is the identity matrix. The perturbed matrix A_ε is well-conditioned. The perturbed matrix A_ε is used to solve the integral equation (3.4). The solution to the perturbed integral equation is denoted by σ_ε. The solution σ_ε is given by

$$\sigma_\varepsilon = A_\varepsilon^{-1} b \qquad (3.10)$$

The solution σ_ε converges to the solution σ as ε tends to zero. The convergence of the solution σ_ε to the solution σ is guaranteed by the theory of regularization methods. The theory of regularization methods is beyond the scope of this paper. The interested reader is referred to the literature for more information. The regularization method is used to solve the integral equation (3.4). The solution to the integral equation (3.4) is used to compute the scattered wave u. The scattered wave u is given by the single-layer potential (3.3). The single-layer potential (3.3) is evaluated at the midpoints of the elements Δ_j. The midpoints of the elements Δ_j are denoted by x_i. The scattered wave u is given by

$$u(x_i) = \sum_{j=1}^{N} \sigma_j \int_{\Delta_j} \Phi(x_i,y)\, ds(y), \quad i = 1, 2, \ldots, N \qquad (3.11)$$

The scattered wave u is used to compute the far-field pattern. The far-field pattern is denoted by F. The far-field pattern F is given by

$$F(\hat{x}) = \sum_{j=1}^{N} \sigma_j \int_{\Delta_j} e^{-ik\hat{x}\cdot y}\, ds(y) \qquad (3.12)$$

where $\hat{x}$ is the unit vector in the direction of the observation point. The far-field pattern F is used to compute the radar cross section. The radar cross section is denoted by σ_{RCS}. The radar cross section σ_{RCS} is given by

$$\sigma_{RCS} = \frac{4\pi}{k^2} |F|^2 \qquad (3.13)$$

The radar cross section σ_{RCS} is used to compute the scattering cross section. The scattering cross section is denoted by σ_{SCS}. The scattering cross section σ_{SCS} is given by

$$\sigma_{SCS} = \int_{S^2} |F(\hat{x})|^2\, d\hat{x} \qquad (3.14)$$

where S^2 is the unit sphere. The scattering cross section σ_{SCS} is used to compute the extinction cross section. The extinction cross section is denoted by σ_{ECS}. The extinction cross section σ_{ECS} is given by

$$\sigma_{ECS} = \sigma_{SCS} + \sigma_{ABS} \qquad (3.15)$$

where σ_{ABS} is the absorption cross section. The absorption cross section σ_{ABS} is zero for a perfectly conducting obstacle. The extinction cross section σ_{ECS} is equal to the scattering cross section σ_{SCS} for a perfectly conducting obstacle.

6.2 Amplification factor B_ν. Spectral equilibrium

Our assumption would be to replace the initial equation (6.1) by the following form

$$\frac{dI_\nu}{dx} = \frac{\Omega}{4\pi} \frac{dN_{\nu,x}}{dx}$$

$$\frac{dI_\nu}{dx} = \frac{\Omega}{4\pi} \frac{dN_{\nu,x}}{dx} \qquad (6.1a)$$

However proceed to derive the relation for the term and the two regions and for the fixed value of the angle by applying the polynomial for the region of positive angle polynomial for the perception of the fixed point and the space-angle position between the boundary of the emitting region. The boundary of the region is a convex polyhedron and is defined by $\frac{dN_{\nu,x}}{dx}$ in terms of the equation (6.1a) relation

$$\frac{d^2 I_\nu}{dx^2} = \frac{d}{dx}\left(\frac{\Omega}{4\pi}\frac{dN_{\nu,x}}{dx}\right) \qquad (6.1)$$

$$\frac{d^2 I_\nu}{dx^2} = \frac{\Omega}{4\pi}\frac{d^2 N_{\nu,x}}{dx^2} \qquad (6.1a)$$

Using the approximation of the relation $\frac{dN_{\nu,x}}{dx} = \frac{N_{\nu,x+\Delta x} - N_{\nu,x}}{\Delta x}$ for the two regions and from the equation (6.1a) and $\frac{d^2 N_{\nu,x}}{dx^2}$ the two-region equation is approximated

$$\frac{d^2 I_\nu}{dx^2} + \frac{d^2 N_{\nu,x}}{dx^2} + \frac{dN_{\nu,x}}{dx} = \frac{dN_{\nu,x}}{dx} \qquad (6.1b)$$

Since the complex wavelength of the boundary polynomial is much smaller than the wavelength of the light field, the approximation $\frac{d^2 N_{\nu,x}}{dx^2} \approx 0$ is valid over the fixed region. The general solution of the above equation in terms of successive exponential functions of the first kind $E_1(x)$ can be written down as

$$I_\nu(x) = A e^{-\frac{x}{\lambda_\nu}} + B(x) \qquad (6.1c)$$

Here λ_ν is the relation

$$\lambda_\nu = \frac{1}{\sigma_\nu + \kappa_\nu} \qquad (6.1d)$$

and $B(x)$ is the solution of the integral equation

$$B(x) = \frac{\sigma_\nu}{\sigma_\nu + \kappa_\nu} \int_0^x E_1\left(\frac{|x-x'|}{\lambda_\nu}\right) B(x')\,dx' + \frac{\kappa_\nu}{\sigma_\nu + \kappa_\nu} B_\nu(T) \qquad (6.1e)$$

We are interested to find out a simple solution using the following conditions on the observed position where the two solutions must match each other. In this respect we need to consider the large x behaviour of the above expression. The $B(x)$ is the largest x behaviour

$$B(x) \sim \frac{\sigma_\nu}{\sigma_\nu + \kappa_\nu} \int_0^\infty E_1\left(\frac{|x-x'|}{\lambda_\nu}\right) B(x')\,dx' + \frac{\kappa_\nu}{\sigma_\nu + \kappa_\nu} B_\nu(T) \qquad (6.1f)$$

A. AMPLIFICATION FACTOR B. PERTURBATION ANALYSIS

For the following we include the equation that sets $p = \ldots$ in order to find $p^{2} = \ldots$ We only display all the terms except those which describe the non-conservative contributions and that are equation (A 31) is

$$\frac{d^{2}A_{n}(x)}{dx^{2}} + \frac{\ldots}{dx}\frac{dA_{n}(x)}{dx} + \ldots \frac{\ldots}{x^{2}} \ldots A_{n}(x) = \qquad (A\ 32)$$

where $k_{y} = \ldots \sqrt{\ldots}$ Equation (A32) has the general solution

$$A_{n}(x) = \ldots \frac{\ldots}{\ldots} H_{\ldots}(\ldots) + \frac{\sqrt{\ldots}}{\ldots} \ldots \frac{\ldots}{\ldots} \ldots + \ldots + \ldots \ldots \frac{\ldots}{\ldots} H_{\ldots}(\ldots) \ldots \frac{\sqrt{\ldots}}{\ldots} \ldots \frac{\ldots}{\ldots} \qquad (A\ 33)$$

Here $H_{\ldots}(\ldots)$ is a Hermite polynomial of order $\ldots$ and $\ldots$ is the Hermite function of order $\ldots$ In order to match the solution with $\ldots$ we must take the small y behaviour of the solution (A 33). For small y $\ldots$ the equation (A 33) becomes

$$A_{n}(x) \ldots \frac{\ldots}{\ldots} \ldots \frac{\ldots}{\ldots} + \ldots \frac{\ldots}{\ldots} \qquad (A\ 34)$$

The solutions (A 33) and (A 34) are acceptable for matching across the two boundaries between the three regions of interest. The matching at the asymptotic solutions (A 33) and (A 34) enables us to compute the complex transmission and reflection coefficients $\ldots$ and $\ldots$ as

$$\ldots = \frac{\ldots}{\ldots} \qquad (A\ 35)$$

$$\ldots = \frac{\ldots}{\ldots} \qquad (A\ 36)$$

We expand equation (A 31) around the boundary at which we expand the variable

$$\ldots \frac{\ldots}{\ldots} \ldots \qquad \ldots \frac{\ldots}{\ldots} \ldots \qquad \ldots \frac{\ldots}{\ldots} \ldots$$

$$\ldots \frac{\ldots}{\ldots} \ldots \qquad \ldots \frac{\ldots}{\ldots} \ldots \qquad \ldots \frac{\ldots}{\ldots} \ldots$$

Multiplying the approximate equation $\ldots$ by $\ldots$ and grouping the terms with the same order of $\ldots$ we find the matching equation (A 31)

$$\ldots \qquad \ldots \qquad \ldots \qquad \ldots \qquad \ldots \to \infty$$

we get

$$\ldots = \ldots \qquad \ldots \to \ldots \qquad \ldots \frac{\ldots}{\ldots} \ldots \frac{\ldots}{\ldots} \ldots$$

$$\ldots \to \ldots \qquad \ldots \frac{\ldots}{\ldots} \ldots \frac{\ldots}{\ldots} \ldots$$

and

$$\ldots = \ldots \qquad \ldots \to \ldots \qquad \ldots \frac{\ldots}{\ldots} \ldots \frac{\ldots}{\ldots} \ldots$$

$$\ldots \to \ldots \qquad \ldots \frac{\ldots}{\ldots} \ldots \frac{\ldots}{\ldots} \ldots$$

Substituting the expressions of [illegible] from Eq. [illegible] into the above expressions, we have [illegible]

$$[illegible]$$

and

$$[illegible]$$

The amplification factor is finally written as

$$[illegible] \quad [illegible]$$

Equation [illegible] is a general expression of the amplification factor obtained by making use of the asymptotic matching method. When [illegible] acquires a value greater than unity, there will be a gain in amplification factor that corresponds to superradiance phenomena. However, a negative value of the amplification factor indicates [illegible] to the occurrence of [illegible]. To [illegible] the effect of [illegible] on the superradiance phenomena, [illegible] in plotting [illegible] for different values of [illegible]. In Fig. [illegible] we present the variation of [illegible] versus [illegible] for the leading multipoles [illegible] and [illegible] taking different values [illegible] and [illegible] of the [illegible] parameter. From the Fig. [illegible] in line with Fig. [illegible] that superradiance [illegible] occurs when the [illegible] are satisfied [illegible].

The negative amplification factor [illegible] value which refers to the non occurrence of superradiance. The plots also show [illegible] that with the decrease in the value of the [illegible] parameter the superradiance process enhances and the reverse is the case when the value of the [illegible] parameter decreases. In Fig. [illegible] we have also studied the effect of the parameter [illegible] on the superradiance scenario. It shows that the superradiance scenario gets diminished with the increase in the value of the parameter [illegible]. However, with the increase in [illegible] the superradiance effect increases as is found from Fig. [illegible]

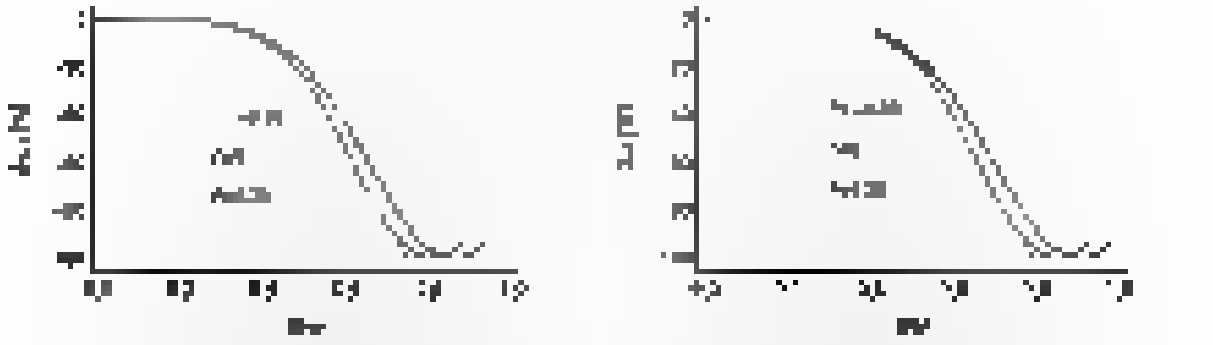

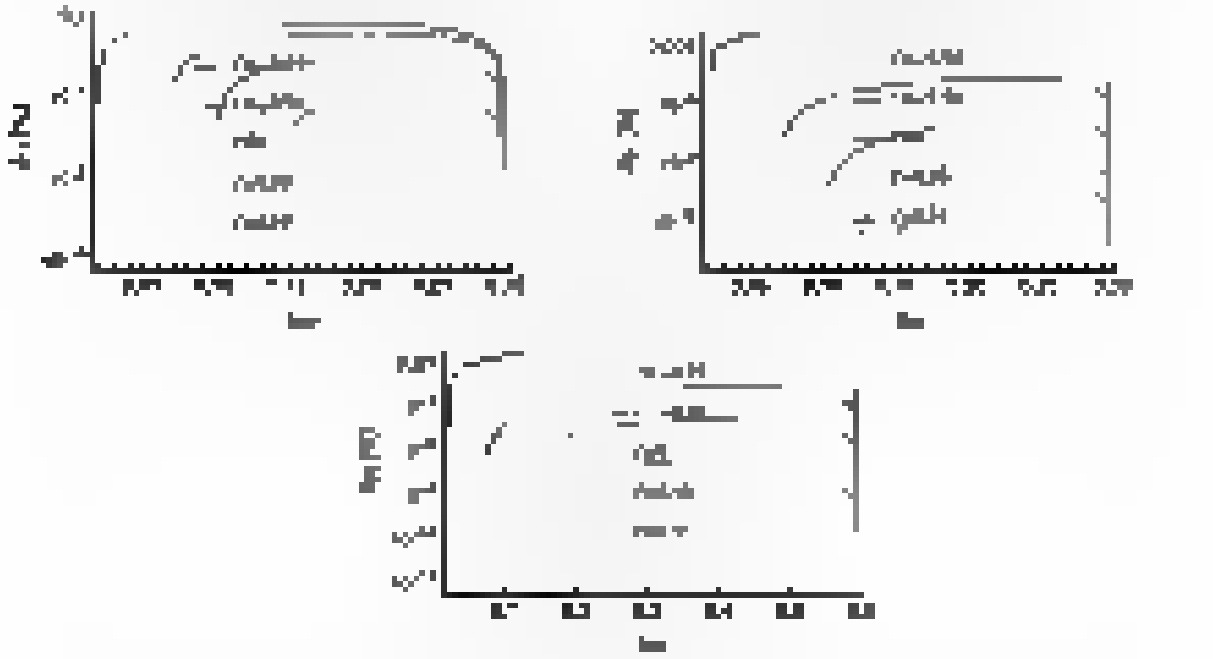

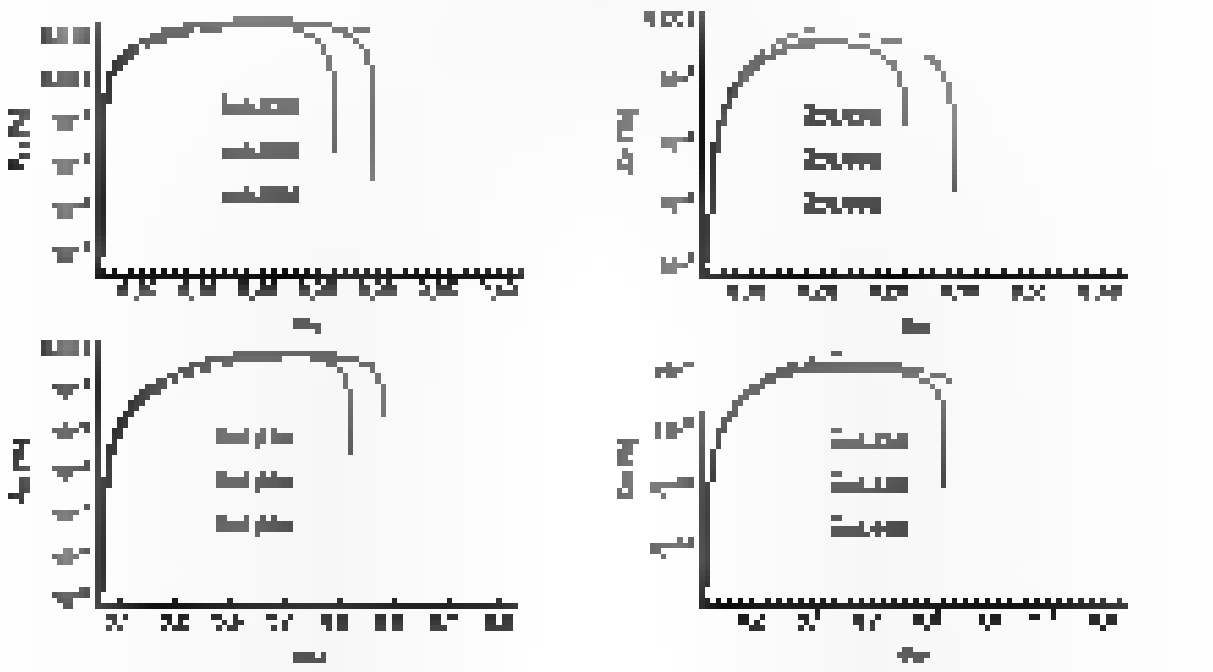

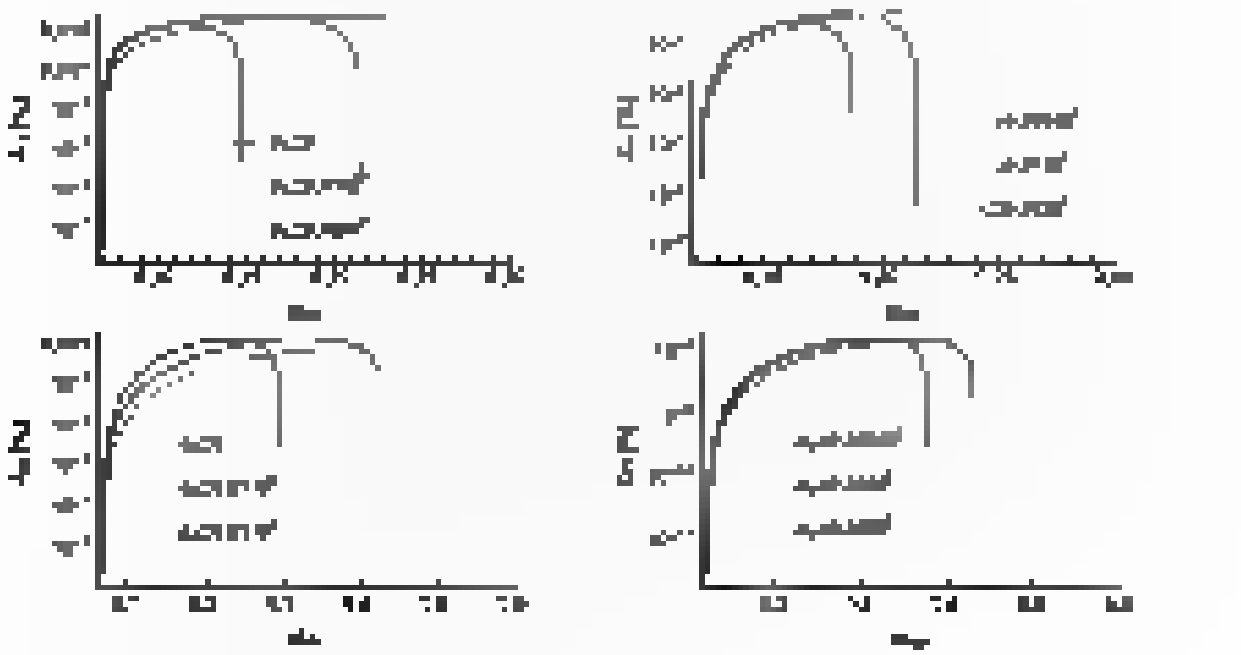

Figure 6.1 [illegible]

6.3 Superradiant instability for Lorentz violating and non-commutative Kerr-like black hole

From equation (3.7) we can write

$$\frac{1}{r^2}\frac{d}{dr}\left(\Delta\frac{dR_{\omega lm}}{dr}\right) + \left[\frac{K^2}{\Delta} - \lambda_{lm} + \right] R_{\omega lm} = 0 \tag{6.25}$$

where for slowly rotating black hole ($a \ll 1$)

$$\lambda_{lm} = l(l+1) - \frac{2ma}{l(l+1)} + \mathcal{O}(a^2) \tag{6.26}$$

Now we are going to find the black hole bound wavefunction, we should have the following solutions to the radial equation (6.25)

$$R_{\omega lm} \sim \begin{cases} \text{[illegible]} & r \to r_+ \\ \text{[illegible]} & r \to \infty \end{cases} \tag{6.27}$$

The above solution approach the event horizon and infinity respectively. Now the probability density of the black hole bound state is slowly varying with time, so we are interested in studying superradiant phenomena provided that $\omega^2 < 0$. With the same method as before

$$\omega_{lm} = -i\sqrt{\Omega}\,\mathcal{E}_{\omega lm} \tag{6.28}$$

the radial equation (6.25) turns into

$$\frac{d^2}{dr^2} - \left[\quad\right] R_{\omega lm} = 0 \tag{6.29}$$

with

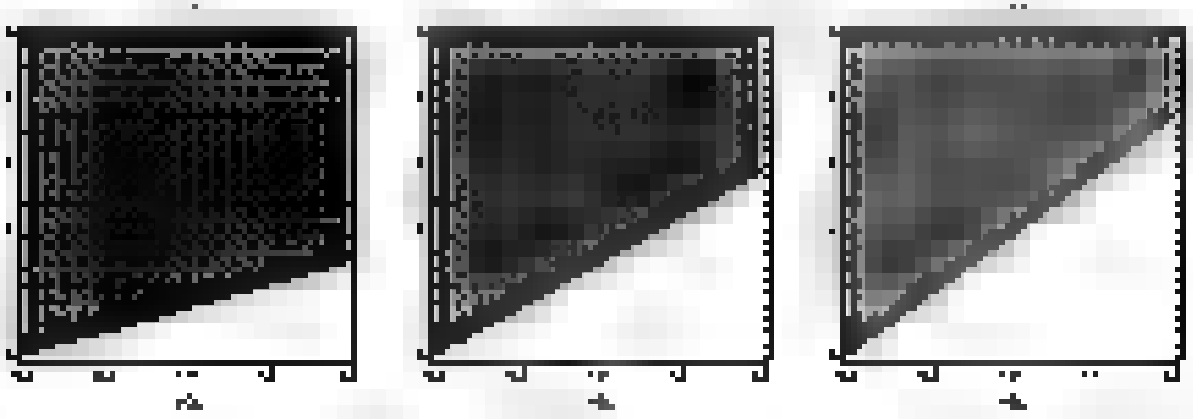

[illegible]

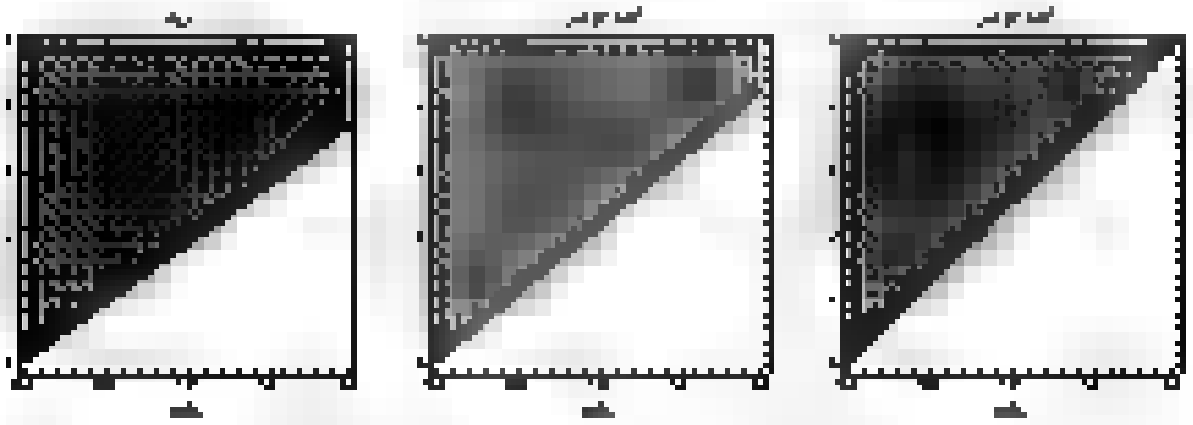

[illegible]

$$[illegible] \tag{illegible}$$

[illegible]

$$[illegible] \tag{illegible}$$

[illegible]

$$\frac{[illegible]}{[illegible]} \tag{illegible}$$

[illegible]

4.4 Superradiance scattering of the scalar field off Reissner-Nordström black holes

To obtain the superradiance scattering of scalar field with small μ we consider the Klein-Gordon equation (4.1) and the equation (4.2). For the Reissner-Nordström black hole, we can separate the variables of the Klein-Gordon equation [156]

$$\frac{1}{r^2}\frac{d}{dr}\left(\Delta\frac{dR_{\omega lm}(r)}{dr}\right)+\left(\frac{\omega^2 r^2}{\Delta}-\frac{\lambda_{lm}r^2}{\Delta}\right)R_{\omega lm}(r)$$

$$=\left(\mu^2+\frac{2Mr-Q^2}{r^2}\right)\sqrt{\frac{(2l+1)(l-m)!}{4\pi(l+m)!}}\,P_{lm}(\cos\theta)\qquad (4.57)$$

and for the angular part we have

$$\sin\theta\frac{d}{d\theta}\left(\sin\theta\frac{dP_{lm}(\theta)}{d\theta}\right)+\left(\lambda_{lm}\sin^2\theta-m^2\right)P_{lm}(\theta)$$

$$=\sqrt{\frac{(2l+1)(l-m)!}{4\pi(l+m)!}}\,m^2\,P_{lm}(\theta)\qquad (4.58)$$

where we have $\Delta=r^2-2Mr+Q^2$. The angular eigenvalue λ_{lm} in Reissner-Nordström black hole is given by

$$\lambda_{lm}=\lambda_{lm}^{(0)}+\frac{\mu^2(Q^2-2M^2)}{2}+\cdots\qquad (4.59)$$

For simplicity, we consider the case of $\mu M\ll 1$. We can obtain the eigenvalue λ_{lm} as $\sqrt{\lambda_{lm}+\frac{1}{2}}=l+\frac{1}{2}$ when $\mu=0$. Then, we can expand the angular eigenvalue λ_{lm} in terms of μM as follows:

$$\lambda_{lm}=l(l+1)-\frac{\mu^2Q^2}{2}+\cdots\qquad (4.60)$$

The effective potential that governs scattering reads

$$V_{\omega lm}(r)=\frac{\Delta}{r^4}\left(\mu^2+\frac{2Mr-Q^2}{r^2}\right)\sqrt{\frac{(2l+1)(l-m)!}{4\pi(l+m)!}}\,P_{lm}(\cos\theta)$$

$$+\sqrt{\frac{(2l+1)(l-m)!}{4\pi(l+m)!}}\,\frac{\Delta}{r^4}\,m^2\,P_{lm}(\cos\theta)\qquad (4.61)$$

where $m=0,1,2,\cdots,l$. We are now in a position to study the scattering of the scalar field around Reissner-Nordström black hole. We have presented the numerical method to study the scattering of the scalar field in the previous section. In the asymptotic region, the solutions of the radial equation have the form

$$\lim_{r\to\infty}R_{\omega lm}(r)=\frac{1}{\sqrt{2\omega}}\left(e^{-i\omega r_*}+\mathcal{R}e^{i\omega r_*}\right),\qquad r_*=r+\cdots\qquad (4.62)$$

where $r_*=r+\frac{2M-Q^2}{r-r_+}\ln\frac{r-r_+}{M}+\cdots$ and the reflection coefficient $\mathcal{R}$ is given by

$$\frac{\mathcal{R}}{\mathcal{I}}=\frac{\omega^2(r_+-r_-)^2-(\lambda_{lm}+1)^2}{2i\omega(\lambda_{lm}+1)},\qquad r_\pm=M\pm\sqrt{M^2-Q^2}\qquad (4.63)$$

Note that in the low-frequency regime, wave function and partial absorption cross section are typically characterized by the s-wave. However, the absorption of the massless scalar field is suppressed.

We are now in a position to study the superradiant behavior of the radial equation. In the near-horizon region, the radial equation (4.46) has the following asymptotic behavior

$$R_{\omega lm}(r)\to\begin{cases}\dfrac{e^{-i(\omega-m\Omega_H)r_*}}{\sqrt{2(\omega-m\Omega_H)}}+\mathcal{R}\dfrac{e^{i(\omega-m\Omega_H)r_*}}{\sqrt{2(\omega-m\Omega_H)}} & \text{for } r_*\to-\infty\\ \mathcal{I}\dfrac{e^{-i\omega r_*}}{\sqrt{2\omega}} & \text{for } r_*\to\infty\end{cases}\qquad (4.64)$$

4.5 Calculation of the amplification factor Z_2 for superheating

Here $\sigma^{(1)}$ represents the amplitude of the moving wall. We first calculate $\sigma_0^{(1)}$ in the corresponding quantity of the corresponding problem with stability and then we calculate the perturbed part of the quantity $\sigma^{(1)}$ by $\sigma_0^{(1)}$.

Let us now compute the Wronskian for the region near the interface and infinity. It is found that the solution in that region is

$$W_{\sigma} \quad \sigma^{(1)} \frac{d\sigma_0^{(1)}}{d\sigma} \quad \sigma_0^{(1)} \frac{d\sigma^{(1)}}{d\sigma} \tag{4.45}$$

and the Wronskian in the region is

$$W \quad \Gamma \frac{d\sigma}{d\sigma} \quad \sigma \frac{d\Gamma}{d\sigma} \tag{4.46}$$

The relation we should calculate. Using knowledge of standard theory of acoustic diffusion, the solution should be found that there is a relation with the amplitude of the pressure. Then, the Wronskian is given by the pressure relation between the amplitude of the pressure and the velocity in the interface region of the wall

$$\sigma_0^{(1)} \quad \sigma_0^{(1)} \quad \frac{\sigma}{\sigma_0} \sigma^{(1)} \tag{4.47}$$

The above equation is valid for $\sigma \quad \sigma^{(1)}$ the solution is valid for superheating and the amplified solution is the solution for the region $\sigma^{(1)} \quad \sigma^{(1)}$ holds superheating

4.5 Calculation of the amplification factor Z_2 for superheating

We consider the initial solution (4.50) as

$$\sigma^{(1)} \frac{d^2\sigma_{\sigma\sigma}}{d\sigma^2} \quad \frac{\sigma}{\sigma} \quad \frac{d\sigma_{\sigma\sigma}}{d\sigma} \tag{4.48}$$

$$+ \quad \frac{\sigma(\sigma) \quad \sigma(\sigma + \sigma^{(1)}) \quad \sigma\sigma}{\sigma} \quad \sigma \, \sigma^{(1)}(\sigma) \quad \sigma(\sigma + \sigma) \quad \sigma(\sigma) \quad \text{where} \quad \sigma_{\sigma} \quad \sigma$$

We will derive the same method and the boundary conditions are to find such a single solution satisfying the outer region in stability and the region solution is at initial point. We apply the change of variable $\sigma = \sigma(\sigma)$. Using the change of variable equation (4.48) under the approximation $\sigma \ll \sigma$ becomes

$$\frac{\sigma(\sigma) \quad \sigma(\sigma)}{\sigma \quad \sigma} \frac{d^2\sigma_{\sigma\sigma}}{d\sigma^2} + \sigma \frac{\sigma(\sigma) \quad \sigma(\sigma)}{\sigma(\sigma) \quad \sigma(\sigma)} \frac{d\sigma_{\sigma\sigma}}{d\sigma} \tag{4.49}$$

$$\sigma^{(1)} + \sigma^{(1)} \frac{\sigma(\sigma) \quad \sigma(\sigma)}{\sigma(\sigma + \sigma)} \quad \sigma(\sigma) + \quad \sigma^{(1)} \sigma(\sigma) + \quad \frac{\sigma \sigma \sigma(\sigma)}{\sigma} \quad \sigma(\sigma)$$

$$\frac{\sigma^{(1)}\sigma}{\sigma} \sigma(\sigma + \sigma) \quad \sigma^{(1)} \sigma(\sigma) + \sigma \quad \sigma(\sigma) = \sigma$$

where $\sigma = \sigma(\sigma \quad \sigma)$ and $\sigma = \frac{\sigma \sigma \sigma(\sigma)}{\sigma}$. Now we neglect the terms $\sigma(\sigma)$ and $\sigma^{(1)}\sigma(\sigma)$ and hence the above equation reduces to

$$\sigma^{(1)}(\sigma) \quad \sigma(\sigma) \frac{d^2\sigma_{\sigma\sigma}}{d\sigma^2} \quad \sigma(\sigma) + \sigma(\sigma) \quad \sigma(\sigma) \frac{d\sigma_{\sigma\sigma}}{d\sigma} \quad \sigma(\sigma) \quad \sigma^{(1)} \quad \sigma(\sigma) + \sigma(\sigma) \quad \sigma(\sigma) \sigma(\sigma) \quad \sigma \tag{4.50}$$

The approximation $\sigma(\sigma) \sigma$ is obtained from the consideration that the amplitude wavelength of the boundary perturbation. We assume the physical parameters are such that the wavelength is

A2 CALCULATION OF THE AMPLIFICATION FACTOR A_n FOR SUPERRADIANCE

The general solution of the above equation is a linear combination of Legendre functions of the first kind $P_n(x)$ and the second kind $Q_n(x)$:

$$R_{n\omega}(r) = \alpha P_n\left(\frac{r}{r_+}\right) + \beta Q_n\left(\frac{r}{r_+}\right) \qquad (A.51)$$

Here α and β are constants.

$$P_n(x) = \frac{1}{2^n n!}\frac{d^n}{dx^n}(x^2-1)^n \qquad Q_n(x) = \frac{1}{2}P_n(x)\ln\frac{x+1}{x-1} - W_{n-1}(x) \qquad (A.52)$$

where $W_{n-1}(x)$ is a polynomial of degree $n-1$. The Legendre function of the second kind $Q_n(x)$ has a logarithmic singularity at $x=1$:

$$Q_n(x) \sim -\frac{1}{2}\ln(x-1) + \frac{1}{2}\ln 2 - \sum_{k=1}^{n}\frac{1}{k} \qquad (A.53)$$

The regular solution is obtained by imposing the condition that at the event horizon there is no outgoing mode. In the near region, we can neglect the ω dependence of the above expression. The case of $\omega M \ll 1$ for large n is considered.

$$R_{n\omega} \sim \frac{\Gamma(n+1)\Gamma(2n+1)\left(\frac{r}{r_+}-1\right)^{n/2}}{\Gamma(n+1)\Gamma(2n+1)\left(\frac{r}{r_+}-1\right)^{n/2}} + \frac{\Gamma(n+1)\Gamma(2n+1)\left(\frac{r}{r_+}-1\right)^{n/2}}{\Gamma(n+1)\Gamma(2n+1)\left(\frac{r}{r_+}-1\right)^{n/2}} \qquad (A.54)$$

For large n, we can use the approximation $\Gamma(n+1) \sim n!$ and $\Gamma(2n+1) \sim (2n)!$. We may drop all the terms except those which contribute the leading order in n, and the radial equation (A.49) reduces to

$$\frac{d^2R_{n\omega}}{dr^2} + \frac{dR_{n\omega}/dr}{r-r_+} - \frac{n(n+1)}{r(r-r_+)}R_{n\omega} = 0 \qquad (A.55)$$

where $r_+ = 2M$. Equation (A.55) is the general solution

$$R_{n\omega}(r) = \alpha\left(\frac{r}{r_+}-1\right)^{n/2}\left(\frac{r}{r_+}\right)^{n/2}\left(\frac{r}{r_+}+\frac{1}{2}\right)^{n/2} + \beta\left(\frac{r}{r_+}-1\right)^{n/2}\left(\frac{r}{r_+}\right)^{n/2}\left(\frac{r}{r_+}+\frac{1}{2}\right)^{n/2}\ln\left(\frac{r}{r_+}-1\right) + \cdots \qquad (A.56)$$

where α and β are constants. The boundary condition requires that the solution (A.56) must be regular. Therefore, we must set $\beta = 0$. Then the equation (A.56) takes the form

$$R_{n\omega}(r) = \alpha\left(\frac{r}{r_+}-1\right)^{n/2}\left(\frac{r}{r_+}\right)^{n/2}\left(\frac{r}{r_+}+\frac{1}{2}\right)^{n/2} \qquad (A.57)$$

The solutions (A.54) and (A.57) have overlapping regions and are reasonable for matching. The matching of the asymptotic solutions (A.54) and (A.57) enables us to determine the constant α as follows:

$$\alpha = \frac{\Gamma(n+1)\Gamma(2n+1)}{\Gamma(n+1)\Gamma(2n+1)}$$

4.2 CALCULATION OF THE AMPLIFICATION FACTOR A_{ij} FOR SUPERRADIANCE

$$A_{ij} = \frac{\sqrt{\text{[illegible]}}}{\text{[illegible]}} \tag{4.24}$$

The optical equation (4.24) should be solved, which gives

$$\text{[illegible]}$$

$$\text{[illegible]}$$

With the approximation [illegible] the equation (4.24) is reduced to the above equation. For initial inversion (4.25)

$$\text{[illegible]}$$

we get

$$\text{[illegible]} \tag{4.26}$$

and

$$\text{[illegible]} \tag{4.27}$$

Putting the value of [illegible] from (4.26) into the above equation we get [134]

$$\text{[illegible]} \tag{4.28}$$

[illegible]

The amplification factor is given by

$$A_{vm} = \frac{|A_v|^2}{[illegible]} \qquad (3.43)$$

Equation (3.43) is a general expression of amplification factor. It is used in finding gain of the asymptotic and mid-frequency regions. When $\frac{C_{gd}}{[illegible]}$ is equal to zero, that is only there will be gain in amplification. [illegible] corresponds to zero impedance. However, when the amplification factor is negative, it indicates a loss which corresponds to the [illegible] of the amplification.

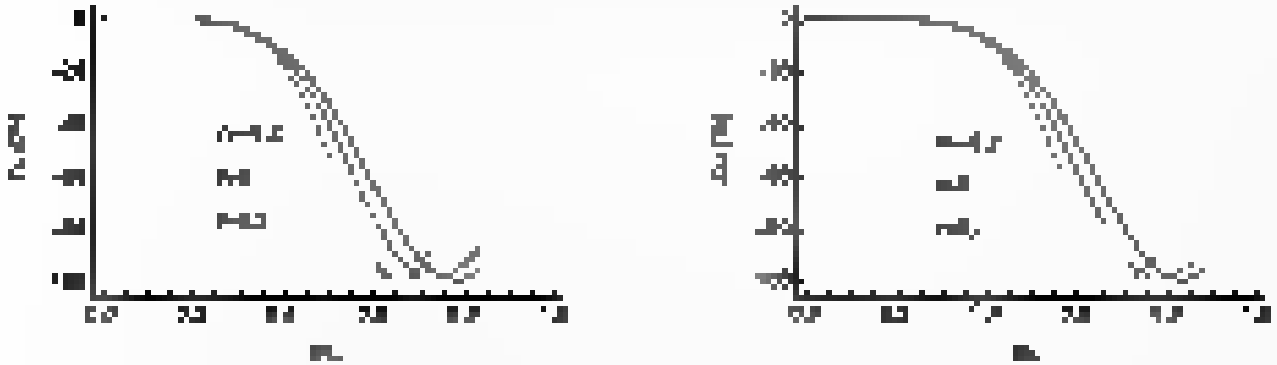

Fig. 3.17 Comparison of amplification between [illegible] and [illegible]

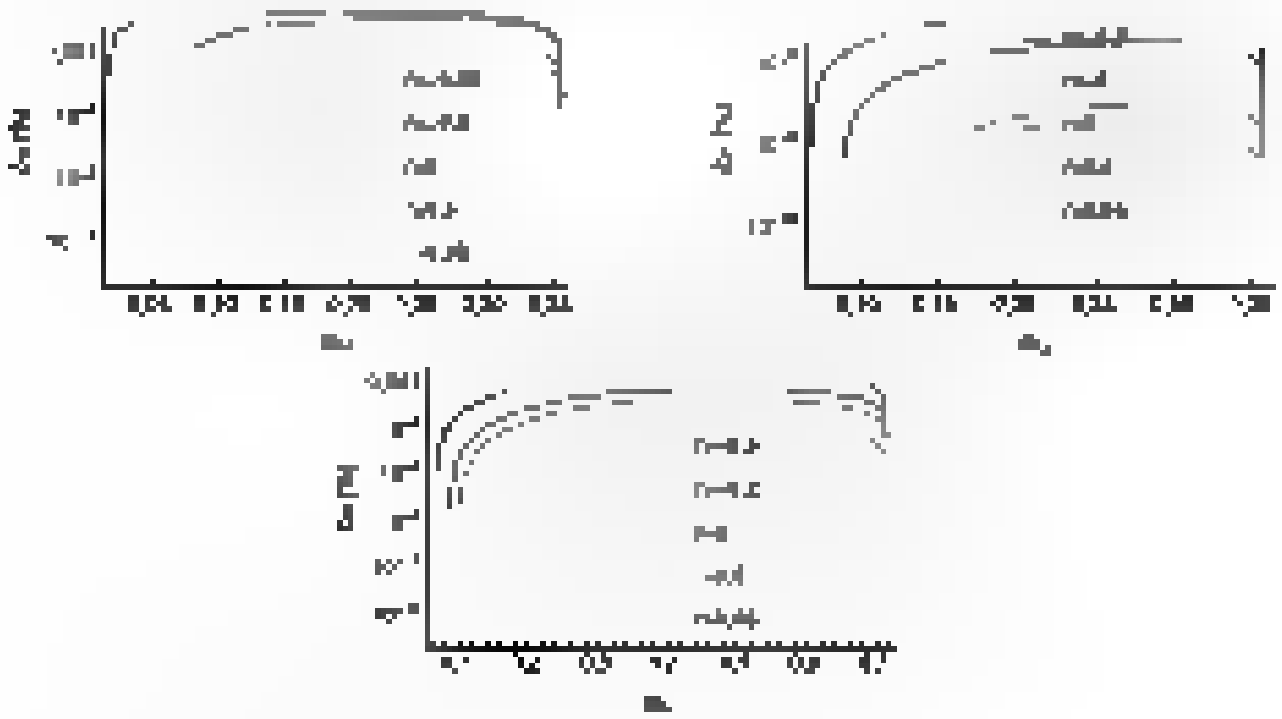

[illegible]

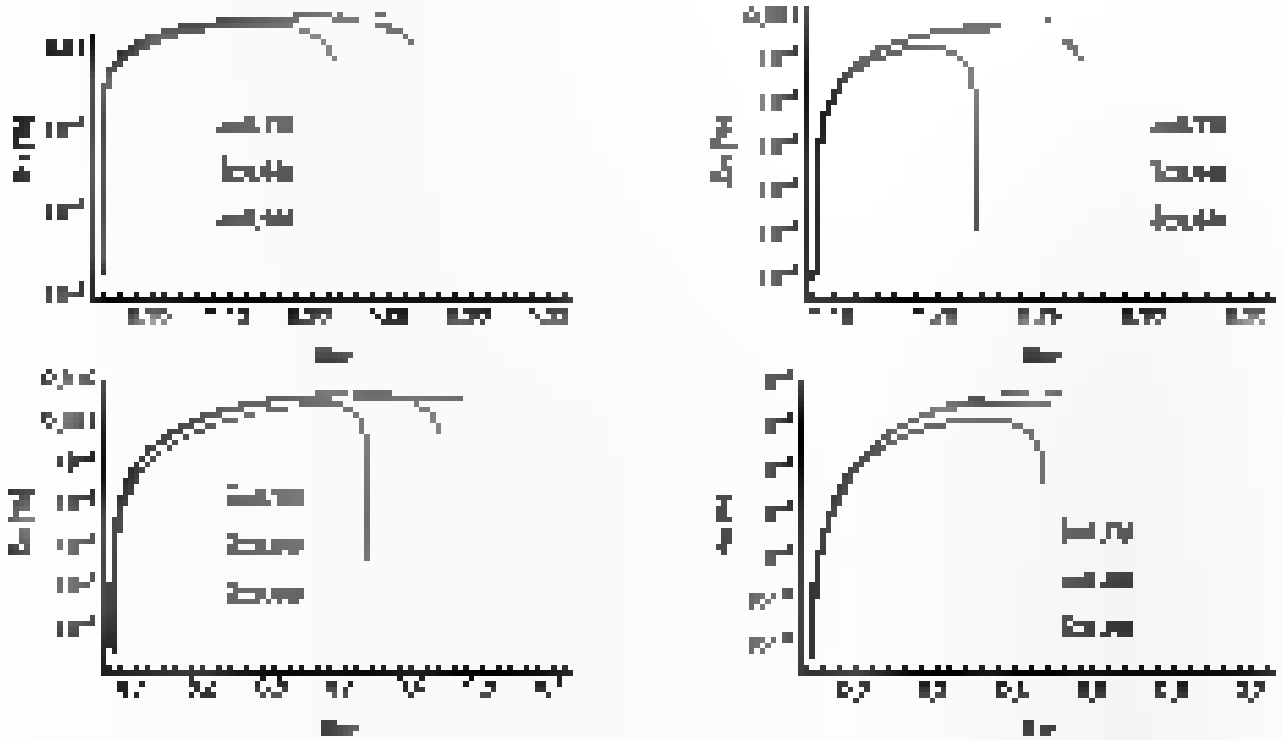

[illegible]

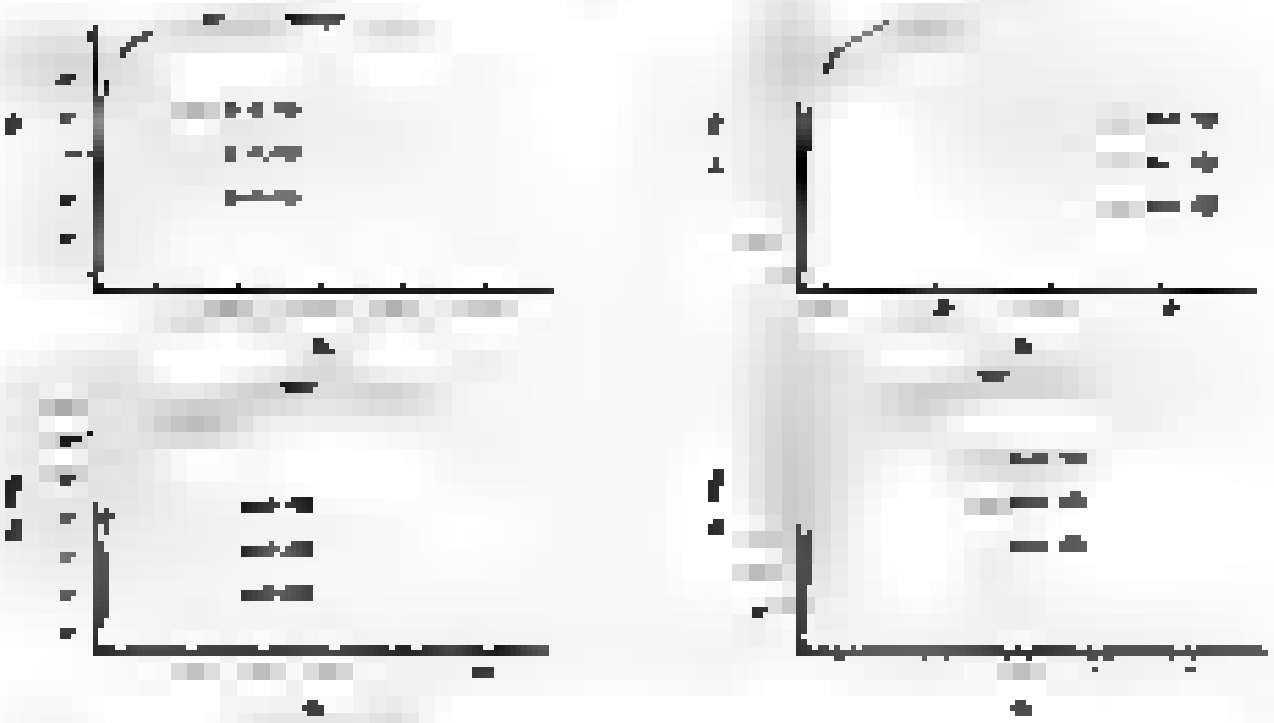

Demanding the black hole bomb mechanism, we should have the following solution for the radial equation (4.64) [illegible]

$$[illegible] \tag{4.66}$$

The above solution represents the physical boundary conditions that the wave is [illegible] at the black hole horizon [illegible] while [illegible] spatially decaying exponentially (bounded) provided that [illegible]. With the new radial function

$$[illegible] \tag{4.67}$$

the radial equation (4.65) becomes

$$[illegible] \tag{4.68}$$

with

$$[illegible] \tag{4.69}$$

where [illegible] Regge-Wheeler equation. Asymptotic form of the effective potential [illegible]

$$[illegible] \tag{4.70}$$

[illegible]

$$[illegible] \tag{4.71}$$

[illegible]

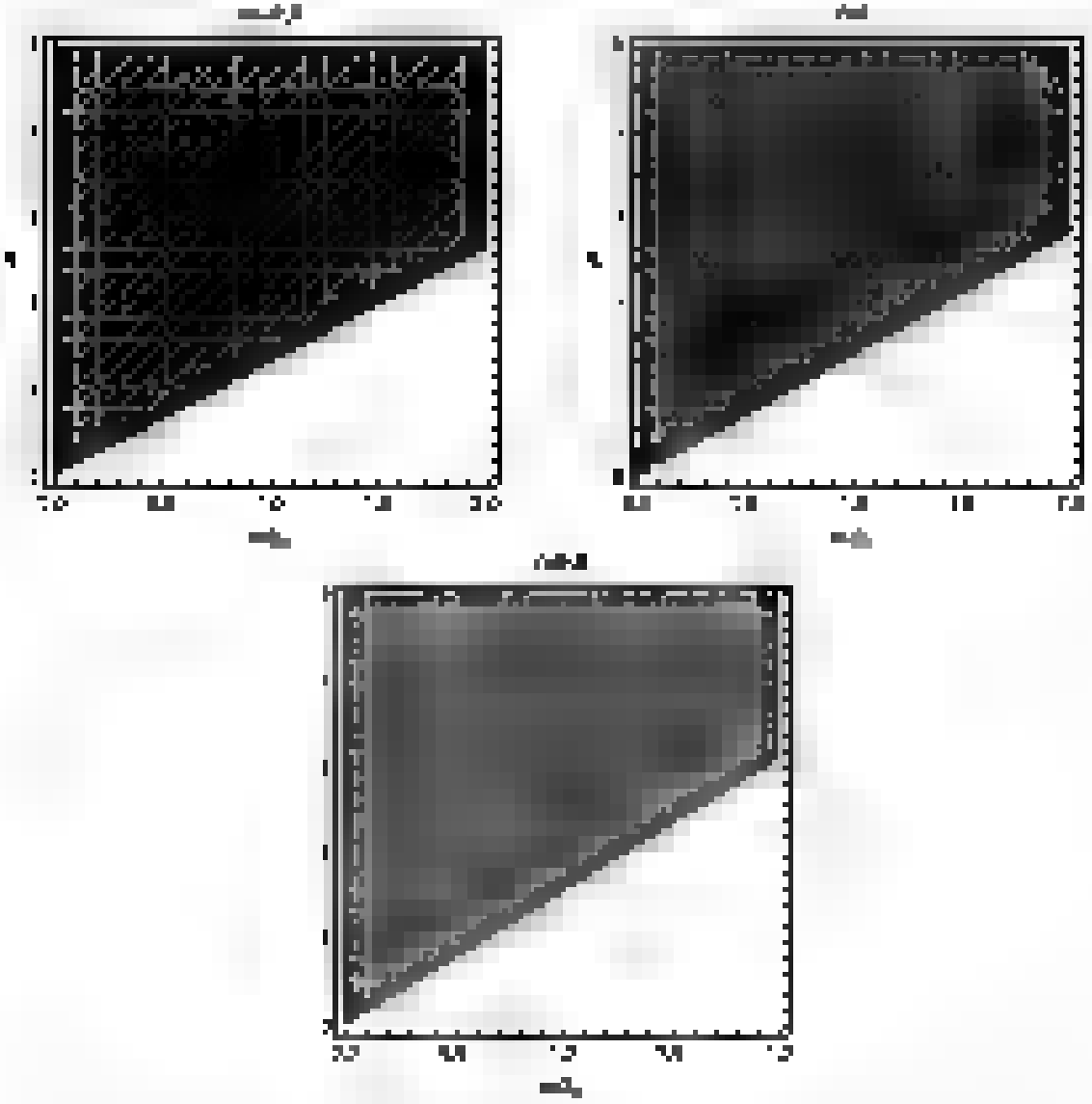

Figure [illegible]

Chapter 7

Constraining parameters involved in modified gravity using observational data for M87* black hole

[illegible]

5.1 Constraining the parameters for the Kerr-Sen-like black hole surrounded by plasma

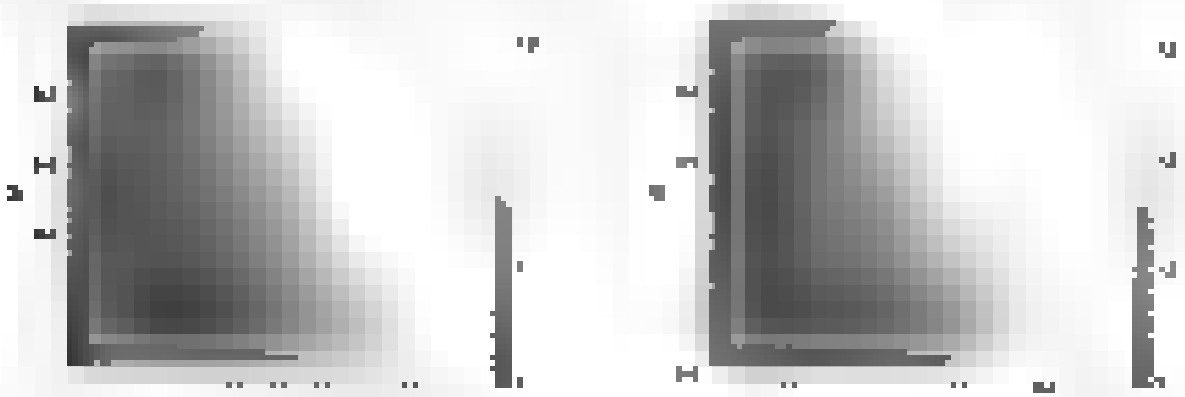

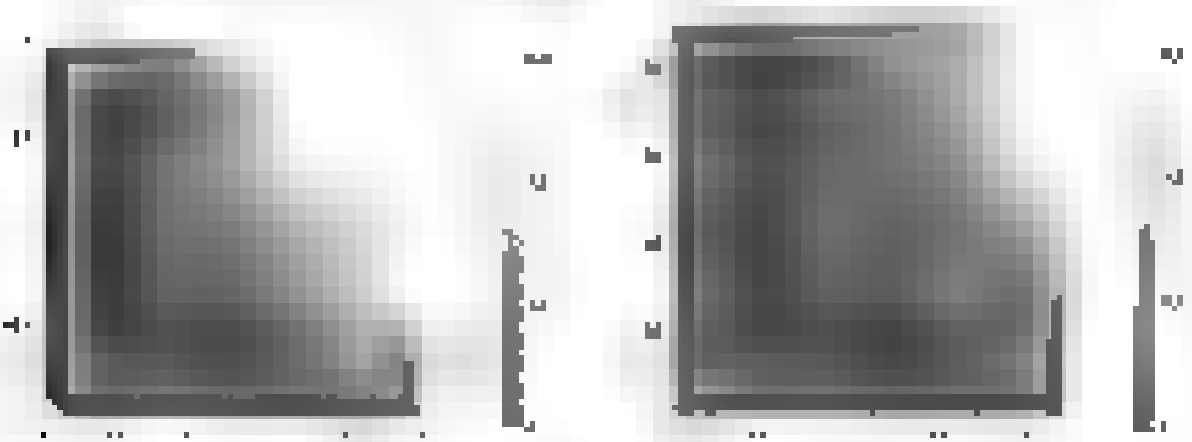

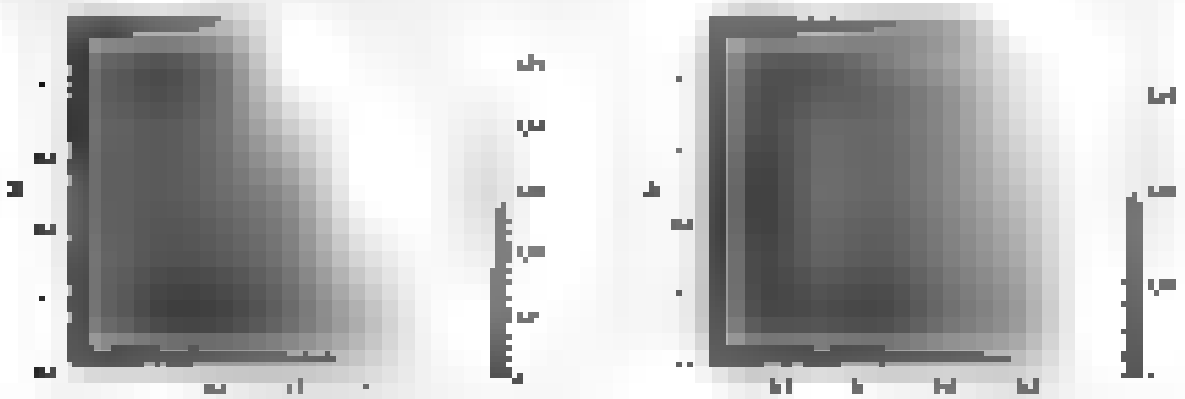

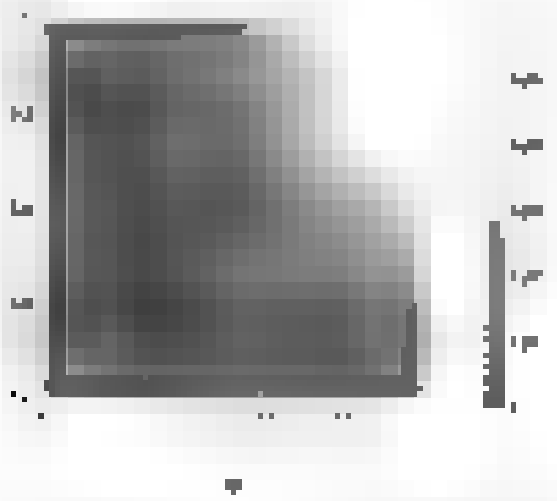

Figure 10. The above plot is for the relative error $\Delta\Omega_{\rm QNM}/\Omega_{\rm QNM}$ as a function of black hole parameters. The left is for [illegible] and the right is for [illegible].

Figure 11. [illegible] The above plot is for the relative error $\Delta\Omega_{\rm QNM}/\Omega_{\rm QNM}$ as a function of black hole parameters. The left is for [illegible] and the right is for [illegible].

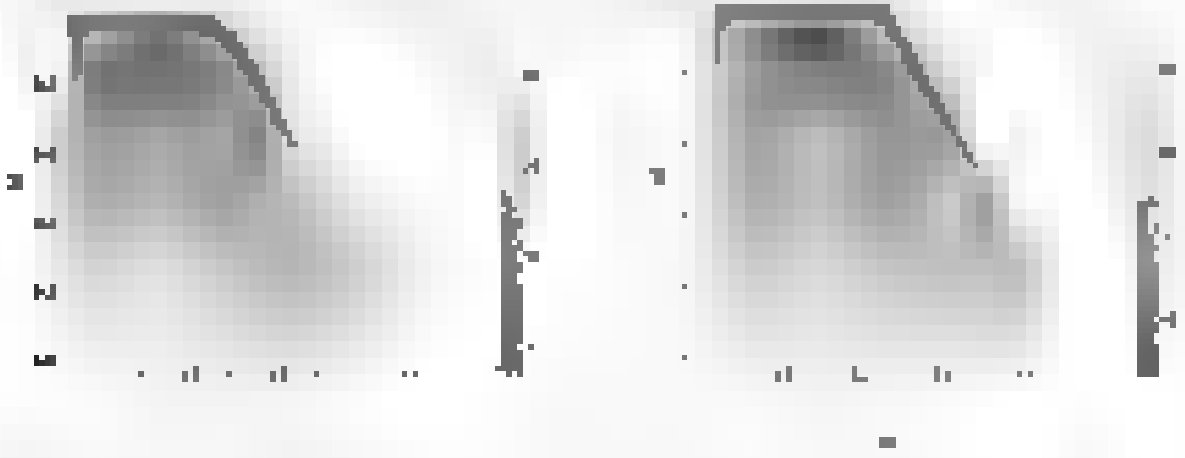

Figure 12. The above plot is for angular [illegible] as a function of black hole parameters. The left is for [illegible] and the right is for [illegible]. The right is for [illegible] and the left is for [illegible].

Figure 13. The above plot is for angular [illegible] as a function of black hole parameters. The left is for [illegible] and the right is for [illegible]. The right is for [illegible] and the left is for [illegible].

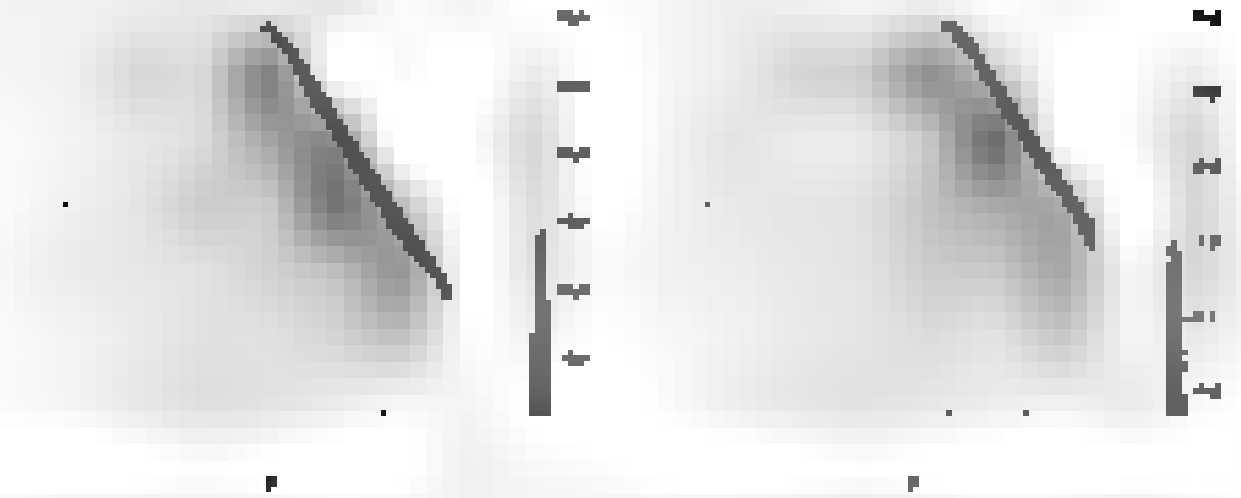

7.1 Constraining the charge parameter in Kerr-Sen-like black hole in accretion from the observed data for M87*

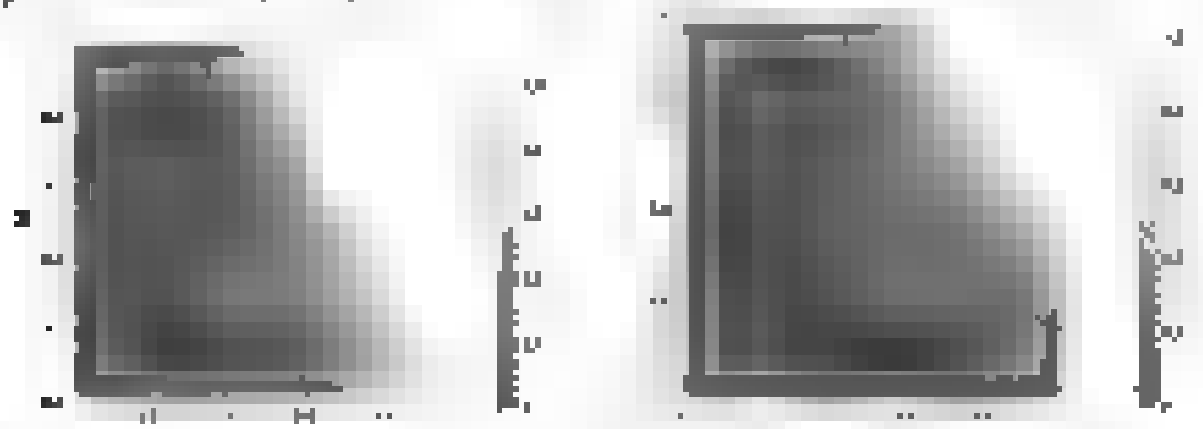

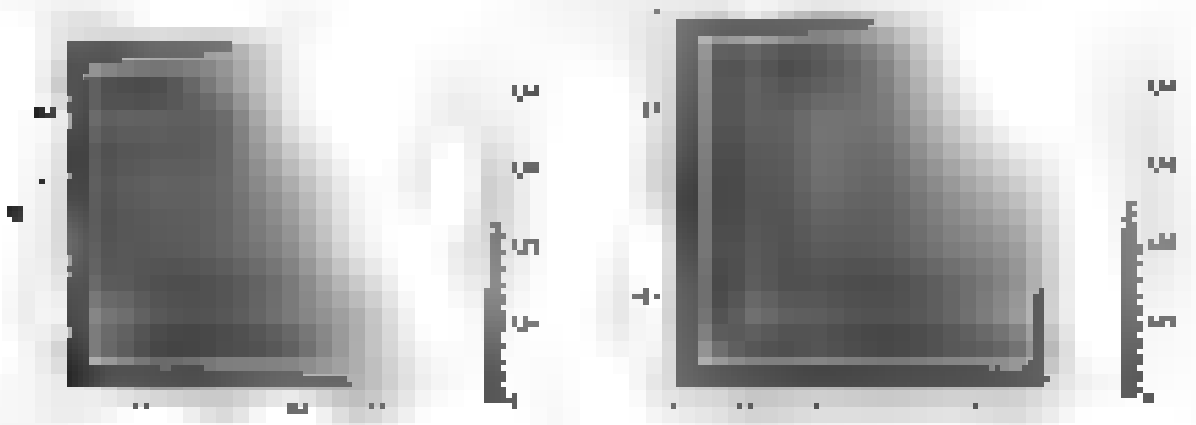

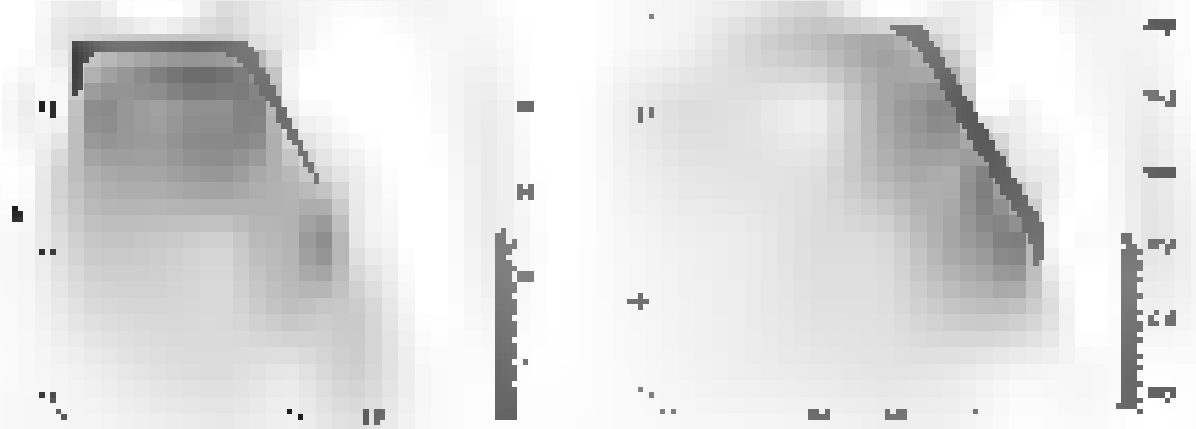

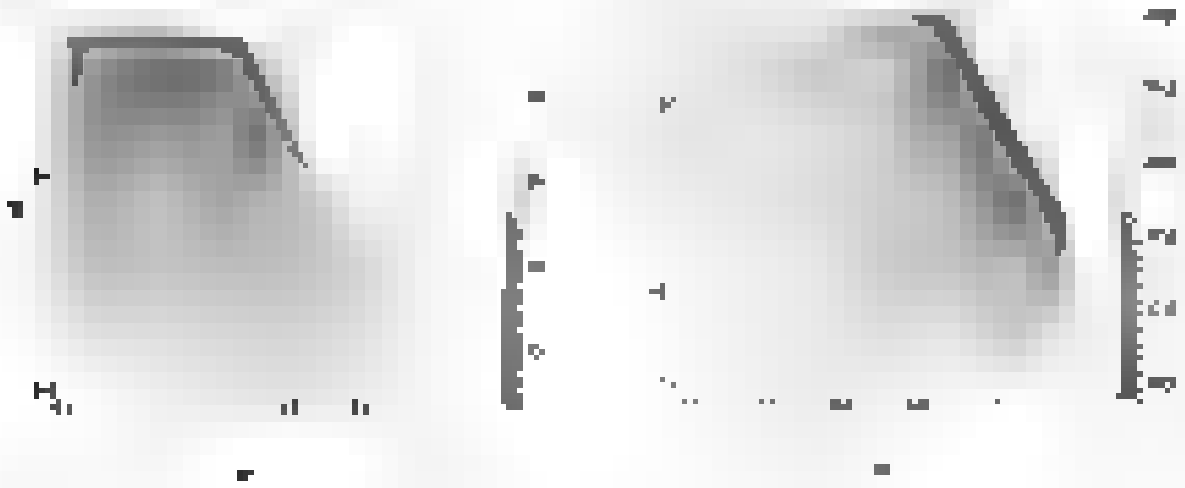

Figure 11. The left panel shows the [illegible] and the right panel shows the [illegible] The thick solid line [illegible]

[illegible]

5.3 Constraining the main-sequence tidal parameter Q_* from the observed data for HAT

[illegible]

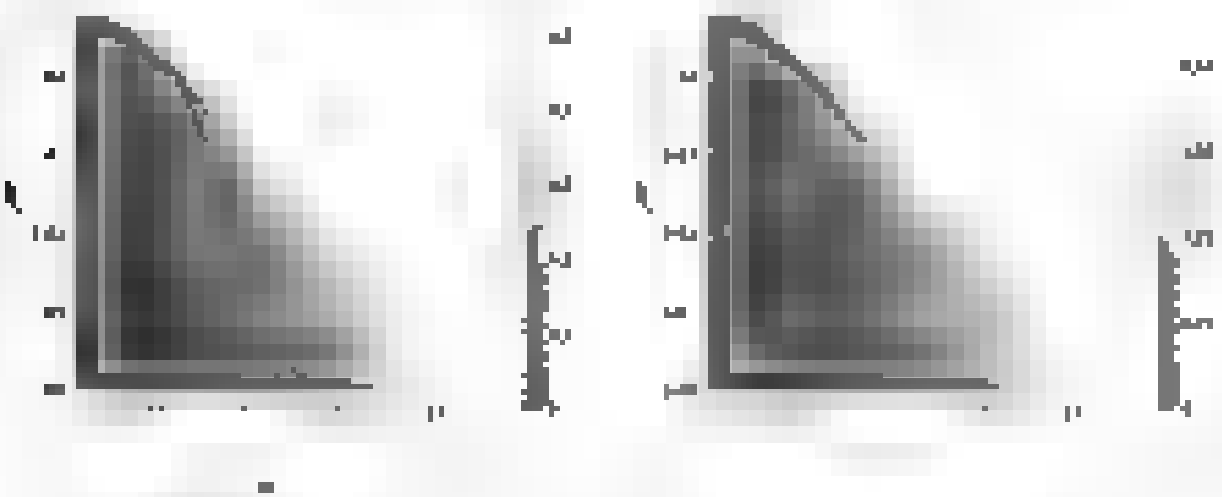

Figure 12. [illegible]

[illegible]

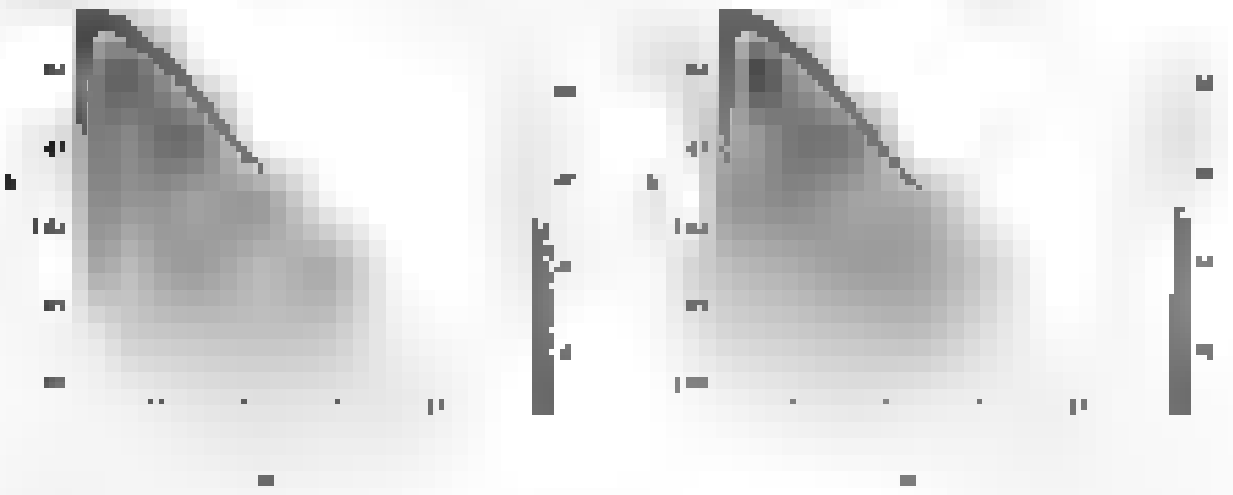

Figure 10: Panels left panel the mean convergence angle κ and on the right panel the deflection angle α [illegible]

From the plot [illegible] the convergence angle κ [illegible] and α [illegible] the corresponding [illegible] is [illegible] [illegible] and [illegible] parameter space. The cumulative [illegible] in the [illegible] [illegible] [illegible]

Chapter 3

[illegible]

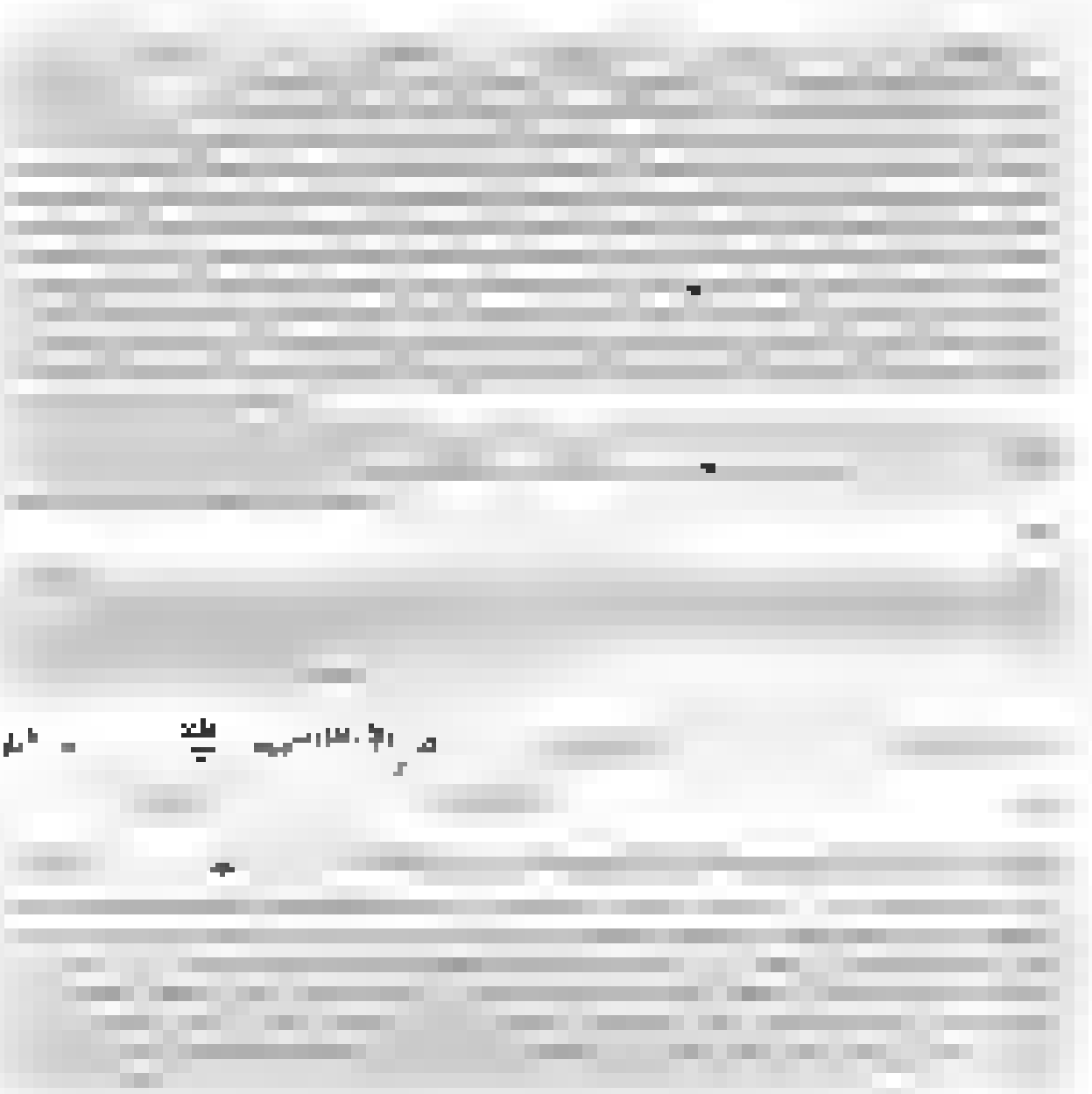

For a lens at z_l and source at z_s, the deflection angle from the lensing term [Section 3.1]

$$\hat{\alpha}(\boldsymbol{\theta}) = \frac{4GM}{c^2}\frac{D_{ls}}{D_l D_s}\frac{2}{\theta - \theta'} \quad \text{for } \theta \gg \theta_E \tag{4.1}$$

where the lens equation $\beta = \theta - \alpha(\theta)$ is given by

$$\beta(\theta) = \theta - \frac{\theta_E^2}{\theta} \quad \text{and} \quad \beta(\theta) = \theta - \frac{\theta_E^2}{\theta} \tag{4.2}$$

The solution of the lens equation is obtained by solving the quadratic

$$\theta^2 - \beta\theta - \theta_E^2 = 0 \tag{4.3}$$

which has two solutions for different values of β. For a fixed value of β and θ_E, there are two different values of θ corresponding to the two images formed by the lens, as described by the lens equation (4.1).

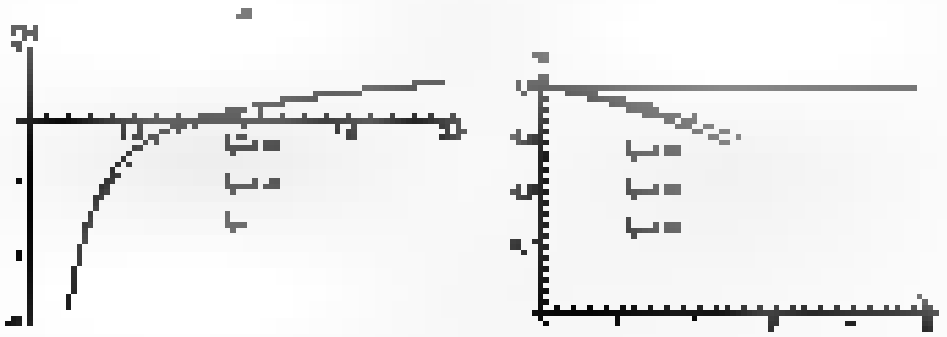

Figure 4. The left panel shows the two solutions of the lens equation, θ_+ and θ_-, as functions of the source position β. The right panel shows the magnification of each image as a function of β, for various values of θ_E.

Figure 4 shows that the two images are always on opposite sides of the lens, with one image always being brighter than the other. Note that for $\beta \gg \theta_E$, the brighter image is very close to the source position, while the fainter image is very close to the lens. However, as β decreases, the two images become more and more similar in brightness, and for $\beta = 0$ (perfect alignment) the two images merge into a ring of radius θ_E, known as the Einstein ring. Note that the total magnification of the two images is always greater than 1, so lensing always increases the total observed flux of a source, even though it redistributes the light into two separate images.

4. Strong and weak gravitational lensing

The lens equation we derived in the previous section applies to a point mass lens. In reality, lenses are extended objects, and the deflection of light rays depends on the mass distribution of the lens. For a lens with surface mass density $\Sigma(\boldsymbol{\theta})$, the deflection angle is given by the two-dimensional integral

$$\hat{\boldsymbol{\alpha}}(\boldsymbol{\theta}) = \frac{4G}{c^2}\frac{D_{ls}}{D_l D_s}\int \Sigma(\boldsymbol{\theta}')\,\frac{\boldsymbol{\theta} - \boldsymbol{\theta}'}{|\boldsymbol{\theta} - \boldsymbol{\theta}'|^2}\,d^2\theta' \tag{4.4}$$

In the strong and weak gravitational lensing regimes, we are interested in the case where the source is close to the optical axis, so that the deflection angle is small. In this limit, we can expand the lens equation to first order in θ/θ_E, and the resulting linear mapping between source and image positions can be written in matrix form as

$$\begin{pmatrix} \beta_1 \\ \beta_2 \end{pmatrix} = \begin{pmatrix} 1 - \kappa - \gamma_1 & -\gamma_2 \\ -\gamma_2 & 1 - \kappa + \gamma_1 \end{pmatrix} \begin{pmatrix} \theta_1 \\ \theta_2 \end{pmatrix} \tag{4.5}$$

where κ is the convergence, which measures the magnification of the image, and $\gamma = \gamma_1 + i\gamma_2$ is the complex shear, which describes the stretching of the image along a preferred direction. The magnification matrix $\mathcal{A} = \partial\beta/\partial\theta$ is the inverse of the Jacobian matrix of the lens mapping, and its determinant $\det \mathcal{A} = (1-\kappa)^2 - |\gamma|^2$ gives the magnification of the image. Critical curves, where the magnification formally diverges, occur when $\det \mathcal{A} = 0$, and their corresponding caustics in the source plane are the images of the critical curves under the lens mapping.

A. STRONG AND WEAK GRAVITATIONAL COUPLING

Inflaton In the slow-roll approximation along the gradient flow from Eq. (A4) and Eq. (A5) we obtain the following equations for the scalar problem

$$\frac{d\phi}{dt} = -\frac{1}{3H}\frac{dV}{d\phi} \tag{A34}$$

Thus, the effective potential $V_{\rm eff}(\phi)$ cannot vanish to be

$$V_{\rm eff}(\phi) = \frac{\partial^2 V(\phi)}{\partial(\phi)} = \frac{\partial^2}{\partial \phi} \qquad + \text{const.} \tag{A35}$$

For circular photon orbits of radius r, the effective potential must satisfy the conditions

$$\frac{dV_{\rm eff}}{dr}\Big|_{r_c} = 0 \tag{A36}$$

which implies

$$\frac{\partial^2 V(\phi)}{\partial(\phi)} = \frac{\partial \quad \partial}{\partial \phi \partial} \tag{A37}$$

Using the result of the above equations we have

$$\frac{\partial}{\partial} \quad \frac{\partial^2}{\partial(\phi)} \quad \frac{\partial}{\partial} \quad \frac{\partial}{\partial(\phi)} + \quad = 0 \tag{A38}$$

Now, the condition $\frac{\partial^2 V}{\partial \phi^2} < 0$ for a maximum and the fact that the value of the potential at the point is zero, we can obtain the gravitational coupling constant α and the effective mass $m_{\rm eff}$ of the photon. The photon enters the effective large distance region that approximates the black hole environment. Such particles by the following a maximum distance $r_{\rm max}$ and the effective mass $m_{\rm eff}$ of the photon by the following. The impact parameter $b_{\rm crit}$ and the maximum distance $r_{\rm max}$ are related to each other through the equation

$$b_{\rm crit} = \sqrt{\frac{r_{\rm max}}{V_{\rm eff}(r_{\rm max})}} \tag{A39}$$

where $V_{\rm eff}$ is given by

$$V_{\rm eff}(r_{\rm max}) = \frac{1}{2} + \quad + \quad = \frac{1}{2} \tag{A40}$$

The impact parameter corresponding to $r_{\rm max}$.

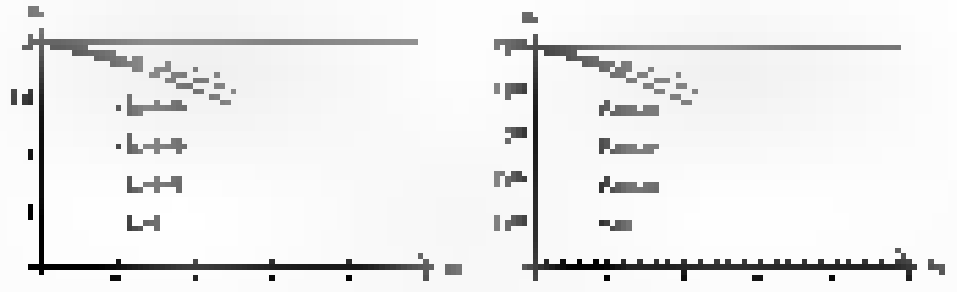

Figure 4 The shadowing effect of the [illegible] and the corresponding [illegible]

The curve in the figure shows the relation between the impact parameter $b_{\rm crit}$ and the maximum distance $r_{\rm max}$ which is the shadow region. The curve is obtained by the numerical calculation of the gravitational coupling constant α and the effective mass $m_{\rm eff}$ of the photon. The [illegible] is calculated

$$= [\text{illegible}] \tag{A41}$$

where

$$\cdots \qquad (6.7)$$

In the absence of a black hole, a photon would travel on a straight line separated by a minimum distance $\cdots$ from the center of the black hole. Due to the gravitational attraction of the black hole, the photon's trajectory is bent, resulting in a deflection angle $\cdots$. The deflection angle $\cdots$ depends on the impact parameter $\cdots$ and is determined by the mass of the black hole. More specifically, the impact parameter $\cdots$ is related to the deflection angle $\cdots$ by the equation $\cdots$. As the photon approaches the black hole, the deflection angle $\cdots$ increases, and the photon can even be captured by the black hole if it comes within the photon sphere, which is the region where the gravitational pull is strong enough to trap photons in orbit around the black hole.

Bozza et al. [41] developed an approximate analytical method to calculate the deflection angle of light rays in the strong field limit, which is particularly useful for studying the behavior of photons near black holes. According to this method, the deflection angle $\cdots$ can be approximated as a function of the impact parameter $\cdots$ and the photon sphere radius $\cdots$:

$$\cdots \qquad (6.8)$$

where $\cdots$ is a function that depends on the properties of the black hole, such as its mass and spin. The function $\cdots$ can be expressed as a power series in terms of the difference between the impact parameter and the photon sphere radius:

$$\cdots \qquad (6.9)$$

$$\cdots \qquad (6.10)$$

The function $\cdots$ is regular for all possible values of $\cdots$ and can be expanded as a Taylor series around the point $\cdots$. The coefficients $\cdots$ and $\cdots$ in the series are determined by the properties of the black hole and the geometry of the photon sphere. To calculate the deflection angle in the strong field limit, we can substitute the expansion of $\cdots$ into the equation for $\cdots$ and integrate over the appropriate range of $\cdots$. The result is an expression for $\cdots$ in terms of the impact parameter $\cdots$ and the photon sphere radius $\cdots$:

$$\cdots \qquad (6.11)$$

where $\cdots$ and $\cdots$ are given by the following integral expressions:

$$\cdots \qquad (6.12)$$

$$\cdots \qquad (6.13)$$

The gravitational lensing equation in the strong field limit can be written as [42]:

$$\cdots \qquad (6.14)$$

Explicitly, the components are

$$\cdots \qquad (6.15)$$

$$\cdots \qquad (6.16)$$

Here, $\cdots$ is the angular radius of the photon sphere. The function $\cdots$ is given by $\cdots$, which makes the integrand in $\cdots$ divergent. In order to regularize the integral, we can subtract the divergent part and define a new function $\cdots$ as follows:

$$\cdots \qquad (6.17)$$

6. STRONG AND WEAK GRAVITATIONAL FIELDS

Next, we expand $\gamma_{\mu\nu}(x,\eta)$ in the following fashion

$$\gamma_{\mu\nu}(x,\eta) = \frac{m_0 c^2 r_s}{M(\eta)} \gamma^{(0)}_{\mu\nu}(x) + \gamma^{(1)}_{\mu\nu}(x) + \mathcal{O}(\eta^2) \tag{6.37}$$

and we take the inner product $\langle \gamma_{\mu\nu}, \gamma_{\rho\sigma} \rangle$. With this, we can rewrite Eq. (6.36) as

$$\Gamma^{\mu}_{\nu\rho}(x,\eta) = \eta \ln\left(\frac{r_0}{r_s}\right) \gamma^{(0)}_{\mu\nu}(x) + \Gamma^{\mu}_{\nu\rho}(x,\eta) \tag{6.38}$$

where $\gamma^{(0)}_{\mu\nu}$ is given by

$$\frac{\eta^2 r_s}{\sqrt{-g^{(0)}}} \tag{6.39}$$

$$\Gamma^{\mu}_{\nu\rho} = \frac{\Lambda r_s}{\sqrt{-g^{(0)}}} \log\left(\frac{M r_s}{r_0^2}\right) \tag{6.40}$$

If we now expand Eq. (6.38) to second order in η, we can rewrite the Christoffel symbol as

$$\Gamma^{\mu}_{\nu\rho}(x,\eta) = \int \gamma^{(0)}_{\mu\nu}(x) \, \Gamma^{\mu}_{\nu\rho}(x,\eta) \, d\eta \tag{6.41}$$

$$= \Gamma^{\mu}_{\nu\rho}(x,\eta) \tag{6.42}$$

where

$$\Gamma^{\mu}_{\nu\rho} = \Gamma^{\mu}_{\nu\rho}(x,\eta) \tag{6.43}$$

Therefore, we can write the Christoffel symbol as

$$\Gamma^{\mu}_{\nu\rho}(x,\eta) = \Gamma^{\mu}_{\nu\rho} + \eta \, \Gamma^{\mu}_{\nu\rho}(x) \tag{6.44}$$

where

$$\Gamma^{\mu}_{\nu\rho}(x) = \frac{\gamma^{(0)}_{\mu\nu}(x)}{\sqrt{-g^{(0)}}} \frac{M r_s}{r_0^2} \tag{6.45}$$

Using the Christoffel symbol in Eq. (6.44) and the Riemann tensor in Eq. (6.45), we can now calculate the deflection angle of light in the weak gravitational field.

$$\alpha = \frac{4GM}{c^2 b} + \mathcal{O}\left(\frac{GM}{c^2 b}\right)^2 \tag{6.46}$$

where

$$\alpha = \frac{4}{\pi} \frac{\Gamma(\frac{3}{4})^2}{\Gamma(\frac{1}{4})^2} \tag{6.47}$$

$$\Gamma = \frac{\Gamma(\frac{3}{4})^2}{\Gamma(\frac{1}{4})^2} \tag{6.48}$$

In the limit of small η, we can recover the well-known result of general relativity. Therefore, our theory of gravity is consistent with the observations of light deflection in the weak gravitational field.

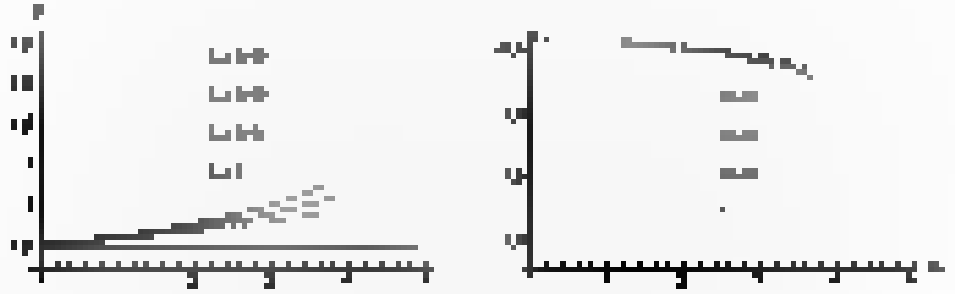

Figure 5. Plot showing the magnification of image 1 as a function of source position for a point mass lens with

As can be seen in Fig. 5, the magnification of image 1 increases as the source approaches the lens, and diverges when the source is exactly behind the lens. However, as the source position is increased, the magnification decreases rapidly, and becomes equal to 1 when the source is exactly behind the lens. This is because the image is demagnified in the direction perpendicular to the direction of motion of the source, and the source is stretched into a ring when it is exactly behind the lens. The image is then said to be an Einstein ring. The radius of the Einstein ring is called the Einstein radius. In the following, we will derive the relationship between the deflection angle and the impact parameter, and then we will derive the lens equation.

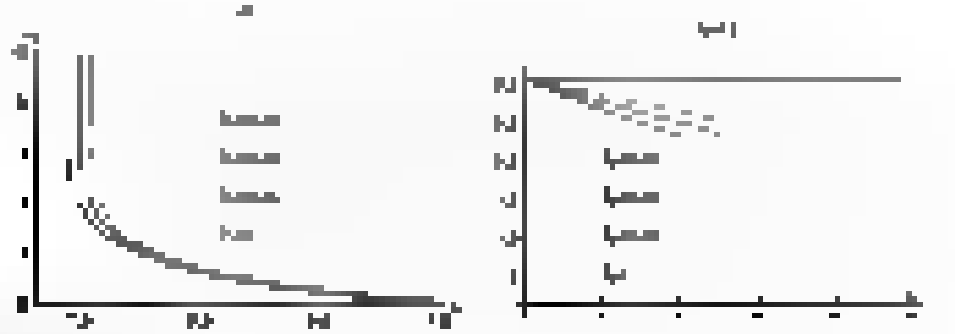

Figure 6. The left panel shows the variation of the deflection angle with respect to the impact parameter for different values of the mass. The right panel shows the variation of the deflection angle with respect to the mass for a fixed impact parameter.

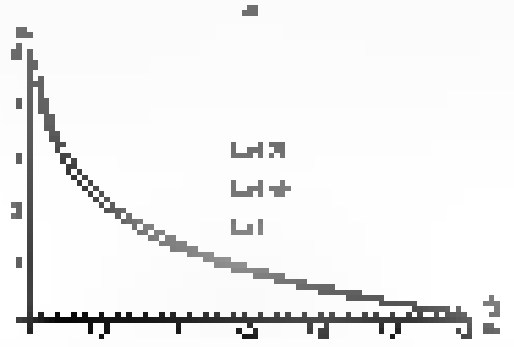

Figure 7. Relation between the deflection angle and the impact parameter for different values of the mass.

From the above relation we see that the deflection angle decreases with the impact parameter and increases with the mass of the lens (Fig. 6). Now, we see that the light ray passing close to the lens is deflected more than the light ray passing far away from the lens. This is because the gravitational force is stronger when the distance between the lens and the light ray is smaller. Now, we will derive the lens equation. We will first derive the relation between the deflection angle and the impact parameter. Here, we have $\alpha = \frac{4GM}{c^2 r_0}$ and $\beta = \theta - \frac{D_{LS}}{D_S}\alpha$. The deflection angle is a function of

[illegible]

[illegible] Observables in the strong field limit

[illegible]

$$r_n \qquad \frac{L\sin\theta}{} \tag{3.83}$$

Therefore we consider $\delta\theta$ $\theta_0^{\prime}$ and expand $\sin\theta$ around θ θ_0 in order to compute small angle. Then we can use the following Taylor expansion of the sine angle

$$\Delta\omega_0 \qquad \frac{\partial\Pi_{n1}}{\hbar\omega_1}\Delta\theta_n \tag{3.84}$$

Then we use the expression $\theta = \theta_0^{\prime} + \Delta\theta_n$ in Eq. (3.83) we obtain the following algebraic expression for η

$$\eta = \theta_0^{\prime} \quad \omega t_0 \qquad \frac{\cdot\omega_0 D_{1n}}{\hbar\omega_1 D_{0n}} \quad \Delta\theta_1 \tag{3.85}$$

Summation over n D holds for physically acceptable cases we can neglect the second term in the above equation as it depends on the last term. Hence the position of the n^{th} image is approximated by [illegible]

$$R_n \quad \theta_0^{\prime} \qquad \frac{\omega_0 D_{1n} \quad \theta_0^{\prime}}{2\hbar\omega_1 D_{0n}} \tag{3.86}$$

When $\theta = \theta_0^{\prime}$ the position of the image and the source coincide. It implies that the n^{th} source ray is not scattered any correction. Therefore, Eq. (3.86) will describe an image on the source and will vanish the medium although. To get the position of the image on the other side of the source, we must replace θ with $-\theta$

The study of the magnification of the image is also interesting. Magnification of the image is another good source of information [3,11] in addition to the position of the source. The magnification of the image is given by

$$M_n \quad = \quad \left|\frac{\Delta_n}{\partial\theta}\right|_{\theta} \tag{3.87}$$

$$= \quad \omega_0 \frac{\cdot\omega_0 \quad \cdot\omega_0 D_{1n}}{\omega_0 \cdot \hbar\omega_1 D_{0n}} \tag{3.88}$$

It is consequent from the Eq. (3.87) that the magnification decreases with an increase in n. It is beneficial for us to consider a special situation where the astronomical single image R_n measured to appear (practically) as a single image with n. The other (secondary) images are suppressed in the noise background itself. Then the resolution power for astronomy here can be given by

$$\theta_n \qquad \frac{\theta_n}{\Delta\omega_1} \tag{3.89}$$

$$\eta \quad \cdot \quad \theta_0 \quad \Delta\omega \tag{3.90}$$

$$\frac{\Pi}{\sum_{n=1}^{\Pi}\Pi_{n1}\eta} = \Delta\omega \qquad \omega_1 \qquad \cdot\log|\cdot| = \frac{\omega_0}{\Delta\omega_1} \tag{3.91}$$

Here θ_n gives the position of the n^{th} source of particular image, given by angular separation between the first image and the n^{th} image and η gives the ratio of the flux from the n^{th} image to that from the remaining images. It must be noted that although θ_n and η depend on the distance between black hole and the observer, ω_{min} does not depend on this.

Now we consider the supermassive black hole Sgr A* and M87* as well as the double image gravitational lens system quasar Q0957+561. The angular separation between the two images is $\theta_0 = 6.1''$ and $\theta_0 = 1.5''$ respectively and the distance between black hole and the observer D_{0n} [illegible]

Fig. 3 demonstrates the variation of image magnification with respect to ω_0 for different values of n for the Sgr A* and M87* black holes. We can also see that the position R_n and image magnification with the increase in n, otherwise these two images with an increase in n. The image magnification

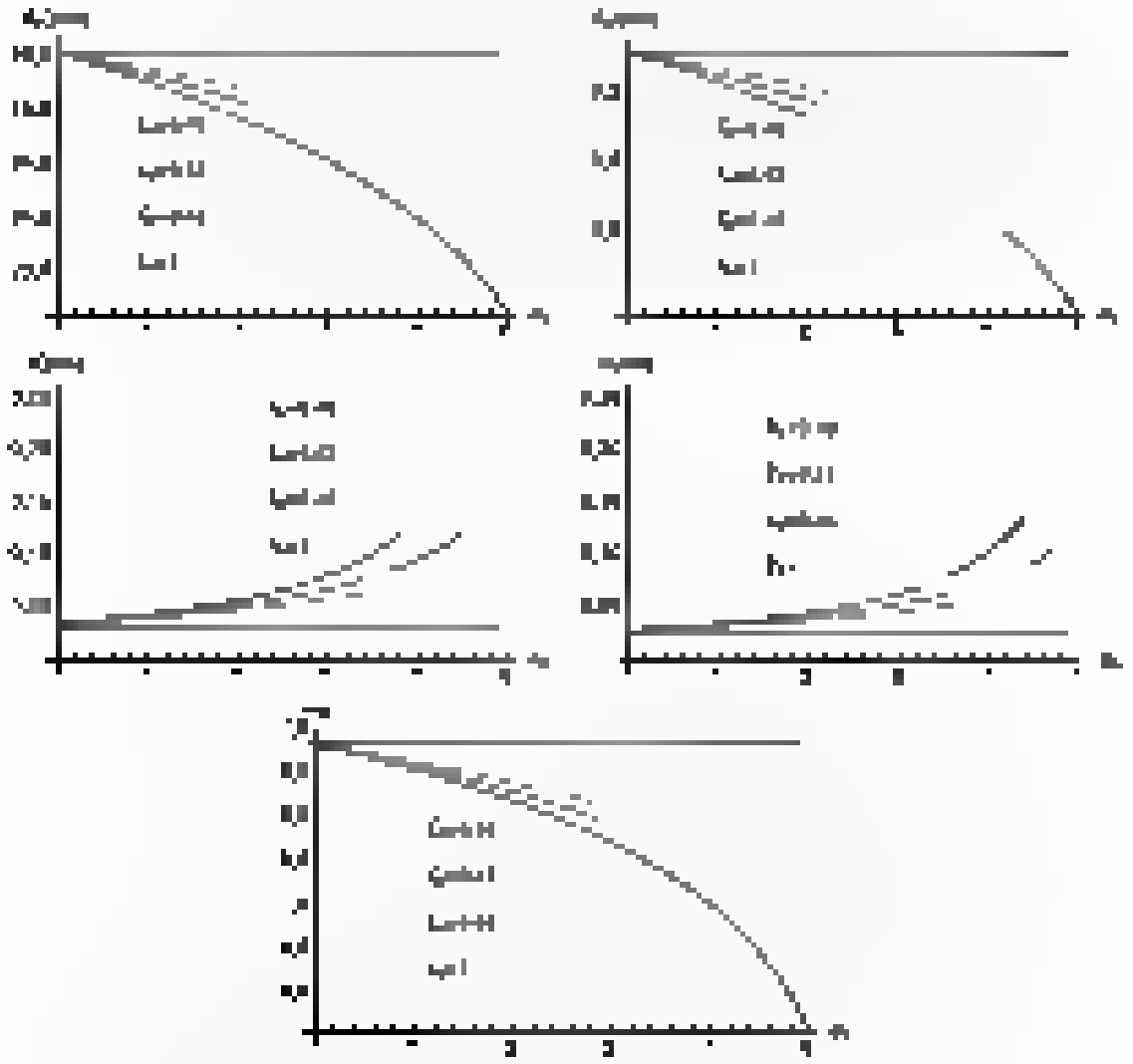

[illegible]

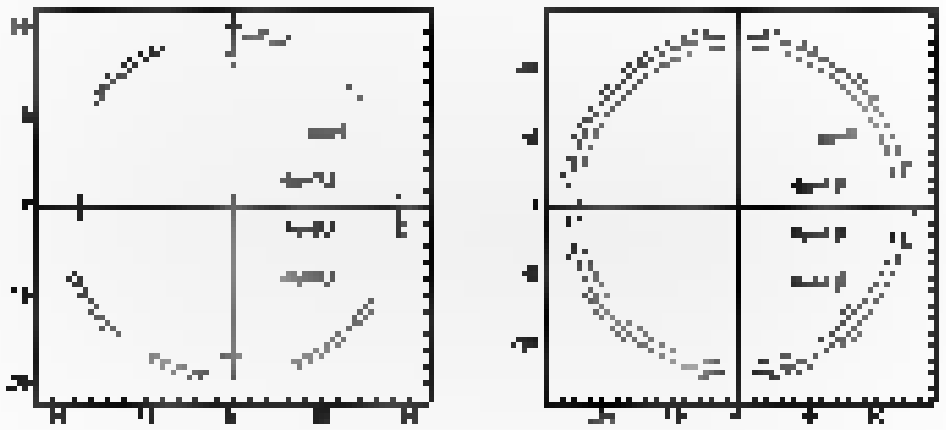

[illegible]

		[illegible]		[illegible]		
[illegible]		[illegible]	[illegible]	[illegible]	[illegible]	[illegible]
	[illegible]	[illegible]	[illegible]	[illegible]	[illegible]	[illegible]
	[illegible]	[illegible]	[illegible]	[illegible]	[illegible]	[illegible]
	[illegible]	[illegible]	[illegible]	[illegible]	[illegible]	[illegible]
	[illegible]	[illegible]	[illegible]	[illegible]	[illegible]	[illegible]
	[illegible]	[illegible]	[illegible]	[illegible]	[illegible]	[illegible]
	[illegible]	[illegible]	[illegible]	[illegible]	[illegible]	[illegible]
	[illegible]	[illegible]	[illegible]	[illegible]	[illegible]	[illegible]
[illegible]	[illegible]	[illegible]	[illegible]	[illegible]	[illegible]	[illegible]
	[illegible]	[illegible]	[illegible]	[illegible]	[illegible]	[illegible]

Table [illegible]

[illegible]

$$[illegible] \quad [illegible]$$

[illegible]

$$[illegible] \quad [illegible]$$

[illegible]

[illegible] Time delay

In this section, we study the time delay between [illegible]

$$[illegible] \quad [illegible]$$

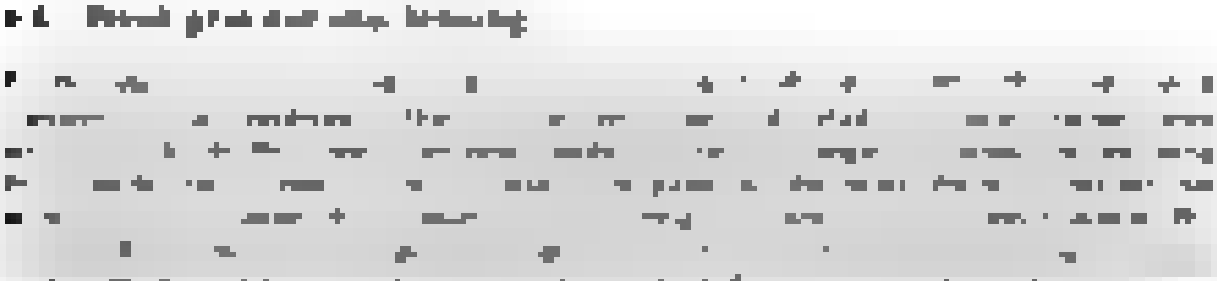

Galaxy	$M_{\rm BH}/M_\odot$	$D_{\rm OL}$/Mpc	$M/L_V/\Upsilon_\odot$	$\Delta T_{\rm S}$	$\Delta T_{\rm S}$	$\Delta T_{\rm L}$
				$\gamma_{\rm g}=1$	$\gamma_{\rm g}=0$	$\gamma_{\rm g}=1$
Milky Way	4.3×10^6	0.008	2.5×10^{11}	11.4 s	0.9 ms	11.4 s
M49	3.5×10^9	16.8	6.1×10^{11}	1.9 d	164.7 s	1.9 d
NGC 4472	2.5×10^9	16.7	8.9×10^{11}	4.6 d	398.0 s	4.6 d
NGC 4552	4.8×10^8	15.3	6.3×10^{11}	1.7 d	147.4 s	1.7 d
NGC 4649	2.0×10^9	16.5	9.1×10^{11}	4.9 d	423.8 s	4.9 d
M87	3.2×10^9	16.4	7.4×10^{11}	3.3 d	285.2 s	3.3 d
NGC 4374	1.5×10^9	18.5	8.2×10^{11}	3.9 d	337.6 s	3.9 d
NGC 4486B	5.0×10^8	16.3	5.8×10^{11}	1.5 d	134.6 s	1.5 d
NGC 4261	5.2×10^8	31.6	7.1×10^{11}	2.8 d	242.0 s	2.8 d
NGC 7052	3.7×10^8	66.4	6.6×10^{11}	2.4 d	207.3 s	2.4 d
NGC 6251	5.9×10^8	104.6	5.4×10^{11}	1.8 d	155.9 s	1.8 d
NGC 4594	1.0×10^9	9.8	4.9×10^{11}	1.4 d	120.9 s	1.4 d
NGC 3379	1.1×10^8	10.6	3.8×10^{11}	0.9 d	79.2 s	0.9 d
NGC 4486	3.4×10^9	16.1	7.6×10^{11}	3.6 d	311.0 s	3.6 d
NGC 1399	5.1×10^8	20.9	6.9×10^{11}	2.2 d	190.8 s	2.2 d
NGC 5128	5.5×10^7	3.8	2.1×10^{11}	0.4 d	34.6 s	0.4 d
NGC 1316	1.5×10^8	21.5	4.4×10^{11}	1.1 d	95.0 s	1.1 d
NGC 1052	2.1×10^8	19.4	5.1×10^{11}	1.4 d	121.0 s	1.4 d
NGC 4636	7.9×10^8	14.7	6.0×10^{11}	1.9 d	164.2 s	1.9 d
NGC 4697	1.7×10^8	11.4	4.2×10^{11}	1.0 d	86.4 s	1.0 d
NGC 3115	1.0×10^9	9.7	5.5×10^{11}	1.6 d	138.2 s	1.6 d

TABLE I. Estimated arrival delays for a hypothetical faster-than-light signal propagating through the gravitational field of various galaxies. Values are computed using the Schwarzschild metric with $\gamma_{\rm g}=1$ (general relativity) and $\gamma_{\rm g}=0$ (Newtonian limit). The last column gives the Shapiro delay.

which is the well-known logarithmic divergence of the Newtonian potential. We regularize by introducing a cutoff at the galaxy's virial radius $r_{\rm vir}$, which for a singular isothermal sphere is related to the velocity dispersion σ by $r_{\rm vir}=\sqrt{2}\,\sigma/H_0$. The resulting expression is

$$\Delta T_{\rm S}(b)=\frac{4GM_{\rm BH}}{c^3}\left[\ln\!\left(\frac{2r_{\rm vir}}{b}\right)+\frac{1}{2}\right]\left(1+\gamma_{\rm g}\right), \tag{3}$$

where b is the impact parameter of the photon trajectory relative to the lens center, and we have kept the $+\tfrac{1}{2}$ term that arises from the exact integration of the Schwarzschild line element rather than the thin-lens approximation. The factor $(1+\gamma_{\rm g})$ vanishes in general relativity ($\gamma_{\rm g}=1$) and equals two in a Newtonian theory with $\gamma_{\rm g}=0$, so the entire signal is a direct measure of the deviation from Einstein gravity.

For a source at redshift $z_{\rm s}$ behind a lens at redshift $z_{\rm l}$, the impact parameter is related to the angular separation θ on the sky by $b=D_{\rm OL}\,\theta$, where $D_{\rm OL}$ is the angular-diameter distance from observer to lens. The total delay between two images separated by θ is therefore

$$\Delta T(\theta)=\frac{4GM_{\rm BH}}{c^3}\left[\ln\!\left(\frac{2r_{\rm vir}}{D_{\rm OL}\,\theta}\right)+\frac{1}{2}\right]\left(1+\gamma_{\rm g}\right)-\frac{4GM_{\rm BH}}{c^3}\left[\ln\!\left(\frac{2r_{\rm vir}}{D_{\rm OL}\,\theta_0}\right)+\frac{1}{2}\right]\left(1+\gamma_{\rm g}\right), \tag{4}$$

where θ_0 is a reference separation chosen so that the second term cancels the first when $\gamma_{\rm g}=1$. Equation (4) reduces to $\Delta T=0$ identically in general relativity, as it must, and to $\Delta T=8GM_{\rm BH}/c^3\,\ln(\theta_0/\theta)$ in the Newtonian limit.

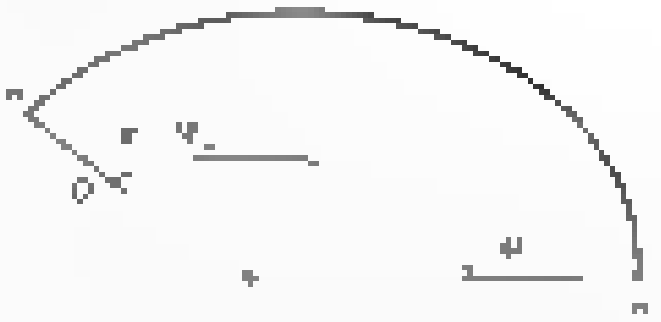

Figure 8.4 Schematic diagram of the gravitational bending of light by a massive object.

MAY with the binding radius is

$$M \quad \frac{\partial \mathcal{L}}{\partial \dot{q}} \quad \frac{\partial}{\partial t} \cdot \quad [\alpha] \quad \frac{\partial \mathcal{L}}{\partial \dot{q}} \quad \mu \quad \frac{\partial \mathcal{L}}{\partial \dot{q}} \quad \omega \quad \frac{\partial \mathcal{L}}{\partial \dot{q}}

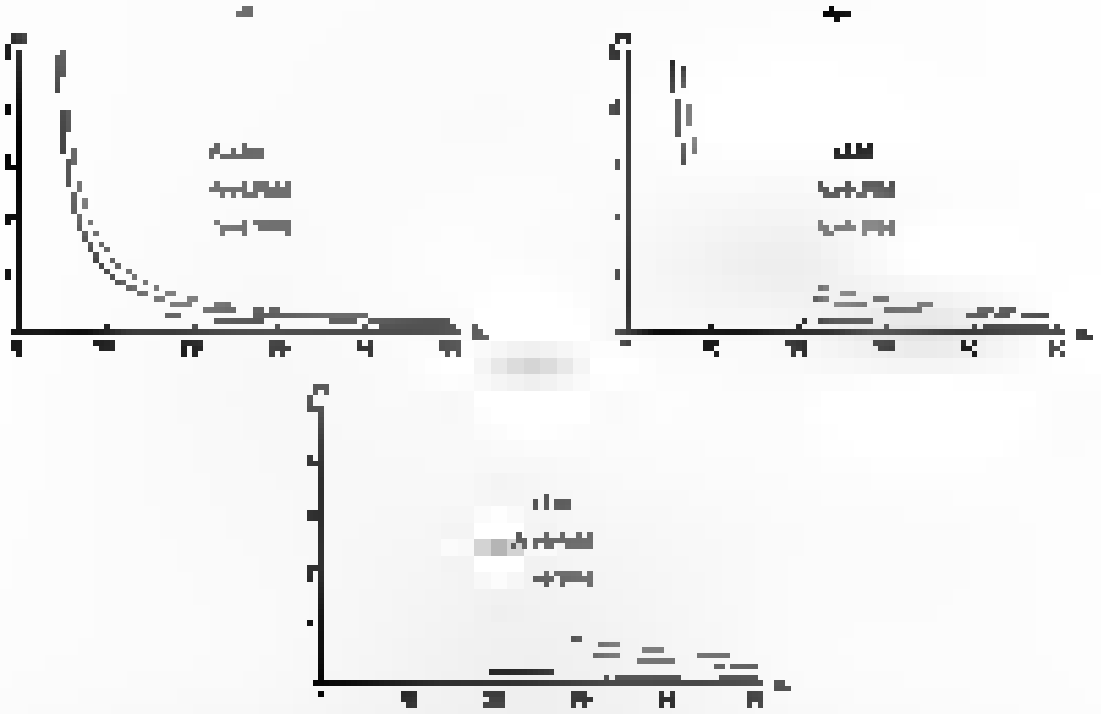

Figure 8. [illegible] for weak gravitational lensing. The upper left panel shows [illegible] the upper right panel [illegible] the lower panel [illegible].

The plots in Figure 8 show the deflection angle in weak gravitational lensing, for a source with the same [illegible] but varying impact parameter. [illegible] The impact parameter is given in units of the Schwarzschild radius, which is the radius at which the escape velocity is equal to the speed of light. The deflection angle is given in radians. The plots show that the deflection angle is [illegible] the impact parameter. The deflection angle is also [illegible].

	[illegible]	[illegible]
	[illegible]	[illegible]
	[illegible]	[illegible]
	[illegible]	[illegible]
[illegible]	[illegible]	[illegible]
	[illegible]	[illegible]
	[illegible]	[illegible]
	[illegible]	[illegible]
[illegible]	[illegible]	[illegible]
	[illegible]	[illegible]

Table 1. [illegible] for the deflection angle in weak gravitational lensing, as in Figure 8. The [illegible] for the impact parameter, [illegible].

References

[1] [illegible]

[2] [illegible]

[3] [illegible]

[4] [illegible]

[5] [illegible]

[6] [illegible]

[7] [illegible]

[8] [illegible]

[9] [illegible]

[10] [illegible]

[11] [illegible]

[12] [illegible]

[13] [illegible]

[14] [illegible]

[15] [illegible]

[16] [illegible]

[17] [illegible]

[18] [illegible]

[19] [illegible]

[20] [illegible]

[21] [illegible]

[22] [illegible]

[23] [illegible]

[48] A. Allen, G. Parisi, Phys. Rev. D 67 (2003) 065004. arXiv:hep-th/0208047, doi:10.1103/PhysRevD.67.065004.

[49] V.A. Kostelecký, M. Mewes, Phys. Rev. D 66 (2002) 056005. arXiv:hep-ph/0205211, doi:10.1103/PhysRevD.66.056005.

[50] R. F. Streater, Phys. Rev. 104 (1956) 554. doi:10.1103/PhysRev.104.554.

[51] R. Jackiw, Rev. Mod. Phys. 52 (1980) 661. doi:10.1103/RevModPhys.52.661.

[52] R. Jackiw, Phys. Rev. D 59 (1999) 065013. arXiv:hep-th/9809071, doi:10.1103/PhysRevD.59.065013.

[53] F. Wang, J. P. Yang, G. H. Yang, J. Li, B. Zhou, Phys. Rev. D 69 (2004) 065008. arXiv:hep-th/0311184, doi:10.1103/PhysRevD.69.065008.

[54] M. Berger, V. A. Kostelecký, Phys. Rev. D 65 (2002) 091701. arXiv:hep-ph/0112207, doi:10.1103/PhysRevD.65.091701.

[55] R. Lehnert, J. Math. Phys. 45 (2004) 3399. arXiv:hep-ph/0403083, doi:10.1063/1.1778168.

[56] V. A. Kostelecký, R. Lehnert, Phys. Rev. D 63 (2001) 065008. arXiv:hep-th/0012060, doi:10.1103/PhysRevD.63.065008.

[57] R. Lehnert, R. Potting, Phys. Rev. Lett. 93 (2004) 110403. arXiv:hep-ph/0406064, doi:10.1103/PhysRevLett.93.110403.

[58] R. Lehnert, R. Potting, Phys. Rev. D 70 (2004) 125010. arXiv:hep-th/0408285, doi:10.1103/PhysRevD.70.125010.

[59] R. Lehnert, R. Potting, Phys. Rev. Lett. 93 (2004) 100402. arXiv:hep-th/0406272, doi:10.1103/PhysRevLett.93.100402.

[60] D. Colladay, V. A. Kostelecký, Phys. Rev. D 55 (1997) 6760. arXiv:hep-ph/9703464, doi:10.1103/PhysRevD.55.6760.

[61] D. Colladay, V. A. Kostelecký, Phys. Rev. D 58 (1998) 116002. arXiv:hep-ph/9809521, doi:10.1103/PhysRevD.58.116002.

[62] R. Lehnert, Lorentz invariance violation and Cherenkov radiation, in: Proceedings of the 2nd Summer School in Modern Mathematical Physics, Belgrade, Serbia, 2005, pp. 127–137. arXiv:hep-ph/0603086.

[63] R. Lehnert, W. Dvornikov, Phys. Rev. D 73 (2006) 065022. arXiv:hep-ph/0512074, doi:10.1103/PhysRevD.73.065022.

[64] R. Lehnert, Phys. Rev. D 68 (2003) 085003. arXiv:hep-ph/0305179, doi:10.1103/PhysRevD.68.085003.

[65] R. Lehnert, Dispersion relations and vacuum refraction in Lorentz-violating QED, in: Proceedings of the 5th Colloquium on Group Theoretical Methods in Physics, Instituto Superior Técnico, Lisbon, Portugal, 2004, pp. 1–5. arXiv:hep-ph/0412080.

[66] R. Lehnert, Lorentz invariance violation and Cherenkov radiation, in: Proceedings of the 2nd Summer School in Modern Mathematical Physics, Belgrade, Serbia, 2005, pp. 127–137. arXiv:hep-ph/0603086.

[67] R. Lehnert, Dispersion relations and vacuum Cherenkov radiation, in: Proceedings of the 5th Colloquium on Group Theoretical Methods in Physics, Instituto Superior Técnico, Lisbon, Portugal, 2004, pp. 1–5. arXiv:hep-ph/0412080.

[68] A. Kostelecký, R. Lehnert, Phys. Rev. D 63 (2001) 065008. arXiv:hep-th/0012060, doi:10.1103/PhysRevD.63.065008.

[69] R. Lehnert, Phys. Rev. D 68 (2003) 085003. arXiv:hep-ph/0305179, doi:10.1103/PhysRevD.68.085003.

[70] R. Lehnert, R. Potting, Phys. Rev. Lett. 93 (2004) 110403. arXiv:hep-ph/0406064, doi:10.1103/PhysRevLett.93.110403.

[71] R. Lehnert, R. Potting, Phys. Rev. D 70 (2004) 125010. arXiv:hep-th/0408285, doi:10.1103/PhysRevD.70.125010.

[72] R. Lehnert, R. Potting, Phys. Rev. Lett. 93 (2004) 100402. arXiv:hep-th/0406272, doi:10.1103/PhysRevLett.93.100402.

[73] R. Lehnert, Lorentz invariance violation and Cherenkov radiation, in: Proceedings of the 2nd Summer School in Modern Mathematical Physics, Belgrade, Serbia, 2005, pp. 127–137. arXiv:hep-ph/0603086.

[74] R. Lehnert, Dispersion relations and vacuum Cherenkov radiation, in: Proceedings of the 5th Colloquium on Group Theoretical Methods in Physics, Instituto Superior Técnico, Lisbon, Portugal, 2004, pp. 1–5. arXiv:hep-ph/0412080.

[1] K. Kowalski and S. H. Mehdipour, Chaos Quantum Gas, 23, 1750135 (2018).

[2] M. A. Amooshahi, F. A. Barati, A. V. Kamyabi, Fortsch. Phys. 66, 1800044 (2018).

[3] A. Abdolmaleki, B. Ahmadabadi, A. Abdolmaleki, Phys. Rev. A 97, 062309 (2018).

[4] R. G. Jafarzadeh, Int. J. Theor. Phys. 57, 3696 (2018).

[5] Shu-Min Wu, Hui Li, Shu-Shen Jia, CAP 7, 063 (2017).

[6] V. Protopopescu, V. Tsoukalas, Phys. Rev. A 91, 042303 (2015).

[7] A. Abdolmaleki, B. Tanhayarian, Z. Amirzadeh, B. Ahmadabadi, Int. J. Theor. Phys. 56, 1750 (2017).

[8] G. Z. Bakmaz, A. Z. Bakmaz, F. Arsenijevic, Chaos Phys. Rev. 2, 1 (2018).

[9] B. Abdolmaleki, Phys. Rev. D 96, 1 (2017).

[10] A. Abdolmaleki, M. Najafi, B. Ahmadabadi, S. Ghaemi, Phys. Rev. D 93, 1 (2016).

[11] S. Lee, C. Chang, Chang and F. Chen, Ann. Phys. 93, 1 (1984).

[12] B. Hamaide and A. Dembarre, Phys. Rev. 97, 1 (2018).

[13] S. M. Wu, F. Chang, Y. Chang and S. N. Chen, Fortsch. Phys. 66, 1 (2018).

[14] Liu, Q. Ma, M. Hou, and T. Tsuchiya, Phys. Rev. D 94, 1 (2016).

[15] A. A. Saharian, Int. J. Mod. Phys. A 23, 1 (2008).

[16] A. A. Saharian, Int. J. Mod. Phys. A 23, 1 (2008).

[17] B. Hamaide, M. Hamaide, P. D. Piyadigama, Chaos Solitons Fract. 11, 1 (2018).

[18] D. O. Mukhanov, F. Johansen, Phys. Rev. Lett. 73, 1 (1994).

[19] D. O. Mukhanov, B. L. Zhou, E. D. Herbst, Fortsch. Phys. Rev. Lett. 24, 1 (1970).

[20] G. Bakmaz, Kaplan and A. Tanhayarian, Mod. Phys. B, Astron. Soc. 1, 1 (2018).

[21] K. Jha, A. Subramanian, Rev. Phys. 2, 1 (2018).

[22] Phys. Rev. 97, 1 (2018).

[23] P. Ahmadabadi, B. Ahmadabadi, A. Abdolmaleki, Phys. Rev. 92, 1 (2015).

[24] A. Kaplan, Mod. Phys. Rev. Astron. Soc. 451, 1 (2015).

[25] G. Z. Bakmaz, A. Z. Bakmaz, F. Arsenijevic, Gen. Relativ. Gravit. 1, 1 (2018).

[26] A. Tanhayarian and G. A. Barnaveli, Gravitation and Cosmology, 1, 1 (2018).

[27] A. Abdolmaleki, B. Tanhayarian, Astron. Nucl. Phys. A, Astrophys. Int. J. Mod. Phys. 26, 1750181 (2017).

[28] V. Tsoukalas and G. A. Barnaveli, Gravitation and Cosmology 19, 1 (2013).

[29] G. V. Tsoukalas and G. A. Barnaveli, Gravitation and Cosmology 19, 1 (2013).

[30] V. Protopopescu, B. Ahmadabadi and A. A. Saharian, Astrophys. Space Sci. 361, 1 (2016).

[31] B. Tanhayarian, Gravitation Cosmology Relativistic Astrophysics, Phys. Rev. 91, 1 (2015).

[32] V. B. Bezerra, Fortsch. Phys. Rev. 14, 1 (1976). Erratum-ibid. 14, 109 (1977).

[1] [illegible]

[2] [illegible]

[3] [illegible]

[4] [illegible]

[5] [illegible]

[6] [illegible]

[7] [illegible]

[8] [illegible]

[9] [illegible]

[10] [illegible]

[11] [illegible]

[12] [illegible]

[13] [illegible]

[14] [illegible]

[15] [illegible]

[16] [illegible]

[17] [illegible]

[18] [illegible]

[19] [illegible]

[20] [illegible]

[21] [illegible]

[22] [illegible]

[23] [illegible]

[24] [illegible]

[25] [illegible]

[26] [illegible]

[27] [illegible]

[28] [illegible]

[29] [illegible]

[30] [illegible]

[1] [illegible]

[2] [illegible]

[3] [illegible]

[4] [illegible]

[5] [illegible]

[6] [illegible]

[7] [illegible]

[8] [illegible]

[9] [illegible]

[10] [illegible]

[11] [illegible]

[12] [illegible]

[13] [illegible]

[14] [illegible]

[15] [illegible]

[16] [illegible]

[17] [illegible]

[18] [illegible]

[19] [illegible]

[20] [illegible]

[1] [illegible]

[2] [illegible]

[3] [illegible]

[4] [illegible]

[5] [illegible]

[6] [illegible]

[7] [illegible]

[8] [illegible]

[9] [illegible]

[10] [illegible]

[11] [illegible]

[12] [illegible]

[13] [illegible]

[14] [illegible]

[15] [illegible]

[16] [illegible]

[17] [illegible]

[18] [illegible]

[19] [illegible]

[20] [illegible]

[21] [illegible]

[147] [illegible] and B. Considine, Revised Extended Gluon Topology. Nuclear Physics Reports, [illegible]

[148] [illegible] and V. [illegible], Topological [illegible], vol. [illegible], [illegible]

[149] [illegible] and [illegible], [illegible], vol. [illegible], [illegible]

[150] A. Christensen and [illegible], Topological [illegible], [illegible]

[151] [illegible] and [illegible], Topological [illegible], vol. [illegible], [illegible]

[152] G. [illegible], A. [illegible], [illegible], Topological [illegible], [illegible]

[153] [illegible], [illegible], [illegible], [illegible], [illegible], [illegible]

[154] [illegible] and [illegible], [illegible], [illegible]

[155] [illegible], [illegible], [illegible], [illegible], [illegible], [illegible]

[156] [illegible], [illegible], [illegible], [illegible], [illegible], [illegible]

[157] [illegible], [illegible], [illegible], [illegible], [illegible], [illegible]

[158] [illegible], [illegible], [illegible], [illegible], [illegible], [illegible]

[159] [illegible], [illegible], [illegible], [illegible], [illegible], [illegible]

[160] [illegible], [illegible], [illegible], [illegible], [illegible], [illegible]

[161] [illegible], [illegible], [illegible], [illegible], [illegible], [illegible]

[162] [illegible], [illegible], [illegible], [illegible], [illegible], [illegible]

[163] [illegible], [illegible], [illegible], [illegible], [illegible], [illegible]

[164] [illegible], [illegible], [illegible], [illegible], [illegible], [illegible]

[165] [illegible], [illegible], [illegible], [illegible], [illegible], [illegible]

[166] [illegible], [illegible], [illegible], [illegible], [illegible], [illegible]

[167] [illegible], [illegible], [illegible], [illegible], [illegible], [illegible]

[168] [illegible], [illegible], [illegible], [illegible], [illegible], [illegible]

[169] [illegible], [illegible], [illegible], [illegible], [illegible], [illegible]

[170] [illegible], [illegible], [illegible], [illegible], [illegible], [illegible]

[171] [illegible], [illegible], [illegible], [illegible], [illegible], [illegible]

[172] [illegible], [illegible], [illegible], [illegible], [illegible], [illegible]

[173] [illegible], [illegible], [illegible], [illegible], [illegible], [illegible]

[174] [illegible], [illegible], [illegible], [illegible], [illegible], [illegible]

[175] [illegible], [illegible], [illegible], [illegible], [illegible], [illegible]

[176] [illegible], [illegible], [illegible], [illegible], [illegible], [illegible]

[177] [illegible], [illegible], [illegible], [illegible], [illegible], [illegible]

[178] [illegible], [illegible], [illegible], [illegible], [illegible], [illegible]

[179] [illegible], [illegible], [illegible], [illegible], [illegible], [illegible]

[180] [illegible], [illegible], [illegible], [illegible], [illegible], [illegible]

Published Papers

The inflationary scenario in the f(R) gravity Model with a R² term

[illegible]

[illegible]

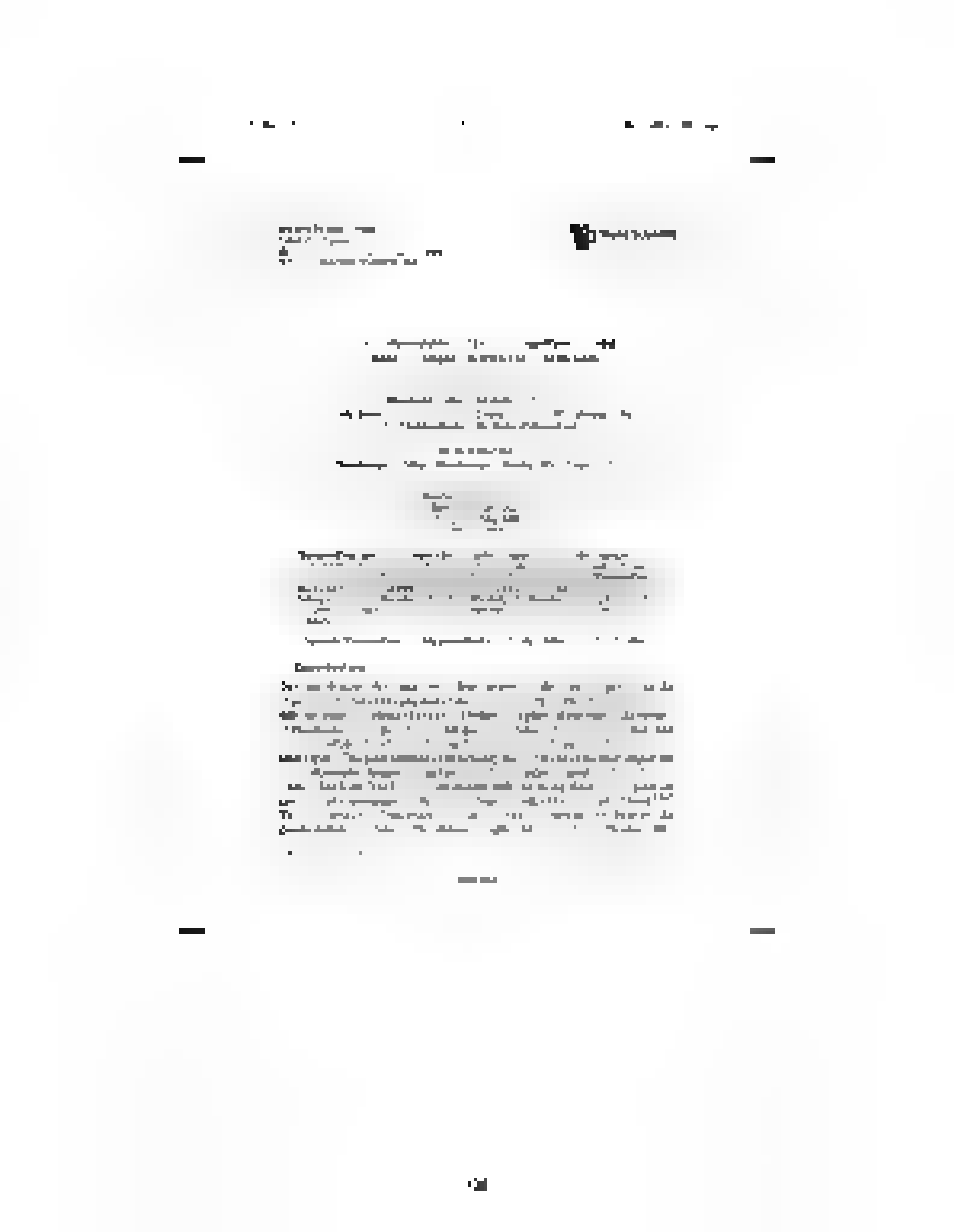

Study of black holes in standard and modified gravity

Thesis submitted for the award of
Doctor of Philosophy in Science (Physics)
of
The University of Burdwan

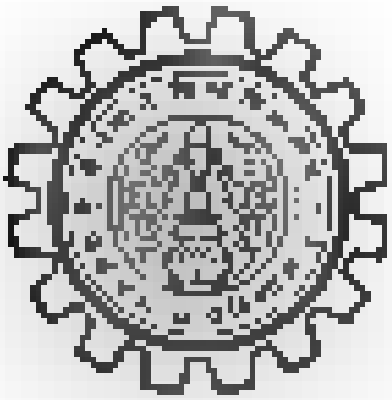

Submitted by

SOHAN KUMAR JHA

(M.Sc. Dated 24.06.2013)

Under the Supervision of Dr. Anusar Rahaman (WBES)

Durgapur Govt. College, Durgapur, Burdwan

Work done in

Hooghly Mohsin College, Chinsurah, Hooghly

And

Durgapur Govt. College, Durgapur, Burdwan

Chapter 9

[redacted]

appears because of the use of non-commutative spacetime proposed by Snyder. The interfering terms that appear are very very small since the term contains the product of two very small factors λ_s and ℓ. Although the interfering term is negligibly small, it has some theoretical consequences, e.g., symmetric contribution may get disturbed by an asymmetric term - the reverse perhaps does not get so. It is true that both the parameters λ_s and ℓ are small. A physical model containing some arbitrary parameter would be physically sensitive if the parameters can be constrained from experimental observations. Both the parameters can be put under constraints using the same arguments available in [65] and [64]. The conjecture used there is that the correction would be of the order of general relativistic correction. Here, we can, indeed, put a restriction on the parameters λ_s and ℓ following the same argument. The upper bound of the predicted values of the parameters is given in Table (2.1). Note that the predicted values of ℓ are identical to the values obtained in the article [65]. It is indeed the expected result. Our study enables us to put another constraint on the parameter λ_s when the constraint on ℓ is known. If it is taken into consideration that the correction that appeared in the form of interference which is proportional to $\lambda_s\ell$ would be of the same order of magnitude of the pure terms. Note that the first-order correction term is proportional to $\lambda_s\ell$. So if we are intended to constrain the interfering term it will provide new information that the parameters may have reciprocal contributions between each other. When the contribution through one parameter dominates, the contribution from the other will get suppressed automatically.

Chapter III contains a description to establish that Kerr-Sen-like spacetime is a viable solution of Einstein-bumblebee gravity model [76] where LV scenario gets involved through the real bumblebee field vector B_μ. Then, it has been extended to study the properties of the shadow it is supposed to cast. To this end, the effective potential that results from the null geodesics in the bumblebee rotating black hole spacetime is computed that in turn helps to get the tentative nature of the motion of photon predicted for different choices of the parameters a, b, and ℓ. Then the nature of shadow is studied and how does the shadow gets deformed has also been studied for different variations of a, b, and ℓ. We observe that the shadow gets shifted towards the right for positive ℓ and shifted towards left for negative ℓ when a and b remain fixed. However, shifting is always towards the right when b increases whatever the set of values of ℓ and a are taken. We have also studied the rate of emission of energy for this type of black hole. The emission rate decreases when b increases for any set of fixed values of a and ℓ. It also decreases when ℓ increases for an arbitrary set of fixed values of a and b. A crucial difference however in the situation is noticed when ℓ increases. The emission rate although decreases with the increase of ℓ like the case when b increases, the peak of the curve gets shifted towards lower ω in the situation when ℓ increases. The deformation of the shadow for the Kerr-Sen-like black hole in the Einstein-bumblebee gravity model with the variation of ℓ observed here is a theoretical prediction. It shows that it enhances the distortion of shadow, and it would be detected by the next generation gravitational antennas.

Chapter IV deals naturally with the investigation effect on the Kerr-Sen-like spacetime which has been found as a solution to the equations developed from Einstein-bumblebee gravity in [76] which has a LV parameter ℓ. This modified spacetime is used to study the propagation of light in a non-magnetized pressureless plasma in [115]. We have considered the plasma as a medium with dispersive properties given by a frequency-dependent index of refraction. The gravitational field is determined by the mass, the spin, and the bumblebee parameter. The Gravitational field due to plasma is neglected here. We have studied how the nature of shadows gets affected by the LV effect associated with the bumblebee field in the pressure-less nonmagnetic plasma. We have also studied the energy emission rate and the weak field lensing in the Kerr-Sen-like spacetime due to Einstein-bumblebee gravity background when it is veiled in a plasma medium. The results for Kerr, Kerr-like, and Schwarzschild black holes can, as well, be obtained from this result with a suitable limit. We have investigated in detail the impact of the charge ($Q^2 = N$), plasma parameter k, and the Lorentz violating bumblebee parameter ℓ on the structure of shadow, on the lensing effect of light, and on the energy emission due to black hole radiation. It has been found that the new parameters quantitatively influence the structure of the event horizon by altering the radius significantly. It is observed that the size of the shadow viewed by a distant observer reduces with an increase in the charge Q and the size of the shadow appears to be larger with the increase in the plasma parameter k. Therefore, the

Kerr-like black hole model in order to study the shadow in presence of plasma as well. Since the energy liberated from the black hole depends on the area of the shadow, the rate of energy emission from the black hole is higher when the black hole is surrounded by plasma. As far as the angle of deflection is concerned, the photons are observed to experience an increase in the deviation as the plasma factor k increases. While on the other hand, the angle of deflection reduces sufficiently when the spin axis of charge parameter increases. It is also observed that the deflection angle increases with an increase in the value of the IV parameter ℓ. Sufficient negative ℓ may cause the lensing effect too!

Chapter V is devoted to constraining the free parameters that have entered into the modified models adopted here. The idea behind this is as follows. The theory of general relativity predicts that the Kerr metric is capable of describing astrophysical black holes. However, such black holes may not exist in a perfect vacuum, due to the presence of surrounding matter, like plasma, dark matter, etc. The accretion disks may also alter the black hole, which may not fit with the Kerr metric. The Lorentz-violation-inspired Kerr spacetime enables the incorporation of potential deviations from the Kerr metric through the additional deviation parameters. The advantage of this type of modified gravity is that it is a generic one and it has the ability to cover the prediction of the Kerr metric since the introduced parameters can be chosen in such a way that it makes the null deviation of the shadow from Kerr spacetime. There is a theoretical motivation for modified theories of gravity indeed, however the constraining of the free parameter from the experimental observation allows us to examine the viability of the model. In this context the information of the captured image by the EHT collaboration becomes instrumental.

The EHT collaboration has captured the image of supermassive black hole M87* exhibiting a deviation from circularity $\Delta C \leq 0.10$. The observation did not say anything about modified theories of gravity or suggest any alternatives to the Kerr black hole. Motivated by this, we considered Kerr-Sen-like modified black holes, which have additional deviation parameters ℓ and k to the Kerr black hole. The presence of Plasma adds an additional parameter. We use the deviation from circularity $\Delta C \leq 0.10$ as declared by the EHT collaboration to constrain the Kerr-Sen-like black hole parameters. We have observed that the bound $\Delta C \leq 0.10$ is satisfied by black hole shadows over a finite parameter space both in the presence of plasma and in the absence of it. Besides, the information available from the article [137] allows us to put constrain on the value of ℓ. We have found that the value of the parameter $\ell > -1$ and the upper bound of it is 0.601691. So ℓ can take both positive and negative values. We would like to mention that in the calculation of the rate of energy emission, we did not consider the greybody factor. The mathematical formulation of it is much involved for any black hole. Moreover, it is important when quantitative estimation is brought under consideration. Unfortunately, there is no available data to compare it with the real situation. A fascinating and involved extension of this work would be to evaluate it theoretically.

We have described the superradiance phenomena of the scalar field scattered off Kerr-Sen-like black holes in detail in Chapter VI. The contents of this chapter have been studied in [156]. We have already mentioned that this is a black hole solution to Einstein-bumblebee gravity model. A Lorentz violating parameter is there in the spacetime metric of this modified gravity. Here, Lorentz violation takes place via a spontaneous symmetry breaking where the pseudovector field of the Einstein-bumble model receives a vacuum expectation value. We have also studied superradiance instability. We have studied here how the superradiance phenomena and related instability scenario gets influenced by the Lorentz violation effect through the Kerr-Sen-like background which is the outcome of the Einstein-bumblebee gravity model. Employing asymptotic matching of the scalar wave, it has been established that in the low-frequency limit, i.e., for $\omega < m\Omega_{+}$, the scalar waves become superradiant amplified. The numerical computation, however, shows that for $m < 0$ the massive scalar field has a non-superradiant mode. For $m \geq 0$ it is superradiant. The superradiant process enhances with the decrease of the Lorentz violation parameter and the reverse is the case when the Lorentz violation parameter increases irrespective of the sign of the value of this parameter. We have also demonstrated how the superradiant process gets influenced by the parameter k. From Fig. (6.10) it is clear that superradiance enhances with the decrease of the positive value of the parameter k. Note that $k = \frac{\alpha^2}{M^2}$. So it cannot be negative. Moreover, extending the issue of the black hole bomb, the analytical study of superradiant instability is made. The plot in Fig. (6.11) related to the study reveal

that the LV parameter remarkably affects the instability regime. In the background with the negative LV parameters, the scalar field has more chances to acquire unstable dynamics and for the positive values of the LV parameter it is less. Therefore, the Lorentz violation has a significant influence on the superradiance scattering phenomena and the corresponding instability linked with it.

As an extension, we describe in Chapter VII how a framework is developed where quantum correction due to the Lorentz violation and non-commutative character of spacetime has been taken into account on the rates leaving [121]. The spacetime background studies a non-commutative Kerr-like Lorentz symmetry violating black hole. We have extensively studied different aspects of the non-commutative and Lorentz violating Kerr-like black hole. The spin, the mass, the Lorentz violation parameter, and the non-commutative parameter involved in it determine the gravitational field of this black hole. First of all, we study geometry in detail concerning its horizon structure and ergosphere. The article [121] contains the study of two important optical phenomena in the vicinity of this black hole. In this report, we have considered the superradiance phenomena and find that it crucially depends on the parameter ℓ and θ_0, apart from its dependence on a which is linked with the spin of the black hole. The superradiance process enhances with the decrease in the value of the Lorentz violation parameter and it diminishes when we increase the value of the Lorentz violation parameter. We also observe that with the increase in the value of the parameter θ_0, the superradiance process gets diminished. However, with the increase in the value of a the superradiance process increases. Next, we have brought into our investigation the effect of Lorentz violating parameter ℓ and non-commutative parameter θ_0 on the size of the black hole shadow. We have observed that the size of the black hole shadow increases with an increase in the value of the parameter ℓ and it decreases with an increase in the value of the parameter θ_0. Thus, it can be safely concluded that Lorentz violation and non-commutativity, both, have significant impacts on black hole shadow. We have also studied energy emission rates. These results have clearly established the influence of the Lorentz violation parameter and non-commutative parameter on emission rate. We observe that the energy emission rate decreases with an increase in the value of ℓ for any set of fixed values of a and ℓ. It also decreases with an increase in the value of ℓ, when a and b are held fixed, and with an increase in the value of a, if ℓ and b are kept fixed.

We have been able to constrain the parameters even in the modified theories augmented with the combined effect of Lorentz violation and the non-commutative character of spacetime using the observations of EHT collaboration. For inclination angle $\theta = 90^\circ$, the deviation from circularity $\Delta C \leq 0.1$ and angular diameter $\theta_d = 42 \pm 3\mu as$ within 1σ region are satisfied for finite parameter space $(\frac{1}{10} - \frac{1}{5})$. For inclination angle $\theta = 17^\circ$, the circularity deviation $\Delta C \leq 0.1$ is satisfied for the entire parameter space $(\frac{1}{10} - \frac{1}{5})$. The angular diameter $\theta_d = 42 \pm 3\mu as$ within 1σ is satisfied for finite parameter space $[\frac{1}{10} - \frac{1}{8}]$. The axis ratio D_X satisfies the constraint $1 < D_X \leq 4/3$ for the entire parameter space at both the inclination angles $\theta = 90^\circ$ as well as $\theta = 17^\circ$. Therefore our study enables us to establish the fact that non-commutative Kerr-like black holes are remarkably consistent with EHT images of M87*. It demands that ruling out non-commutative Kerr-like black holes from the observational data of black hole shadow would be illogical. Thus, non-commutative Kerr-like black hole may be considered a suitable candidate for the astrophysical black hole. It has also been shown that the possible upper bound of θ_0, which is associated with the non-commutativity is $0.0003597 M^2$. It is intriguing and indeed a novel way to constrain the parameter associated with the non-commutativity from the shadow of an astrophysical black hole. Till now we do not have any available data to constrain the parameter ℓ and θ_0 from the superradiance effect and from the energy emission process. So, the parameters cannot be constrained by knowledge of the superradiance phenomena and the energy emission process. We have made all the plots for the superradiance and the energy emission process maintaining the constraints obtained from the EHT data concerning the shadow of the M87*.

Chapter VIII is devoted to study the strong as well as weak lensing due to the black hole modified with scalar hair. Black holes have been considered more than basic results of the Einstein equations for quite some time now. Nonetheless, it is only recently that their direct existence was detected substantially due to the report of the results of the Event Horizon Telescope Collaborations. So, the study of aspects of black holes and the consequences of their presence have now gathered with new elevation. In this environment, we study strong as well as weak lensing in the background of a

modified black hole. Hence, modification due to scalar hair is considered in [34] and a study has been made to study lensing properties and how the presence of hair influence the lensing property. The relativistic telescope here evokes the no hair theorem since the hair is examined in the manner by which we come to know the surroundings such as dark matter, which is considered to have a constant energy-momentum tensor. This modification permitted us to introduce parameters c_0 and c_2. The former relates back hole to the deformation because of the presence of outside supply and the c_2 is associated with alteration in thermodynamical pursuits because of the presence of hair. We observe that the lensing coefficient $\bar{A}$ increases with c_0 but the lensing coefficient $\bar{B}$ and the impact parameter b_m decrease with the increase of c_0. However, with the increase of c_2 although $\bar{A}$ decrease $\bar{B}$ gets enhanced. The impact parameter b_m increases with the increase of c_2. The values of the parameters resemble to Schwarzschild black hole whenever we put $c_0 = 0$.

The modified models that we have considered in our work have their own advantages in order to understand supermassive black holes through the manner that the observations of the EHT collaboration has opened recently. However, it is still too early to say which model fits the experiment the best or performs better than another models. As a result, numerous investigations in this regard need to be pursued. While considering our research, we focused on the information pertaining to M87*. What further insight does the observation from Sgr A* provide about these modified gravity that we will bring investigated?